As part of the BMBF funding initiative “sustainable bioproduction”, the work reported in this thesis was performed with the goal to reduce the time to market for biocatalytic processes. For this purpose, three kinetic resolutions catalyzed by Candida antarctica lipase B are investigated from a process engineering point of view. A combination of modeling, simulation and miniplant technology* is applied to mimic technical operation at the smallest scale. This involves kinetic analysis, pervaporation and fixed bed reactor catalysis. To top off this work, the sustainability of the three reaction alternatives was analyzed.

Wouter R. Berendsen graduated in 2000 in bioprocess engineering at the University of Wageningen in the Netherlands. During 2000 and 2005, he performed the practical part of his PhD at the Institute of Biochemical Engineering at the University of Stuttgart, Germany. After joining Danone R&D in July 2005, he passed his oral examination with great success on December 18, 2007.

Model Based Development of Continuous Processes for Production of Chiral Glycol Ethers by Biocatalysis

Wouter R. Berendsen

Model Based Development of Continuous Processes for Production of Chiral Glycol Ethers by Biocatalysis

Wouter R. Berendsen

Model Based Development of Continuous Processes for Production of Chiral Glycol Ethers by Biocatalysis

Print and bound in the Netherlands by Grafisch Productiebedrijf Gorter

Model Based Development of Continuous Processes for Production of Chiral Glycol Ethers by Biocatalysis

Modellbasierte Entwicklung Kontinuierlicher Prozesse zur Herstellung Chiraler Glykolether durch Biokatalyse

Von der Fakultät Maschinenbau der Universität Stuttgart
Zur Erlangung der Würde eines Doktors der Ingenieurwissenschaften (Dr.-Ing.)
genehmigte Abhandlung

vorgelegt von

Wouter Robert Berendsen

aus Gouda in den Niederlanden

Vorsitzender:	Prof. Dr.-Ing. Frank Allgöwer
Hauptberichter:	Prof. Dr.-Ing. Matthias Reuss
Mitberichter:	Prof. Dr. rer. nat. Rolf D. Schmid
Tag der mündlichen Prüfung:	18. Dezember 2007

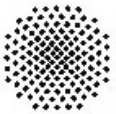

Institut für Bioverfahrenstechnik (IBVT)
Universität Stuttgart
2008

The work described in this thesis was financially supported by the Federal Ministry of Education and Research (BMBF), Germany as part of the program „sustainable bioproduction“ and The Dow Chemical Company, Stade, Germany.

Studies described in this thesis were performed at

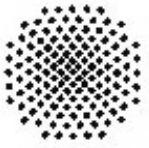

Institute of Biochemical Engineering
University of Stuttgart
Allmandring 31
70569 Stuttgart

Voor

Gert, Franky,

Renske en Wiardi

Acknowledgements

Many people have contributed to this work and I would like to thank them all!

In particular, I would like to thank Prof. Dr.-Ing. Matthias Reuss for giving me the opportunity to perform my PhD research at his institute. Thank you for your motivating ideas and visions, which were a great help and guide to my research.

First, I would like to give special thanks to Markus Samorski and Andreas Freund. Markus, thanks for our stimulating discussions and your valuable suggestions. Andreas, I know you don't like to hear it, but it was your contribution, which made miniplant planning, construction and operation possible! Thanks for your devotion, technical support and interest for detail.

Special thanks are due to my students, Glen Gendrot, Pia Radmer, Christoph Stockert, and Andreas Weiss. Many thanks for your hard work, devotion and input. In particular, I like to thank Renate Moser for helping me with many practicalities.

I would like to acknowledge all employees of the Dow Chemical Company, which helped to make this project a success. Thank you, Wilhelm Leffers and Ioannis Evripidis for our discussions about process design and sustainability. Many thanks also to Sol Resnick for your technical support and for being a great host on our trip to San Diego.

Furthermore, I wish to thank my project colleague, Monika Rusnak and Prof. Dr. rer. nat. Rolf D. Schmid for the good cooperation and pleasant trips to Dow at Schwalbach.

In addition, I would like to thank all my colleagues at the IBVT for providing a fantastic and stimulating working atmosphere. In particular, I would like to thank the "MPI-group", Jochen Schaub, Knut Behrendt, Martin Siemann-Herzberg, Joachim Schmid, Markus Samorski, Klaus Mauch and Oliver Vielhauer for the interesting discussions during lunch, but also Dirk Müller, Prem Kumar Murugan, Timo Hardiman, Christina Fritz, Alexei Lapin, Klaus Maier, and Luciano Aguilera for having much fun during daily work.

My family and friends deserve special thanks for giving me the opportunity to relax. I am particularly grateful for our dear friendship, Erwin van den Born and Nadja Schultz.

My colleagues at Danone, in particular Horst Müller, Heiko Fuhrmeister, Nicole Kleber and Christoph Briegleb also deserve big thanks for their encouragement.

Finally and above all, I would like to thank my parents, Gert and Franky, for encouraging and supporting me at all times and my sister Renske and her husband Wiardi for their interest in my work and for sharing great vacations!

Wouter Robert Berendsen

Table of Contents

Acknowledgements VII

Nomenclature XIII

Abstract XIX

Keywords XX

Zusammenfassung XXI

Schlüsselwörter XXX

Samenvatting XXXI

Sleutelwoorden XXXII

1. Introduction and Outline 1

1.1 Introduction 3

1.2 Outline 9

2. Kinetic Modeling of Lipase Catalyzed Hydrolysis of (R/S)-1-Methoxy-2-propyl-acetate as a Model Reaction for Production of Chiral Secondary Alcohols 11

2.1 Introduction 15

2.2 Results and Discussion 17

2.2.1 Model Development 17

2.2.2 Enantioselectivity and Enantiomeric Ratio 23

2.2.3 Effect of pH on Enzyme Activity 25

2.2.4 The Influence of Temperature on the Enantioselectivity of the Enzyme 25

2.2.5 Estimation of Kinetic Parameters for Reactor Design Studies to Optimize the Operation Temperature 31

2.3 Conclusions 33

3. A Kinetic Study of Lipase-Catalyzed Reversible Kinetic Resolution Involving Verification at Miniplant-Scale 35

3.1 Introduction 39

3.2 Theory 41

3.2.1 Kinetic Model Development 41

3.3 Results and Discussion 44
3.3.1 Model Identification and Parameter Estimation 44
3.4 Conclusions 54
4. Pervaporative Separation of Ethanol from an Alcohol – Ester Quaternary Mixture 55
4.1 Introduction 59
4.2 Theory 60
4.2.1 Models Based on the Concentration Gradient as the Driving Force for Mass Transport 61
4.2.2 The Challenge of Choosing the Right Boundary Conditions 62
4.2.3 Models Based on the Pressure Gradient as the Driving Force for Mass Transport 65
4.3 Results and Discussion 67
4.3.1 Dynamic Behavior of Mass Transport Through Pervap 2256® Membranes 67
4.3.2 Effect of Feed Composition on Permeation Behavior 68
4.3.3 Effect of Temperature on Permeate Flow 73
4.4 Conclusions 76
5. Investigations of Reaction Kinetics for Immobilized Enzymes – Identification of Parameters in the Presence of Diffusion Limitation 77
5.1 Introduction 81
5.2 Theoretical Analysis 84
5.2.1 Coupled Reaction and Diffusion Model 84
5.2.2 Kinetics 86
5.3 Results and Discussion 89
5.3.1 Kinetic Measurements and Modeling 89
5.3.2 The Impact of Diffusion Limitation 96
5.3.3 Investigation of Systems Behavior 99
5.4 Conclusions 101
6. Nonisothermal Lipase-Catalyzed Kinetic Resolution in a Packed Bed Reactor: Modeling, Simulation and Miniplant Studies 103
6.1 Introduction 107
6.2 Mathematical Model Development 109
6.2.1 Mass and Energy Balances 110
6.2.2 Kinetics 113

6.2.3 Calculation of Radial Porosity and Superficial Velocity Profile 114
6.3 Results and Discussion 115
6.4 Conclusions 122
7. Applications of Integrated Miniplant Technology and their Opportunity for Process Development of Enzymatic Reactions 123
7.1 Introduction 127
7.2 Miniplant-Technology 127
7.3 Miniplant Used for Studying Biocatalytic Synthesis of Chiral Glycolethers 128
8. Concluding Remarks and Outlook 133
9. Materials and Methods 137
9.1 Materials 139
9.1.1 Chemicals 139
9.1.2 Enzyme 139
9.1.3 Membrane 139
9.2 Experimental Methods for Determination of Kinetics 140
9.2.1 Time Course Measurements of MPA Hydrolysis 140
9.2.2 Initial Rate Measurements of MP-EA Transesterification 140
9.2.3 Time Course Measurements of MP-VA Transesterification 140
9.3 Miniplant Experiments 141
9.3.1 Design, Construction, Start-up and Operation 141
9.3.2 Typical Miniplant Operation and Measurements 141
9.4 Pervaporation Experiments 142
9.4.1 Setup 142
9.4.2 Procedure 143
9.5 Analytical Methods: Gas Chromatography 144
9.6 Calculation Methods 144
9.6.1 Determination of Kinetic Parameters 144
9.6.2 Performing Reactor Simulations 145
9.6.3 Calculation of Effective Diffusion Coefficient 145
List of Publications 147
References 149

Nomenclature

Symbols

a_i	activity of component i	(mol·m^{-3})
a_p	specific external surface area of the particle per unit reactor volume $= \frac{3 \cdot (1-\varepsilon_l)}{R_p}$	(m^{-1})
A_p	particle surface area $= 4\pi R_p^2$	(m^2)
A_c	surface area of cooling jacket $= 2\pi R_r X$	(m^2)
Bi	Biot number	(-)
B_i, B_{ij}	adjustable parameters	(L·mol^{-1})
c_i, c_j	concentration of compound i or j	(mol·L^{-1})
$c_{l,i}$	concentration in liquid phase	(mol·L^{-1})
$c_{p,c}$	specific heat capacity of cooling medium	(J·kg^{-1}·K^{-1})
$c_{p,l}$	specific heat capacity of liquid	(J·kg^{-1}·K^{-1})
$c_{s,i}$	concentration in solid phase	(mol·L^{-1})
$D_{0,i}$	diffusion coefficient at infinite concentration	(m^2·s^{-1})
$D_{ax,l}$	effective axial dispersion coefficient in liquid $= \frac{\overline{u_0} \cdot 2 \cdot r_p}{Pe_{ax}}$	(m^2·s^{-1})
$D_{ep,l}$	effective dispersion coefficient in particle $= \frac{\overline{u_0} \cdot 2 \cdot r_p}{Pe_{mr}}$	(m^2·s^{-1})
$D_{er,l}$	effective radial diffusion coefficient in liquid phase	(m^2·s^{-1})
D_i	Fick diffusion coefficient	(m^2·s^{-1})
E	enantiomeric ratio / E-value	(-)
$E_{act,a}$	activation energy	(J·mol^{-1})
$E_{D,i}$	Energy of diffusion	(J·mol^{-1})
E_{Eff}	effective enantiomeric ratio	(-)
e.e.	enantiomeric excess	(-)
Fo_i	Fourier number	(-)
$\Delta G°_j$	Gibbs free energy of K_m or K_i-constants	(J·mol^{-1})
$\Delta G^{‡\circ}_j$	transition state energy	(J·mol^{-1})
$\Delta_{R-S}\Delta G^{‡\circ}$	differential transition state energy	(J·mol^{-1})
h	Planck constant	(J·s)

$\Delta H_{act,a}$	activation energy	(J·mol^{-1})
$\Delta H^{\ddagger\circ}{}_j$	reaction enthalpy / activation energy	(J·mol^{-1})
ΔH_m	enthalpy of reaction	(J·mol^{-1})
$\Delta H_{s,i}$	enthalpy of sorption	(J·mol^{-1})
$\Delta_{R-S}\Delta H^{\ddagger\circ}$	differential enthalpy	(J·mol^{-1})
J_i	pervaporation flux	(mol·m^{-2}·s^{-1})
k_B	Bolzmann constant	(J·K^{-1})
$k_{cat,a}$	maximum specific conversion rate	(mol·g^{-1}·s^{-1})
$k^0_{cat,a}$	$k_{cat,a}$ at infinite temperature	(mol·L^{-1}·s^{-1})
$K_{i,i}$, $K_{j,i}$	inhibition constant	(mol·L^{-1})
$K_{eq,}$ K_j	equilibrium constant	(-)
k_h	lumped heat transfer coefficient $= \left(\frac{1}{\alpha_{wl}} + \frac{\delta_w}{\lambda_w} + \frac{1}{\alpha_{wc}} \right)^{-1}$	(W·m^{-2}·K^{-1})
k_l	mass transfer coefficient	(m·s^{-1})
$K_{m,j}$	Michaelis Menten constant	(mol·L^{-1})
k_S	modified first order rate constant	(L·g^{-1}·s^{-1})
$k°_S$	k_s at infinite temperature	(L·g^{-1}·s^{-1})
l	membrane thickness of separating layer	(m)
m	molecularity (1 for uni-, 2 for bimolecular reaction)	(-)
m_E	enzyme concentration	(g·L^{-1})
$m_{E,imm}$	immobilized enzyme concentration	(g·L^{-1})
MW_E	molecular weight of the enzyme	(g·mol^{-1})
p	pressure	(Pa)
$P_{0,i}$	permeability constant	(mol·m^{-1}·s^{-1}·Pa^{-1})
$P'_{0,i}$	lumped permeance constant	(mol·m^{-2}·s^{-1}·Pa^{-1})
$P''_{0,i}$	pure component permeance constant	(mol·m^{-2}·s^{-1}·Pa^{-1})
$P_{crit,i}$	critical pressure	(Pa)
Pe_{ax}	axial Peclet number	(-)
Pe_{mr}	mass radial Peclet number	(-)
Pe_{hr}	heat radial Peclet number	(-)
$p_{f,i}$	partial pressure in the liquid feed	(Pa)
P_i	permeability coefficient	(mol·m^{-1}·s^{-1}·Pa^{-1})
p_{perm}	downstream pressure in the permeate	(Pa)

$p_{perm,i}$	partial pressure in the vapor permeate	(Pa)
$p^s_{f,i}$	saturated partial pressure in the feed	(Pa)
R	universal gas constant	($J \cdot mol^{-1} \cdot K^{-1}$)
Re_p	particle Reynolds $= \frac{\overline{u_0} R_p \rho_l}{2 \cdot \eta_l}$	(-)
r_p	distance from particle center	(m)
R_p	particle radius	(m)
r_{pore}	radius of particle pores	(m)
r_r	distance from reactor center	(m)
R_r	inner reactor radius	(m)
$r_{subs,i}$	substrate radius	(m)
$\Delta S^{\ddagger\circ}{}_j$	reaction entropy	($J \cdot mol^{-1} \cdot K^{-1}$)
$\Delta_{R-S} \Delta S^{\ddagger\circ}$	differential entropy	($J \cdot mol^{-1} \cdot K^{-1}$)
t	time	(s)
T	temperature	(K)
T_c	temperature of cooling medium	(K)
$T_{crit,i}$	critical temperature	(K)
T_l	temperature of liquid	(K)
T_{rac}	temperature, where no enantioselectivity is present	(K)
u_0	superficial velocity	($m \cdot s^{-1}$)
$\overline{u_{0,l}}$	average superficial velocity	($m \cdot s^{-1}$)
x	distance from reactor inlet	(m)
$x_{f,i}$	mole fraction in the feed	($mol \cdot mol^{-1}$)
x_E	enzyme loading	($g \cdot g^{-1}$)
x_i	mol fraction	(-)
$v_{app,i,0}$	initial apparent reaction velocity	($mol \cdot L^{-1} \cdot s^{-1}$)
V_c	volume of cooling jacket $= \pi X \left(R_t^{\,2} - R_r^{\,2} \right)$	(m^3)
v_i	volumetric reaction rate	($mol \cdot L^{-1} \cdot s^{-1}$)
$\hat{V}_j$	saturated liquid volume	($cm^3 \cdot mol^{-1}$)
$v_{eff,a}$	effective reaction rate	($mol \cdot L^{-1} \cdot s^{-1}$)
V_l	specific bulk volume $= V_p \cdot \frac{\varepsilon_l}{1 - \varepsilon_l}$	(L)
$v_{max,a}$	maximum conversion rate	($mol \cdot L^{-1} \cdot s^{-1}$)
$v^\circ_{max,a}$	maximum volumetric rate at T->∞	($mol \cdot L^{-1} \cdot s^{-1}$)

V_p	particle volume $= \frac{4}{3}\pi \cdot R_p^{\,3}$	(m^2)
$y_{perm,i}$	mole fraction in the permeate	($mol \cdot mol^{-1}$)
v_R, v_S	volumetric reaction rate of R or S-enantiospecific substrate	($mol \cdot L^{-1} \cdot s^{-1}$)
x	distance from reactor inlet	(m)
X	reactor height	(m)
z	distance of diffusion	(m)
$Z_{RA,i}$	Rackett parameter	(-)

Greek Letters

α_{lp}	particle-to-fluid heat transfer coefficient	($W \cdot m^{-2} \cdot K^{-1}$)
α_{wc}	heat transfer coefficient between wall and cooling medium	($W \cdot m^{-2} \cdot K^{-1}$)
α_{wl}	heat transfer coefficient between wall and liquid	($W \cdot m^{-2} \cdot K^{-1}$)
δ_c	cooling jacket width	(m)
δ_w	thickness of glass wall between cooling medium and mixture	(m)
ε_p	particle porosity	(-)
ε_l	reactor porosity $= \frac{V_l}{V_l + V_p}$	(-)
ϕ_i	general Thiele modulus	(-)
Φ_i	dimensionless observable modulus	(-)
$\phi_{v,i}$	permeant volume fraction in the membrane polymer	(m^3/m^3)
η_i	effectiveness factor	(-)
η_l	viscosity of liquid phase	(Pa·s)
λ	particle tortuosity	(-)
$\Lambda_{ax,l}$	effective axial heat conduction in liquid phase	($W \cdot m^{-1} \cdot K^{-1}$)
$\Lambda_{ep,l}$	effective heat conduction in particle	($W \cdot m^{-1} \cdot K^{-1}$)
$\Lambda_{er,l}$	effective radial heat conduction in liquid phase	($W \cdot m^{-1} \cdot K^{-1}$)
λ_w	thermal conductivity of the glass reactor wall	($W \cdot m^{-1} \cdot K^{-1}$)
μ_j	viscosity	(cP)
$\mu_{f,i}$	chemical potential	(-)

ρ_c	density of cooling medium	$(kg \cdot L^{-1})$
ρ_l	liquid density	$(kg \cdot L^{-1})$
ρ_p	particle density	$(g \cdot L^{-1})$
$\gamma_{f,i}$	activity coefficient in the feed	(-)
ξ_h	total enantiomer conversion	(-)

Subscripts

0	initial conditions
a	R, S
f	feed
fm	feed – membrane interface
i	compounds, i.e. R-MP, S-MP, EA, VA
inlet	reactor feed
h	MP, MPA
l	liquid phase
mp	membrane-permeate
perm	permeate
p, s	particle or solid phase

Superscripts

‘	dimensionless parameter
d	f, r
f, r	forward or reverse reaction
‡	transition state
°	standard state

Abbreviations

Ac	acetaldehyde
EA	ethyl acetate
EtOH	ethanol
H_2O	water
HAc	acetic acid
MP	1-methoxy-2-propanol
MPA	1-methoxy-2-propyl-acetate
R, S	R- or S-enantiomer
VA	vinyl acetate

Abstract

Chiral secondary alcohols are interesting building blocks for the production of active ingredients for the life-science-industry. A popular method for the synthesis of such chiral compounds is enzyme catalyzed kinetic resolution. While a vast majority of scientific publications deal with kinetic resolutions, actually only a few provide information in terms of reaction kinetics or focus on process engineering. In this thesis, the biocatalytic kinetic resolution of racemic glycol ethers is investigated from a process engineering point of view as a model system for the production of chiral secondary alcohols.

Detailed kinetic analyses are presented for three reaction alternatives catalyzed by immobilized *Candida antarctica* lipase B. The alternatives are: (A) the hydrolysis of (R/S)-1-methoxy-2-propylacetate, (B) the transesterification of (R/S)-1-methoxy-2-propanol with ethyl acetate, and (C) the transesterification of (R/S)-1-methoxy-2-propanol with vinyl acetate. Kinetic models are developed following model discrimination and parameter identification. They are applied in simulation studies to improve the understanding of the investigated reaction systems. The sustainability of the reaction alternatives is discussed briefly.

For reaction alternative (A), a mathematical model is proposed which takes into account competitive inhibition by both enantiomers and product inhibition by (R/S)-1-methoxy-2-propanol. This model is used for mechanistic interpretation from a biochemical point of view and compared to findings in the field of molecular modeling. Overall, this reaction is shown to be a very promising way to produce chiral glycol ethers due to its high enantiomeric ratio and good conversion rate.

In case of alternative (B), an extensive kinetic model is developed based on a reversible ping-pong bi-bi mechanism. Furthermore, the model allows for (1) full reversibility of the reaction, (2) alternative substrate inhibition by each enantiomer, and (3) substrate inhibition by an acyl donor and acceptor. The model is capable of predicting the rate of the bimolecular reaction of both enantiomers at various substrate and product concentrations. It is applied in simulations to study the behavior of the reaction kinetics in a fixed bed reactor. Validation of these simulations is achieved by comparing modeling and experimental results. The experimental results are obtained by performing trials in a fully automated, in-house designed and in-house constructed modular miniplant.

As a result of the reversible nature of reaction alternative (B) the position of the equilibrium influences not only the progress in conversion but also the enantioselectivity. Removal of the byproduct ethanol results in higher conversion and enantioselectivity of the glycol ether and glycol ether acetate. Therefore, pervaporative separation of ethanol

from the quaternary alcohol-ester mixture was studied using a commercial membrane. Pervaporation is found to be strongly impacted by interactions between the permeants and the membrane polymer. The pervaporation behavior is studied to improve understanding of the mass transport mechanism of such concentrated multicomponent mixtures in composite membranes.

The kinetic parameters of the mathematical model for alternative (C) are identified using a new method applicable to reactions with immobilized enzymes, influenced by internal diffusion limitation. This method overcomes conventional sequential procedures by simultaneously solving coupled equations describing intraparticle mass transport and reaction mechanism. Numerical methods are used in combination with direct estimation of parameters. The kinetic model has the ability to describe the enantioselective conversion over a wide range of substrate ratio's (5 - 95%) and temperatures (5 - 56°C). It is used to study the impact of diffusion limitation on kinetic resolution reactions catalyzed by immobilized enzymes.

A sophisticated model is developed for the exothermic transesterification of (R/S)-1-methoxy-2-propanol and vinyl acetate (C) in a fixed bed reactor. The non-isothermal two-dimensional heterogeneous model accounts for irreversible ping-pong bi-bi kinetics (*with alternative substrate inhibition by both enantiomers*) and non-even flow distribution. Model validation is performed by comparing modeling results with experimental investigations obtained in the miniplant reactor.

Altogether, the presented miniplant validated models will be useful to bioengineers with the intent to model biocatalytic processes with all its kinetic constants. The models described in this thesis could be utilized for sustainability studies as well as rational improvement of bioreaction kinetics and/or better control of bioprocesses.

Keywords

Modeling and simulation, ping-pong bi-bi mechanism, kinetics, enzyme catalysis, lipase, miniplant technology, multicomponent pervaporation, kinetic resolution, immobilized enzymes

Zusammenfassung

Chirale sekundäre Alkohole sind interessante Bausteine für die Herstellung von Wirkstoffen für die Life Science Industrie. Eine bekannte Methode für die Synthese solcher chirale Komponente ist die Enzymkatalysierte kinetische Resolution. Während eine große Anzahl wissenschaftlicher Publikationen kinetische Racematspaltungen behandeln, beschreiben nur wenige kinetische Informationen und fokussieren selten auf Verfahrensentwicklung. In diese Doktorarbeit wird die biokatalytische Racematspaltung razemischer Glykolether aus der Perspektive der Verfahrenstechnik betrachtet als Modellsystem für die Herstellung von sekundären Alkoholen.

Diese Doktorarbeit fand im Rahmen des Projektes „Nachhaltige Bioproduktion“ des Bundesministeriums für Bildung und Forschung (BMBF) statt und war Teil eines größeren Projektes, dessen Struktur hier unten erläutert wird:

- Der Industriepartner, The Dow Chemical Company, Midland, MI, U.S.A., war verantwortlich für die Vorarbeiten (Resnick, et al., 2003) und spielte eine entscheidende Rolle bei der Nachhaltigkeitsanalyse.

- Das Institut für Technische Biochemie der Universität Stuttgart war verantwortlich für die Biokatalysatoroptimierung, welches nachzulesen ist in der Doktorarbeit von Monika Rusnak (Rusnak, 2004).

- Das Institut für Bioverfahrenstechnik der Universität Stuttgart befasste sich mit der Prozessentwicklung, welches in dieser Arbeit beschrieben ist.

Das Gesamtziel dieses Projektes war die Verkürzung der Produkteinführungszeit biokatalytischer Prozesse durch „Simultaneous Engineering“. Das heißt, dass die drei Aspekte, die Biokatalysatoroptimierung, die Prozessentwicklung und die Nachhaltigkeits-Analyse gleichzeitig durchgeführt werden.

Die Zielsetzung dieser Doktorarbeit ist die Modellgetriebene Verfahrensentwicklung von drei biokatalytische Reaktionen katalysiert durch *Candida antarctica* Lipase B, die im Verlauf dieser Arbeit mit A, B und C gekennzeichnet werden:

A) Die Hydrolyse von (R/S)-1-Methoxy-2-Propyl-Acetat mit Wasser in (R/S)-1-Methoxy-2-Propanol und Acetat;
B) Die irreversible Transesterifikation von (R/S)-1-Methoxy-2-Propanol mit Ethylacetat in (R/S)-1-Methoxy-2-Propyl-Acetat und Ethanol;
C) Die reversibeler Transesterifikation von (R/S)-1-Methoxy-2-Propanol mit Vinylacetat in (R/S)-1-Methoxy-2-Propyl-Acetat und Acetaldehyd.

Die Themengebiete, womit sich die Arbeit befasst, sind:

- die Kinetik;
- die Pervaporation;
- die Reaktormodellierung und die Validierung im Miniplantmaßstab;
- und eine Nachhaltigkeitsbewertung der drei Reaktionsalternativen (A, B und C).

Die Art der untersuchten Reaktionen ist eine kinetische Resolution. Was ist genau eine kinetische Resolution? Sie ist eine Reaktion, wobei beide Enantiomerenformen des Substrates bei Reaktionsbeginn in gleicher Menge vorliegen und einer der beiden Enantiomere schneller umgesetzt wird als der Andere. Im Falle der hier untersuchten kinetischen Resolutionen ist das R-Enantiomer das Enantiomer, welches schneller umgesetzt wird. Dieses hat zur Folge, dass nach einer gewissen Reaktionszeit das Produkt des R-Enantiomers und das Substrat des S-Enantiomers in höherer Konzentration vorliegen. Da die Stoffeigenschaften dieser Verbindungen unterschiedlich sind, können sie mittels klassischen Trennverfahren geschieden werden.

Die Gliederung der Doktorarbeit orientiert sich an den von uns publizierten Artikeln. Die Einführung in Kapitel 1 beschreibt das Anwendungsgebiet von Reaktionen und deren Produkten. Auch gibt es eine Übersicht der Qualitäten des Enzyms, *Candida antarctica* Lipase B, welches besonders für kinetische Resolutionen ein sehr geeigneter Biokatalysator ist.

Kapitel 2. befasst sich mit der kinetische Modellierung und Simulation einer Lipase-katalysierte Hydrolyse (Reaktion A). Es betrifft die von *Candida antarctica* Lipase B katalysierte Reaktion von (R/S)-1-Methoxy-2-Propyl-Acetat (R/S-MPA) mit Wasser in (R/S)-1-Methoxy-2-Propanol (R/S-MP) und das Nebenprodukt Acetat. Neben die Reaktion des R-Enantiomers findet auch die Reaktion des S-Enantiomers statt, nur wesentlich langsamer.

Für die Erstellung eines kinetischen Modells sind Modellvereinfachung und Parameteridentifikation von wesentlicher Bedeutung. Ausgehende von einem ausführlichen Modell konnte mittels diese Technologien ein kinetisches Modell für Reaktion A hergeleitet werden, welches aus ein Michaelis Menten Mechanismus besteht und sowohl die alternative Inhibierung beider Enantiomere als auch die Produktinhibierung von (R/S)-1-Methoxy-2-Propanol (R/S-MP) berücksichtigt.

Für die kinetische Studien wurden Zeitverlaufsmessungen zu unterschiedliche Anfangssubstratkonzentrationen von R/S-MPA durchgeführt. Zur genaueren Bestimmung des Effektes der Produktinhibierung von (R/S)-MP wurden zusätzlich Zeitverlaufsmessungen zu unterschiedliche Anfangsproduktkonzentrationen und gleiche Anfangssubstrat-Konzentration durchgeführt.

Neben die Konzentrationsabhängigkeit der Kinetik, wurde auch die Temperaturabhängigkeit bestudiert. Die Änderung der Produktkonzentration des R-Enantiomers und die der Substratkonzentration des S-Enantiomers wurden bei unterschiedliche Temperaturen und gleicher Anfangssubstratkonzentration aufgezeichnet.

Da das mathematische Modell nicht nur in der Lage ist, die experimentelle Daten gut zu beschreiben, sondern auch die bestimmte kinetischen Parameter sensitiv sind, wird das Modell eingesetzt für Simulationen und ihre Parameter interpretiert aus einem biochemischen Gesichtspunkt. Die gewonnenen Erkenntnisse werden verglichen mit denen aus dem Gebiet der molekularen Modellierung. Wegen des vorteilhaften Enantiomeren-Verhältnisses und des guten Umsatzes sieht diese Reaktion insgesamt für die Herstellung chiraler Glykolether viel versprechend aus.

Das 3. Kapitel beschreibt die kinetische Studie einer reversiblen kinetischen Resolution mit Validierung im Miniplantmaßstab. Die betrachtete Reaktion ist die von *Candida antarctica* Lipase B katalysierte reversibeler Transesterifikation von (R/S)-1-Methoxy-2-Propanol (R/S-MP) mit Ethylacetat (EA) in (R/S)-1-Methoxy-2-Propyl-Acetat (R/S-MPA) und Ethanol (EtOH) (Reaktion B).

Ein ausführliches kinetisches Modell ist entwickelt worden, dass auf ein Ping-Pong Bi-Bi Mechanismus basiert ist. Außerdem berücksichtigt das Modell

1) die vollständige Reversibilität der Reaktion;
2) die alternative Substratinhibierung jedes Enantiomers als auch
3) die Substratinhibierung von einem Acylspender und -Akzeptor

Da für dieses Modell insgesamt elf kinetische Parameter zu bestimmen sind, ist ein gleichzeitige Anpassung nicht möglich und wurden aus diesem Grund Parameterbestimmungen bei ausgewählten Bedingungen durchgeführt. Wie zum Beispiel für Reaktionszeiten nahe Null, wo die Produktinhibierung als auch die Reversibilität der Reaktion zu vernachlässigen ist. Auf diese Art wurden alle Parameter sensitiv bestimmt.

Die Verifizierung des kompletten kinetischen Modells erfolgt im Miniplantmaßstab in einem Festbettreaktor. Hierfür wurde der enantiomerische Überschuss ($e.e._i$), der Unterschied der Enantiomere geteilt durch ihre Summe, berechnet und aufgetragen gegen den Umsatz. Da das Substrat am Reaktionsanfang razemisch ist, fängt die Kurve vom $e.e._{MP}$ bei Null an. Da das R-Enantiomer von MP schneller umgesetzt wird, steigt der $e.e._{MP}$. Wenn das R-Enantiomer sich im Gleichgewicht befindet, erreicht der $e.e._{MP}$ ein Maximum, da ab diesem Punkt nur noch das S-Enantiomer reagieren kann. Der Verlauf des $e.e._{MPA}$'s fängt bei eins an, da ja das erste Produkt, welches entsteht, sehr enantioselektiv ist. Der $e.e._{MP}$ nimmt dann mit steigender Umsetzung immer weiter ab.

Das hergeleitete kinetische Modell mit elf Parametern ist imstande ohne zusätzliche Parameteranpassung die reversibeler kinetische Resolution der bimolekulare Reaktion der beiden Enantiomere bei unterschiedliche Anfangssubstratkonzentrationen im Festbettreaktor vorherzusagen. Es konnte gezeigt werden, dass das Reaktionsgleichgewicht einen großen Einfluss auf die Enantioselektivität kinetischer Reaktionen hat. Es ist somit ein wichtiger Parameter beim Screening von potentiellen Substraten für industrielle biokatalytische Verfahren.

Im 4. Kapitel wird die pervaporative Trennung eines Alkohol-Ester-Vierstoffgemisches diskutiert. Dank der Umkehrbarkeit der Reaktionsalternative (B), beeinflusst die Lage des Gleichgewichtes nicht nur den Umfang der Umsetzung, sondern auch die Enantioselektivität. Die Abtrennung des Nebenproduktes Ethanol von dem Reaktionsgemisch würde in eine höhere Umsatz und höhere Enantioselektivität des Glykolethers und Glykoletheracetats resultieren. Hierfür wurde eine kommerzielle Pervaporationsmembran eingesetzt.

Bevor die kombinierte Pervaporation und Reaktion bestudiert werden kann, muss die Pervaporation getrennt charakterisiert werden. Dafür ist die Pervaporation bei unterschiedliche Feedmischungen aus EtOH, EA, MP und MPA in einem gerührtem Membranreaktor untersucht worden. Konstante Bedingungen für die Pervaporationsmembran sind durch die Einstellung eines Quasi-Steady-States im Feed gewährleistet.

Wird der Molenanteil des Permeats zu dem Molenanteil des Feeds aufgetragen, wird deutlich, dass das Ethanol am Meisten permeiert, jedoch gleich gefolgt wird durch Ethylacetat und 1-Methoxy-2-Propanol. Die Pervaporation von Ethanol ist somit wie gewünscht am Größten, den Unterschied zu Ethylacetat und 1-Methoxy-2-Propanol jedoch zu gering für einen industriellen Einsatz der Membran.

Bei Pervaporation von Mischungen aus mehreren Komponenten treten oft Interaktionen zwischen den Komponenten (Flusskopplung) und zwischen den Komponenten und der Membran (Plastifizierung) auf. Um die Anwesendheit solcher Interaktionen zu prüfen wurde ein mathematisches Modell für den Molarfluss einer Komponente i aufgestellt, dass:

- diese Interaktionen;
- den Einfluss der Temperatur
- der partielle Druck im Feed
- der partielle Druck im Permeat

beschreiben. Mit Hilfe dieses Modells konnte gezeigt werden, dass die Interaktionen zwischen den Komponenten und/oder zwischen den Komponenten und der Membran eine erhebliche Rolle spielen bei der Pervaporation.

Das 5. Kapitel behandelt die Identifikation kinetischer Parameter von Reaktionen mit immobilisierten Enzymen bei Diffusionslimitierung. Die konventionelle Prozedur der Parameteridentifikation immobilisierter Enzyme besteht aus zwei Schritten:

1) Die Hydrolyse von (R/S)-1-Methoxy-2-Propyl-Acetat mit Wasser in (R/S)-1-Methoxy-2-Propanol und Acetat;
2) Die Bestimmung des immobilisierten Enzyms und die Anpassung der maximale volumetrische Reaktionsrate, $V_{max,i}$.

Hierbei wird automatisch angenommen, dass die Immobilisierung keinen Einfluss auf die Bindungsaffinität ($K_{m,i}$; $K_{i,i}$) hat. Da dieser Effekt durchaus eine Rolle spielen kann, wird in dieses Kapitel eine neue Prozedur vorgestellt. Zusätzlicher Vorteil ist die Reduzierung der notwendigen experimentellen Versuchen und der daraus resultierenden Zeitgewinn für die Prozessentwicklung.

Die neue Prozedur besteht aus die gleichzeitige:

- numerische Lösung von partiellen gekoppelten Differentialgleichungen, die den Massentransport und das Reaktionsmechanismus im Enzympartikel beschreiben;
- und die direkte Anpassung der kinetischen Parameter an den experimentellen Daten.

Für diese neue Prozedur wurde die irreversible Transesterifikation von (R/S)-1-Methoxy-2-Propanol (R/S-MP) mit Vinylacetat (VA) zu (R/S)-1-Methoxy-2-Propyl-Acetat (R/S-MPA) und das Nebenprodukt Acetaldehyd (Ac) katalysiert durch *Candida antarctica* Lipase B untersucht (Reaktion C).

Das hergeleitete kinetische Modell für diese Umsetzung ist ein irreversibler Ping-Pong Bi-Bi Mechanismus unter Berücksichtigung der Substratinhibierung der Enantiomere. Das heißt, das Vinylacetat zuerst am Enzymkomplex bindet, reagiert zu Acetaldehyd, wonach R-MP oder S-MP am modifizierten Enzymkomplex bindet und umgewandelt wird zu R-MPA bzw. S-MPA.

Für die kinetische Studie wurden Zeitverlaufsmessungen bei unterschiedlichen Anfangssubstratkonzentrationen durchgeführt, m.a.w. die Produktkonzentrationen von R-MPA und S-MPA wurden zu unterschiedliche Zeiten gemessen.

Das vorgestellte kinetische Modell besitzt die Fähigkeit die enantioselektive Reaktion C über einem breiten Bereich von Substratverhältnissen (5 - 95% v/v) und Temperaturen (5 - 56°C) zu beschreiben. Die Aussagekraft dieses Modells ist somit geeignet für Prozessentwicklungsstudien und Simulationen.

Mathematische Simulationen können eingesetzt werden um das Verständnis des Systems zu vergrößern, wie zum Beispiel zur Untersuchung des Einflusses der Diffusionslimitierung auf die Kinetik. Hierfür wurden dynamische Profile des Effektivitätsfaktors bestudiert, der sich aus der Division der Reaktionsrate unter diffusionslimitierenden Bedingungen und der Reaktionsrate unter diffusionsfreien Bedingungen berechnen lässt. Wird der Effektivitätsfaktor für das R-Enantiomer gegen die Zeit aufgetragen, ist ersichtlich, dass die Reaktionsrate des R-Enantiomers deutlich durch den Einfluss der Diffusionslimitierung beeinflusst wird für niedrige MP zu VA Anfangsubstratkonzentrationen (MP_0/VA_0 = 5%). Steigt das MP_0/VA_0-Verhältnis, wird dieser Einfluss weniger. Für MP_0/VA_0 > 60% ist erneut ein Effekt zu beobachten. Dieser Effekt wird jedoch nicht durch Diffusionslimitation des R-MP verursacht, sondern durch das VA, da dieser Effekt in gleicher Maße auch beim Effektivitätsfaktor des S-Enantiomers auftritt. Außerdem ist ein Effektivitätsfaktor des S-Enantiomers größer als eins zu beobachten für 5% > MP_0/VA_0 > 60%. Dieses resultiert aus der kompetitiven Hemmung der Enantiomere. Das heißt, dass wenn das R-Enantiomer-Substrat verlangsamt wird durch Diffusionslimitierung, das S-Enantiomer-Substrat einen geringen Geschwindigkeitsschub bekommt.

Die neue Methode zur Bestimmung kinetischer Parameter von Reaktionen mit immobilisierten Enzymen konnte somit nicht nur erfolgreich angewandt werden, sondern die bestimmte Kinetik war auch Basis für Prozesssimulationen und Identifizierung prozessrelevanter Optimierungspotentiale der Enzymeigenschaften, welches die gezielte Lenkung der Enzymoptimierung ermöglicht.

Kapitel 6 befasst sich mit dem Einsatz der Modellierung, Simulation und Miniplant-Technik für die Biokatalyse am Beispiel einer kinetischen Resolution. Die Kombination aus Modellierung, Simulation und Miniplant-Technik wird oft als integrierte Miniplant-Technologie bezeichnet.

Es ist ein ausführliches mathematisches Modell für die exotherme Transesterifizierung von (R/S)-1-Methoxy-2-propanol mit Vinylacetat (Reaktion C) in einem Festbettreaktor entwickelt worden. Dieses nichtisotherme zweidimensionale heterogene Modell besteht aus:

- Stofftransport in der Flüssigphase, welche die axiale und radiale Dispersion, die axiale Konvektion und die Massentransport zwischen Flüssigphase und Partikel berücksichtigt;
- Energietransport in der Flüssigphase, welche aus der radiale effektive Wärmeleitung, der Konvektion und Energietransport zwischen Flüssigphase und Partikel zusammengesetzt ist;
- Stofftransport im Partikel;
- Energietransport im Partikel;
- Randbedingungen am Anfang, am Ende, in der Mitte und an der Wand des Reaktors, sowie im Kern und am Rand des Partikels;
- Anfangsbedingungen;
- Ungleichmäßige Strömungsverteilung, welches gerade bei schmale Festbettreaktoren nicht zu vernachlässigen ist, da die Porosität der Partikel nahe der Reaktorwand niedriger ist, wodurch die Lehrrohrgeschwindigkeit in diesem Bereich wesentlich höher liegt;
- Die in Kapitel 5. bestimmte irreversible Ping-Pong Bi-Bi Kinetik inklusiv alternative Eduktinhibierung beider Enantiomere.

Die Modellvalidierung wurde durchgeführt durch die Modell- und die im Miniplantmaßstab erhaltenen experimentellen Resultate miteinander zu vergleichen. Zum Beispiel wurde der Verlauf der dimensionslose R-MPA und S-MPA Produktkonzentrationen über die dimensionslose Reaktorhöhe für unterschiedliche Lehrrohrgeschwindigkeiten erstellt. Da die Reaktion exotherm ist, wurde der Energietransport mitberücksichtigt und den Verlauf der Temperatur über der dimensionslose Reaktorhöhe für unterschiedliche Lehrrohrgeschwindigkeiten betrachtet. Werden die experimentellen in der Miniplant gewonnen Ergebnisse in der gleichen Darstellung aufgetragen, ist ersichtlich, dass das Modell die Messergebnisse ohne zusätzliche Parameteranpassung gut beschreibt.

Im Kapitel 7 wird eine Übersicht über die Potenziale der integrierten Miniplant-Technologie für die Biokatalyse gegeben. Der Bedeutendste ist die erfolgreiche Realisierung des technischen Betriebs im kleinstmöglichen Maßstab. Dieses ermöglicht:

- die Hochrechnung der Ergebnisse in den Produktionsmaßstab
- die frühzeitige Bestimmung der technische und wissenschaftliche Machbarkeit (oder auch das „*Proof of Concept*“ genannt);
- die langzeitige Beobachtung des Prozesses unter prozessnahe Bedingungen und
- die Produktion van Mustermengen.

Außerdem wird in dieses Kapitel die für die experimentelle Validierungsversuche eingesetzte Miniplant beschrieben, die am Institut für Bioverfahrenstechnik geplant, gebaut und in Betrieb genommen wurde. Sie besteht aus zwei Teile, ein Reaktionsteil mit Substratgefäßen, Pumpen und Festbettreaktor, und ein Trennungsteil mit einer Destillationskolonne mit dreißig theoretischen Trennböden.

Hervorzuheben ist, dass es sich um eine vollautomatisierte Miniplant-Anlage handelt, welches eine stetige Prozessüberwachung, -Steuerung als auch Datenerfassung ermöglicht. Zu dem zeichnet sie sich durch ihre Modularität und Flexibilität aus, die durch die Verwendung schnell verfügbarer Normbauelementen und die Standardisierung der Anschlüsse gewährleistet wurde. Dieses Vorgehen ermöglicht eine systematische Evaluierung verschiedener Verfahrensalternativen, Substrate und Biokatalysatoren unter industrienahen Bedingungen.

Kapitel 8 rundet die Ergebnisse der Arbeit ab, indem es eine Zusammenfassung der wichtigsten Ergebnisse der Doktorarbeit und eine Nachhaltigkeitsbewertung der drei Reaktionsalternativen (A-C) enthält. Diese Nachhaltigkeitsabschätzung berücksichtigt die ökonomischen und ökologischen Aspekte, und basiert auf den im Miniplantmaßstab validierten mathematischen Modellen und die Lebenszyclusanalysemethode EPS 2000.

Die Nachhaltigkeitsstudie ergibt ein interessantes Ergebnis: Entgegen der möglicherweise intuitiv vermuteten Einschätzung ist die irreversible Transesterifizierungsreaktion von (R/S)-MP mit EA (Reaktion C) deutlich weniger nachhaltig (z.B. in den Kategorien Umweltbelastung, Energieverbrauch, Dampf und Kühlwasser) als die reversibeler Transesterifizierungsreaktion von (R/S)-MP mit VA (Reaktion B), in der die toxischeren Verbindungen Vinylacetat und Acetaldehyd eingesetzt werden. Die Ursache hierfür ist die aus der integrierten Miniplant-Technologie erhaltenen Erkenntnis, dass die Enantioselektivität der Reaktion größer für eine im Ethylacetatüberschuss betriebene Reaktion ist und die daraus folgende Notwendigkeit, diesen Überschuss an Ethylacetat zurück zu gewinnen. Dieses zeigt erneut die Relevanz des Reaktionsgleichgewichts für kinetische Resolutionen.

Die irreversible Hydrolysereaktion von MPA (Reaktion A) ist die im Vergleich zu den Transesterifizierungsreaktionen die am wenigsten nachhaltige Prozessvariante, was am Einsatz eines Extraktionslösungsmittels zur Produktaufbereitung liegt.

Zusammenfassend ist somit die Transesterifizierungsreaktion mit Vinylacetat (Reaktion C) die nachhaltigste Alternative.

Schlüsselwörter

Modellierung und Simulation, Ping-Pong Bi-Bi Mechanismus, Kinetik, Enzymkatalyse, Lipase, Miniplant-Technologie, Pervaporation von Multikomponenten, kinetische Racematspaltung, immobilisierte Enzyme

Samenvatting

Chirale secundaire alcoholen zijn interessante bouwstenen voor de productie van actieve ingrediënten voor de Life Science industrie. Een bekende methode voor de synthese van zulke chirale componenten is de enzym gekatalyseerde kinetische resolutie. Terwijl een groot aantal wetenschappelijke publicaties kinetische racemaatsplitsingen behandelen, geven slechts weinige kinetische details. Ook focusseren ze betrekkelijk weinig op procesontwikkeling. In dit proefschrift wordt de biokatalytische racemaatsplitsing van racemische glycol ethers onderzocht vanuit het oogpunt van procestechnologie als model systeem voor de productie van secundaire alcoholen.

Gedetailleerde kinetische analysen worden gepresenteerd voor drie reactie alternatieven, die gekatalyseerd worden door middel van geïmmobiliseerd *Candida antarctica* lipase B. De alternatieven zijn: (A) de hydrolyse van (R/S)-1-methoxy-2-propylacetaat, (B) de transesterificatie van (R/S)-1-methoxy-2-propanol met ethyl acetaat, en (C) de transesterificatie van (R/S)-1-methoxy-2-propanol met vinyl acetaat. Kinetische modellen zijn ontwikkeld met behulp van model-discriminatie en parameter-identificatie. De duurzaamheid van de reacties komt kort aan bod.

Voor reactie alternatief (A) wordt een mathematisch model voorgesteld, dat rekening houdt met onderlinge remming van beide enantiomeren en product inhibitie van (R/S)-1-methoxy-2-propanol. Het model wordt toegepast en geïnterpreteerd vanuit een biochemisch mechanisme en vergeleken met bevindingen uit het gebied van de moleculaire modellering. Het blijkt, dat de deze reactie veelbelovend is vanwege de gunstige enantiomeer verhouding en goede omzettingsgraad.

In het geval van alternatief (B) is een uitgebreid kinetisch model ontwikkeld op basis van een omkeerbaar ping-pong bi-bi mechanisme, dat (1) de volledige omkeerbaarheid van de reactie, (2) de alternatieve substraat inhibitie van elk enantiomeer, alsook (3) de substraat remming van een acyl donor en acceptor bewerkstelligt. Het model is in staat de snelheid van de bimoleculaire reactie van beide enantiomeren bij verschillende substraat- en productconcentraties te voorspellen. Het wordt toegepast in simulaties om het gedrag van de reactiekinetiek in een gepakt bed reactor te bestuderen. Het valideren van deze simulaties is bereikt door model- met experimentele resultaten te vergelijken. De experimentele resultaten zijn verkregen uit proeven met een volledig geautomatiseerde, zelf ontworpen en zelf gebouwde modulaire miniplant.

Dankzij de omkeerbare aard van reactie alternatief (B), beïnvloedt de ligging van het evenwicht niet alleen de mate van omzetting, maar ook de enantioselectiviteit. Scheiden

van het nevenproduct ethanol van het reactiemengsel, resulteert in een hogere omzetting en een hogere enantioselectiviteit van de glycolether en het glycolether acetaat. Hierdoor is het scheiden van ethanol door middel van pervaporatie uit het quaternaire alcohol-ester mengsel onderzocht, waarbij gebruik is gemaakt van een commercieel membraan. Het pervaporative gedrag is bestudeerd om het mechanisme van massatransport van zulke geconcentreerde multicomponenten mengsels in composiet membranen te verbeteren.

De kinetische parameters van het mathematische model voor alternatief (C) zijn geïdentificeerd door gebruik te maken van een nieuwe moduleermethode voor reacties met geïmmobiliseerde enzymen die beïnvloedt worden door interne diffusie begrenzing. Deze methode overtreft conventionele sequentiële methoden, door gelijktijdig gekoppelde vergelijkingen met behulp van numerieke methoden op te lossen in combinatie met het schatten van parameters. De gekoppelde vergelijkingen beschrijven het massatransport en het reactiemechanisme in de drager, waar het enzym aan vastzit. Het kinetische model heeft het vermogen de enantioselectieve omzetting over een breed bereik van substraatverhoudingen (5 - 95% v/v) en temperaturen (5 - 56°C) te beschrijven. Het model wordt gebruikt om de invloed van diffusielimitatie op de door geïmmobiliseerde enzymen gekatalyseerde racemaatsplitsing te bestuderen.

Een uitgebreid model is ontwikkeld voor de exotherme transesterificatie van (R/S)-1-methoxy-2-propanol en vinyl acetaat (C) in een gepakt bed reactor. Het niet-isotherme tweedimensionale heterogene model houdt rekening met irreversibele ping-pong bi-bi kinetiek *(met alternatieve substraat inhibitie van beide enantiomeren)* en ongelijkmatige stromingsverdeling. Model verificatie is uitgevoerd met experimentele resultaten, die verkregen zijn met de miniplant reactor.

Samenvattend kan worden gesteld, dat de hier gepresenteerde miniplant gevalideerde modellen gebruikt kunnen worden door bioprocestechnologen, die biokatalytische processen willen modelleren en kinetische parameters willen bepalen. De in dit proefschrift beschreven modellen kunnen ook van dienst zijn voor duurzaamheidstudies, alsook voor het rationeel verbeteren van bio-reactiekinetiek en/of het gecontroleerder aansturen van bioprocessen.

Sleutelwoorden

Modellering en simulatie, ping-pong bi-bi mechanisme, kinetiek, enzymkatalyse, lipase, miniplant technologie, pervaporation van multicomponenten, kinetische resolutie, geïmmobiliseerde enzymen

1

Introduction and Outline

1.1 Introduction

The chirality or handedness of a molecule is well accepted as an important property of new pharmaceutical active ingredients. Just like the left hand is a mirror of the right hand, the same concept applies to chiral molecules. Although achiral drugs have identical chemical formulas, they may cause different biological reactions in a human body. Mostly, only one of the forms is responsible for the pharmacological desired effect, while the other(s) may cause severe adverse reactions. One of the most infamous examples is the drug Contergan of drug maker Chemie Grünenthal marketed in 1957, which is based on the active ingredient Thalidomide (Figure 1.1). While the S-enantiomer of Thalidomide is a sedative, the R-enantiomer causes severe abnormalities of the spinal column and missing organs in embryos when ingested during pregnancy. It is a very sad demonstration of the importance of chirality.

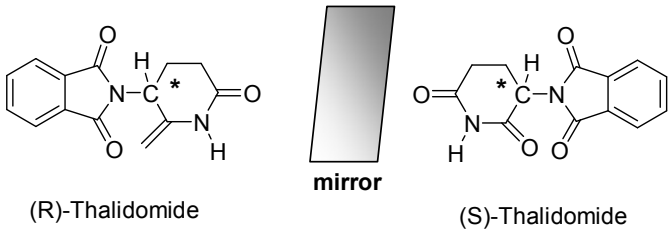

Figure 1.1 Chirality of the infamous drug Thalidomide (* chiral center)

Nowadays, the European Committee for Proprietary Medicinal Products (CPMP) and the Food and Drug Administration (FDA) in the U.S.A. require that the pharmacological effects of each enantiomeric form of a drug are tested separately. Annual sales in chiral drugs is rapidly growing, topping 100 billion dollar in 2000, which represents close to one-third of all drug sales worldwide (Stinson, 2000).

It is for this reason that much research has been directed towards the development of chiral intermediates from which chiral drugs may be synthesized. Other potential applications for chiral intermediates are building blocks for agrochemical and fine chemical ingredients.

Biocatalysis has emerged as a powerful and diverse tool for the synthesis of such chiral intermediates. In particular, reactions catalyzed by lipases (E. C. 3.1.1.3) have been extensively studied for this purpose from a biochemical point of view (Bornscheuer and Kazlauskas, 1999; Rubin and Dennis, 1997a; Rubin and Dennis, 1997b; Drauz and

Waldmann, 1995). Methods for lipase catalyzed enantioselective transformations include (1) asymmetric catalysis starting with a prochiral or meso-compound and (2) resolution of a racemic mixture.

"Racemates [racemic mixtures] are usually easy to access and cheap to produce, so the most economic method can be to make both isomers and then separate them." says Ray McCague, global director for science and technology at Chirotech, a subsidiary of The Dow Chemical Company, Cambridge, UK (Houlton, 2002).

Several methods are available for separation of the enantiomers of such a racemic mixture. One possibility is the attachment of a chiral auxiliary to the enantiomers and separation of the formed diasteriomers by chromatography, recrystilization or distillation. Kinetic resolution, the achievement of enantiomerically enriched compounds resulting from unequal rates of reaction of both enantiomers, is another method (Figure 1.2, Equation 1). In this respect, lipase catalyzed kinetic resolution is an especially promising field. For a recent review the reader is referred to Ghanem and Aboul-Enein (2004a).

One disadvantage of kinetic resolutions is the fact, that theoretically maximum 50% of the starting material can be converted into the desired enantiopure end-product. Hence, methods to recycle the unwanted enantiomer have to be considered. One possibility is the use of a special case of kinetic resolution, i.e. the dynamic kinetic resolution, in which both enantiomers of the starting material are rapidly equilibrated by an additional catalyst (Figure 1.2, Equation 2). Opportunities in this field have been recently summarized by Schnell, et al. (2003), Pamies and Bäckvall (2004) and Turner (2004), who show the employment of racemases and transition metal catalysts for this purpose.

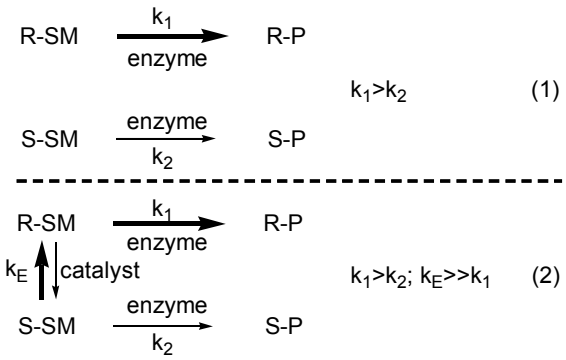

Figure 1.2 Biocatalytic kinetic resolution (1) and dynamic kinetic resolution (2) of a racemic starting material (SM).

Another possibility is to reuse the unwanted enantiomer in an application, where chirality is not needed. The racemic glycol ethers employed in this study are an example for this, as they are presently sold worldwide in multi-tons-scale by global chemical companies, such as Dow Chemical, Midland, MI, U.S.A., BASF, Ludwigshafen, Germany and Shell Chemicals, London, U.K. They are applied in cleaning agents, coatings and electronic applications. Anyhow, the model driven development presented in this thesis can be applied for dynamic kinetic resolutions also, if the additional racemization step is characterized similarly.

An especially suited biocatalyst for kinetic resolutions is lipase B from *Candida antarctica* (CAL-B), which is known to exhibit a wide substrate specificity. It has been employed in an uncountable number of scientific publications. For instance, it has been applied for enantioselective synthesis of full-fledged anti-inflammatory drugs, such as ibuprofen (Henke, et al., 2000), flurbiprofen, (Zhang et al., 2005), ketoprofen (Arroyo and Sinisterra, 1995) and naproxen (Arroyo and Sinisterra, 1994). The enzyme has been extensively investigated for kinetic resolution of secondary alcohols following a hydrolysis, esterification or transesterification mode (e.g. Heinsman, et al., 2001, Rotticci, et al., 2001b). CAL-B can accept highly versatile types of acyl donors, such as esters (Fischman, et al., 2001), acids (Romero, et al., 2005), thioesters (Orrenius, et al., 1998) and carbonates (Al-Azemi and Bisht, 2002).

Next to the broad substrate specificity, the enzyme shows significant activity in apolar and polar organic solvents (Secundo, et al., 2001), in solid/gas systems (Bousquet-Dubouch, et al., 2001) and in ionic liquids (Sheldon, et al., 2002; Noel, et al., 2004). It is active at nearly anhydrous conditions (Lozano, et al., 2003a) and exhibits good long-term stability at ambient temperatures (Orsat et al., 1999). In addition, it was found to maintain stability over a prolonged period of time at temperatures as high as 100-160°C (Overmeyer, et al., 1999; Turner and Vulfson, 2000; Lozano et al., 2003b).

On top of this, CAL-B displays high enantioselectivity towards many secondary alcohols, which is strongly dependent on the type of acyl donor and acceptor. Because of these favorable properties and the fact, that a crystallographic structure is available (Uppenberg, et al., 1994), CAL-B is often selected for molecular modeling studies. These studies aim to predict the enantiopreference of the enzyme, i.e. to determine which enantiomer of a racemic substrate is preferred by the catalyst (Ottosson, 2002; Raza, et al., 2001; Orrenius et al., 1998; Bocola, 2002). Or they focus on rational design of the enzyme's properties through the combination of molecular dynamics simulations and site-directed mutagenesis (Ottosson, et al., 2001; Rotticci, et al., 2001a; Magnusson et al., 2005).

Yet, in spite of widespread research efforts, the number of applications in industrial enantioselective processes with lipases remains rather modest. A successful example is the resolution of 2-halopropionic acids by porcine pancreatic lipase (Kirchner, et al., 1985), which was commercialized by Chemie Linz Co. Austria (now DSM Actis, Austria) as starting material for the synthesis of herbicides. Another example is the commercial application of lipase catalyzed synthesis of (2R, 3S)-3-4-(methoxyphenyl) methyl glycidate (Shibatani et al., 1990), a key intermediate in the manufacture of the optically pure cardiovascular drug Diltiazem, by Sepracor Inc., Marlborough, MA, USA.

Further realization of industrial applications in the field of enantioselective biocatalysis will benefit from process and biochemical engineering. In particular, the combination of modeling, simulation and experimental investigations should help to shorten time-to-market of enzyme catalyzed chiral intermediates.

For this purpose, the kinetic resolution of racemic glycol ethers by CAL-B was selected as a model system and systematically investigated as part of the BMBF funding initiative "sustainable bioproduction" (Figure 1.3). The Institute of Biochemistry (University of Stuttgart, Germany) focused on biocatalyst improvement (Rusnak, 2004), the Dow Chemical Company (Stade, Germany) was responsible for sustainability analysis and the Institute of Biochemical Engineering (University of Stuttgart, Germany) dealt with reaction and process engineering.

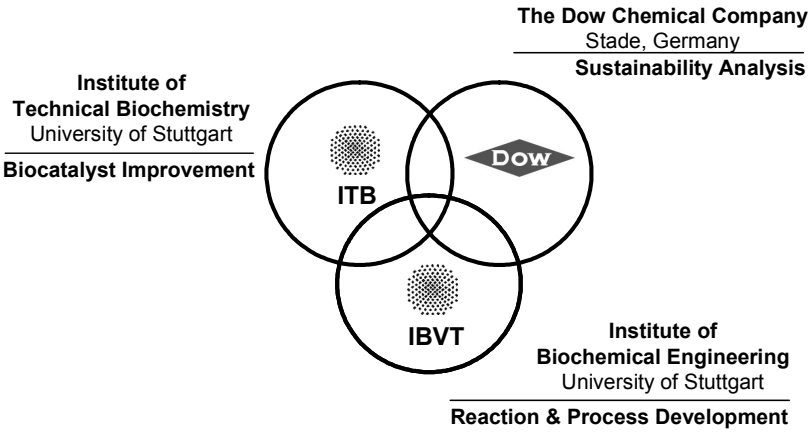

Figure 1.3 Project network and integration

In this thesis, the work performed at the Institute of Biochemical Engineering (IBVT) is reported. Kinetic studies of three reaction alternatives involving model discrimination, parameter determination and experimental validation are described (Scheme 1.1a-c). The impact of the choice of reaction alternative on industrial feasibility is discussed. For example, reaction alternative 1.1c) is shown to be more efficient than alternative 1.1b). Hence, one can argue, the former results in a higher sustainable process even though its acyl donors and acceptors are more toxic versus the latter. As substantial contribution to fast and efficient development of biocatalytic processes, a combination of modeling, simulation and miniplant technology is applied. The modular concept of this in-house planned, constructed and operated state-of-the-art miniplant gives the opportunity to systematically evaluate different process alternatives, process conditions and reaction substrates.

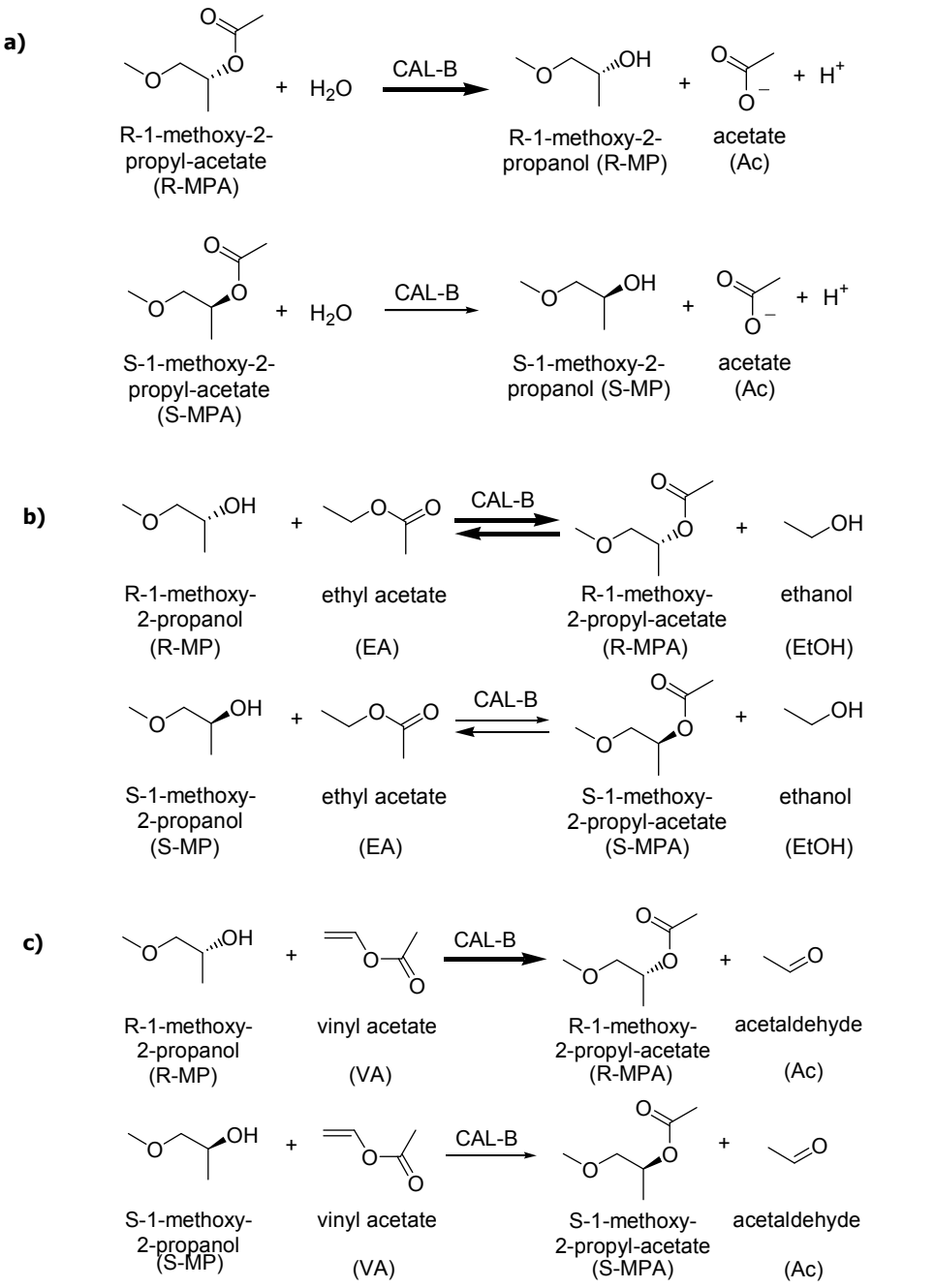

Scheme 1.1 *Candida antarctica* lipase B catalyzed **a)** enantioselective hydrolysis of R/S-1-methoxy-2-propyl acetate, **b)** reversible transesterification of (R/S)-1-methoxy-2-propanol with ethyl acetate, **c)** transesterification of (R/S)-1-methoxy-2-propanol with vinyl acetate.

1.2 Outline

Due to the broad nature of this study, the following chapters are virtually self-contained.

In Chapter 2, the CAL-B catalyzed enantioselective hydrolysis of (R/S)-1-methoxy-2-propyl-acetate is kinetically investigated (Scheme 1.1a). The derived model parameters are used for comparison with findings from the field of molecular modeling. The reaction is shown to be an attractive example for industrial production of secondary alcohols, due to its high enantiomeric ratio and good enzyme stability at low pH-values.

Chapter 3 provides a detailed kinetic study on the enantioselective transesterification of (R/S)-1-methoxy-2-propanol with ethyl acetate catalyzed by the same enzyme (Scheme 1.1b). Like most (trans)-esterifications, this reaction is reversible. A model is presented which is based on a ping-pong bi-bi mechanism, which takes into account the reversibility of the reaction, substrate inhibition by the acyl donor and acceptor as well as alternative substrate inhibition by each enantiomer. Next to initial rate measurements, experiments run at miniplant-scale are employed for model validation.

Model simulations in Chapter 3 indicate that efficient removal of ethanol from this mixture would lead to higher enantioselectivities and conversion. Because of this, in Chapter 4, pervaporative separation of ethanol from the quaternary mixture, (R/S)-1-methoxy-2-propanol / ethyl acetate / (R/S)-1-methoxy-2-propylacetate / ethanol, is examined using a commercial membrane. Pervaporation is shown to be strongly impacted by interactions between the components and the membrane.

In Chapter 5, a method is proposed for identification of kinetic parameters for reactions catalyzed by immobilized enzymes, which are affected by internal diffusion limitation. A mathematical model is derived for the CAL-B catalyzed enantioselective transesterification of (R/S)-1-methoxy-2-propanol with vinyl acetate (Scheme 1.1c).

In Chapter 6, the development of a non-isothermal two-dimensional heterogeneous model is presented for the kinetic resolution of (R/S)-1-methoxy-2-propanol with vinyl acetate in a fixed bed reactor. The model is based on kinetics derived in Chapter 5. Model simulations are validated using experimental results obtained through miniplant operation.

Chapter 7 provides an overview of the application of miniplant technology, modeling and simulation and discusses their potential for the field of enzyme catalysis.

In Chapter 8, the conclusions of this work are presented within the context of future studies. The suitability of the three reaction alternatives for industrialization is discussed briefly.

Chapter 9 explains the materials and methods used throughout this work.

2

Kinetic Modeling of Lipase Catalyzed Hydrolysis of (R/S)-1-Methoxy-2-propyl-acetate as a Model Reaction for Production of Chiral Secondary Alcohols

Published in:

Berendsen, W. R., Gendrot, G., Resnick, S. M., Reuss, M., (2006a)
Journal of Biotechnology, **121**, 213-226

Abstract

The Candida antarctica lipase B catalyzed kinetic resolution of (R/S)-1-methoxy-2-propyl-acetate is studied as a model system for the biocatalytic production of chiral secondary alcohols. For this purpose, a kinetic model is proposed involving both enantiomers of this reaction using model discrimination and parameter identification. Starting from a ping-pong bi-bi mechanism, a simplified model with sensitive parameters is derived for the R- and S-enantiomer, respectively. It is validated at pH 7.0, using time-course measurements at varying temperatures (30-60°C) and initial substrate conditions (0.05-1.5M).

This model is then used for mechanistic interpretation of the kinetic resolution on a biochemical level. The effect of temperature on kinetic parameters and enantiomeric ratio is investigated and compared to findings from the field of molecular modeling to obtain a better understanding of the reaction system for process design. Values of 21.2 kJ·mol^{-1} and 9.7 kJ·mol^{-1} are determined for the enthalpic ($\Delta_{R-S}\Delta H^{\ddagger\circ}$) and the entropic ($-T\cdot\Delta_{R-S}\Delta S^{\ddagger\circ}$) contribution of the difference in transition state energy of both enantiomers at 30°C.

High enantiomeric ratio's (E's of 47-110) especially at lower temperatures, in addition to enzyme activity at a wide pH-range, indicate this biotransformation is a promising example for the industrial production of chiral secondary alcohols.

2.1 Introduction

In recent years, lipases have received much attention as biocatalysts for the acylation of carbohydrates (La Ferla, 2002), modification of triglycerides (Murty et al., 2002) and synthesis of chiral compounds (Kielbasinski, et al., 1998; Patel, 2002; Ghanem and Aboul-Enein, 2004b; Kazlauskas and Bornscheuer 1998). They have been extensively studied for stereo-selective hydrolysis (Rogalska et al., 2000; Patel et al., 1996), esterification (Krishna and Karanth, 2002) and transesterification reactions (Theil, 2001). In particular, chiral compounds have gained much interest in pharmaceutical industry (Lida and Mase, 2002).

Candida antarctica lipase B (CAL-B) has been shown to have high catalytic activity in almost dry solvents (Lozano, et al., 2003a), good long-term and temperature stability (Orsat et al., 1999; Turner and Vulfson, 2000), high enantioselectivity (Hoff et al., 1996; Rotticci et al., 2001b, Anderson, et al., 1998), as well as broad substrate specificity (Otto et al., 2000). Hence, this enzyme is very attractive for industrial chiral biocatalysis.

In the case of secondary alcohols, like glycol ethers, high enantioselectivities have been reported for this enzyme (Orsat et al., 1999; Turner and Vulfson, 2000; Ottosson and Hult, 2001). In addition, screening studies have demonstrated the selectivity of CAL-B for resolution of propylene-oxide derived “P-series” glycol ethers under both hydrolysis and transesterification conditions (Baumann, et al., 2000; Resnick, et al., 2003). Therefore, CAL-B catalyzed enantioselective hydrolysis of 1-methoxy-2-propyl-acetate (MPA) is selected as a model system (Scheme 2.1) for the biocatalytic resolution of this series of secondary alcohols.

A thorough kinetic investigation can be used to evaluate the potential utility of the reaction system and to support reaction engineering investigation for process development. For the kinetic resolution of 2-methyl-pantanol with *Pseudomonas sp.*, Indlekofer et al., (1993) successfully applied a kinetic model based on a Michaelis Menten mechanism taking into account competitive inhibition of both enantiomer substrates. The model derived here has a similar basis. Competitive inhibition of the R-enantiomer product is considered additionally and the maximum velocity ($V_{max,S}$) and affinity constant ($K_{m,S}$) of the slower enantiomer are reduced to a single specificity constant (k_S) due to the limited solubility of MPA in water.

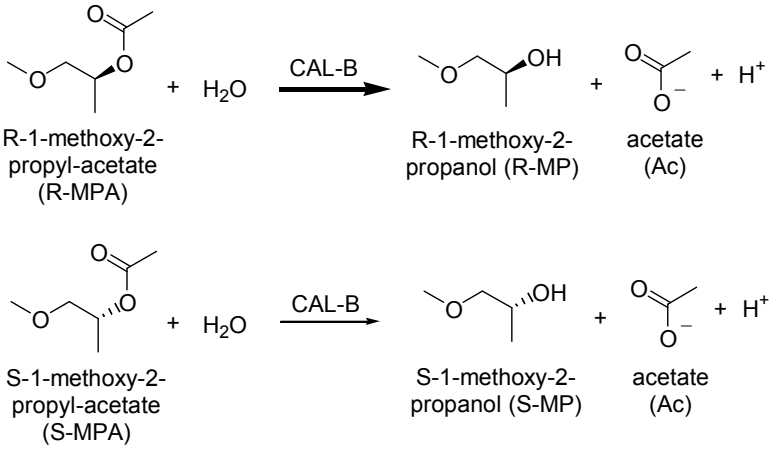

Scheme 2.1 CAL-B catalyzed enantioselective hydrolysis of R/S-1-methoxy-2-propyl acetate catalyzed by *Candida antarctica* lipase B.

Due to the interesting properties of CAL-B, and the fact that a three-dimensional crystal structure is available (Uppenberg, et al., 1995), this enzyme is often used in protein engineering to derive molecular models which predict the enantioselectivity of the enzyme towards a class of substrates like secondary alcohols. In case of (trans)-esterification reactions, the interplay of secondary alcohols with the active site of the enzyme and the resulting enantioselectivity has been studied by various authors (Ottosson, et al., 2002; Bocola, 2002; Raza, et al., 2000; Rotticci, et al., 2001b). These authors have investigated the ability to accomplish such chiral resolutions from a thermodynamic point of view, using the difference in Gibbs free energy of activation, i.e. the difference in absolute transition state energy of the R- and S-enantiomer, $\Delta_{R-S}\Delta G^{\ddagger\circ}$. By factorizing the Gibbs free energy of activation into an enthalpic and entropic contribution, they observed that the entropic contribution plays a major role in enzyme enantioselectivity. Up to now, these molecular modeling and experimental studies are mainly focused on (trans)-esterification reactions using organic solvents as liquid medium.

Depending on the overall goal of kinetic studies, model discrimination and parameter identification are crucial activities for interpretation of modeling results. Whenever the model outcome is to be investigated, insensitive parameters do not thwart interpretation capability, as long as the validity of the model is warranted. If the model parameters themselves are the result, i.e. to enable mechanistic interpretation, both model discrimination and parameter identification are of utmost importance. In this chapter, both aspects are applied using the enantioselective hydrolysis of MPA as an example. The thus obtained parameters are then used for comparison with findings from a molecular modeling point of view.

2.2 Results and Discussion

2.2.1 Model Development

The kinetic mechanism of *Candida antarctica* lipase B has been described as reversible ping-pong bi-bi (Martinelle and Hult, 1995). In addition, for the kinetic resolution of a racemic mixture, the competition of both enantiomers for the same active site should be considered (Indlekofer et al., 1993). For the sake of clarity, this effect is neglected at this point, but will be taken into account at a later stage in model development. Such a system may be described by the following mathematical equations (Segel, 1993):

$$\frac{dc_{R-MPA}}{dt} = -\frac{k^{f}_{cat,R} \cdot k^{r}_{cat,R} \cdot \left(c_{R-MPA} \cdot c_{H_2O} - \frac{c_{R-MP} \cdot c_{HAc}}{K_{eq}} \right) \cdot m_E \cdot x_E}{D_1} \tag{2.1}$$

with: $D_1 = k^{r}_{cat,R} \cdot \left(K_{m,H_2O} \cdot c_{R-MPA} \left(1 + \frac{c_{R-MP}}{K_{i,R-MP}} \right) + K_{m,R-MPA} \cdot c_{H_2O} + c_{R-MPA} \cdot c_{H_2O} \right)$

$$+ \frac{k^{f}_{cat,R}}{K_{eq}} \left(K_{m,R-MP} \cdot c_{HAc} \left(1 + \frac{c_{H_2O}}{K_{i,H_2O}} \right) + K_{m,HAc} \cdot c_{R-MP} + c_{R-MP} \cdot c_{HAc} \right)$$

$$\frac{dc_{S-MPA}}{dt} = -\frac{k^{f}_{cat,S} \cdot k^{r}_{cat,S} \cdot \left(c_{S-MPA} \cdot c_{H_2O} - \frac{c_{S-MP} \cdot c_{HAc}}{K_{eq}} \right) \cdot m_E \cdot x_E}{D_2} \tag{2.2}$$

with: $$D_2 = k^r_{cat,S} \cdot \left(K_{m,H_2O} \cdot c_{S-MPA} \left(1 + \frac{c_{S-MP}}{K_{i,S-MP}} \right) + K_{m,S-MPA} \cdot c_{H_2O} + c_{S-MPA} \cdot c_{H_2O} \right)$$

$$+ \frac{k^f_{cat,S}}{K_{eq}} \left(K_{m,S-MP} \cdot c_{HAc} \left(1 + \frac{c_{H_2O}}{K_{i,H_2O}} \right) + K_{m,HAc} \cdot c_{S-MP} + c_{S-MP} \cdot c_{HAc} \right)$$

$$\frac{dc_{R-MP}}{dt} = -\frac{dc_{R-MPA}}{dt}; \frac{dc_{S-MP}}{dt} = -\frac{dc_{S-MPA}}{dt} \tag{2.3}$$

with:

c_j	compound concentration	($mol \cdot L^{-1}$)
K_{eq}	equilibrium constant	(-)
$k^d_{cat,a}$	maximum specific rate	($mol \cdot g^{-1} \cdot s^{-1}$)
$K_{m,i}$	Michaelis Menten constant	($mol \cdot L^{-1}$)
$K_{i,i}$	inhibition constant	($mol \cdot L^{-1}$)
m_E	enzyme concentration	($g \cdot L^{-1}$)
x_E	enzyme loading	($g \cdot g^{-1}$)

d = f, r; i = R-MPA, S-MPA, R-MP, S-MP, HAc, H_2O

In a reversible ping-pong bi-bi mechanism, the first substrate (glycol ether acetate) binds to the enzyme, after which the corresponding product (glycol ether) is released to form an acyl-enzyme-complex. Next, the second substrate (water) binds to the acyl-enzyme complex to yield the second substrate (acetic acid) and regenerate the enzyme. In aqueous systems, however, where the reactant water is available at saturating conditions, the reversible reaction is negligible ($c_{HAC} << c_{H2O}$, $c_{R\text{-}MP} << c_{H2O}$). Canceling down Equations (2.1) and (2.2) by c_{H2O} results in:

$$\frac{dc_{R-MPA}}{dt} = -\frac{k^f_{cat,R} \cdot c_{R-MPA} \cdot m_E \cdot x_E}{\frac{K_{m,H_2O}}{c_{H_2O}} \cdot c_{R-MPA} \left(1 + \frac{c_{R-MP}}{K_{i,R-MP}} \right) + K_{m,R-MPA} + c_{R-MPA}} \tag{2.4}$$

$$\frac{dc_{S-MPA}}{dt} = -\frac{k^f_{cat,S} \cdot c_{S-MPA} \cdot m_E \cdot x_E}{\frac{K_{m,H_2O}}{c_{H_2O}} \cdot c_{S-MPA} \left(1 + \frac{c_{S-MP}}{K_{i,S-MP}} \right) + K_{m,S-MPA} + c_{S-MPA}} \tag{2.5}$$

Since $c_{H2O}>>c_{R\text{-}MPA}$ and $c_{H2O}>>c_{S\text{-}MPA}$, Equations (2.4) and (2.5) can be further simplified to an irreversible Michaelis Menten mechanism. As mentioned before, the competition of both enantiomers for the same active site should be considered. Based on experimental observations (Figure 2.1), product inhibition of the R-enantiomer needs to be taken into account as well. The corresponding King-Altman-Plot for this system is shown in Scheme 2.2. This leads to the following mathematical equations:

Scheme 2.2 King-Altman plot of an irreversible Michaelis Menten mechanism taking into account competition by both enantiomers and product inhibition by R-MP.

$$\frac{dc_{R-MPA}}{dt} = -\frac{k^{f}_{cat,R} \cdot c_{R-MPA} \cdot m_{E,imm}}{K_{m,R-MPA} \cdot \left(1 + \frac{c_{S-MPA}}{K_{m,S-MPA}} + \frac{c_{R-MP}}{K_{i,R-MP}}\right) + c_{R-MPA}} \tag{2.6}$$

$$\frac{dc_{S-MPA}}{dt} = -\frac{k^{f}_{cat,S} \cdot c_{S-MPA} \cdot m_{E,imm}}{K_{m,S-MPA} \cdot \left(1 + \frac{c_{R-MPA}}{K_{m,R-MPA}} + \frac{c_{R-MP}}{K_{i,R-MP}}\right) + c_{S-MPA}} \tag{2.7}$$

As can be observed in Equations (2.6) and (2.7), product inhibition for the S-enantiomer is not taken into account. This effect is found to be negligible and meets the expectations from a biochemical point of view: The slow-reacting S-enantiomer should have less interaction with the active site of the enzyme and therefore cause less inhibition effects. The enzyme loading, x_E, is unfortunately not known for this commercial available immobilized enzyme preparation. Therefore, the 'concentration of the immobilized enzyme' is used: $m_{E,imm} = m_E \cdot x_E$. Model equations (2.3), (2.6) and (2.7) are used to fit experimental data, shown in Figures (2.1, 2.2a-c). In order to determine kinetic constants, like $k_{cat,S}$ and $K_{m,s\text{-}MPA}$ accurately, measurements should be performed at $c_{s\text{-}MPA,0}>>K_{m,S\text{-}MPA}$. The estimated value of $K_{m,S\text{-}MPA}$ is however much larger than the solubility limit of S-MPA. Because of this, Equations (2.6) and (2.7) are reduced to first order kinetics with respect to the S-enantiomer:

$$\frac{dc_{R-MPA}}{dt} = -\frac{k^{f}_{cat,R} \cdot c_{R-MPA} \cdot m_{E,imm}}{K_{m,R-MPA} \cdot \left(1 + \frac{c_{R-MP}}{K_{i,R-MP}}\right) + c_{R-MPA}} \tag{2.8}$$

$$\frac{dc_{S-MPA}}{dt} = -k_S \cdot \frac{c_{S-MPA} \cdot m_{E,imm}}{1 + \frac{c_{R-MPA}}{K_{m,R-MPA}} + \frac{c_{R-MP}}{K_{i,R-MP}}} \tag{2.9}$$

with:

k_s modified first order rate constant ($L \cdot g^{-1} \cdot s^{-1}$)

$$k_S = \frac{k^{f}_{cat,S}}{K_{m,S-MPA}} \tag{2.10}$$

Due to the limited solubility of MPA in water (1.4M), purified R-MPA is used in two cases, in order to determine $K_{m,R\text{-}MPA}$ and $k^{f}_{cat,R}$ more precisely. The kinetic model describes the experimental data very well at isothermal conditions (Figure 2.1, 2.2a-c). The corresponding parameter set is shown in Table 2.1.

Table 2.1 Estimated kinetic parameters at various temperatures. * Changes in $K_{m,R\text{-}MPA}$ and $K_{i,R\text{-}MP}$ did not impact R- or S- enantiomer conversion. Therefore, both parameters were assumed constant over the temperature range studied.

		T (°C)				
		30	**40**	**50**	**56**	**60**
$\mathbf{k^{f}_{cat,R}}$	$mol \cdot g^{-1} \cdot s^{-1}$	4.80E-05	5.80E-05	6.50E-05	7.70E-05	9.20E-05
$\mathbf{K_{m,R\text{-}MPA}}$	$mol \cdot L^{-1}$	0.39 *				
$\mathbf{K_{i,R\text{-}MP}}$	$mol \cdot L^{-1}$	0.55 *				
$\mathbf{k_S}$	$L \cdot g^{-1} \cdot s^{-1}$	1.30E-06	2.10E-06	2.70E-06	3.40E-06	5.40E-06

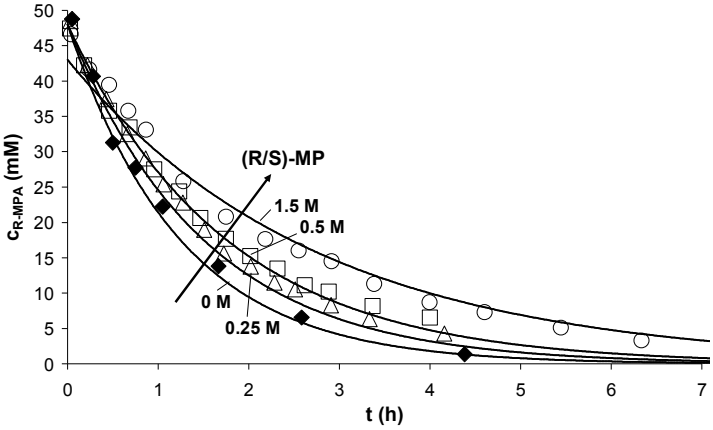

Figure 2.1 Dynamic R-MPA concentration profiles in a stirred tank reactor at varying initial R/S-MP- concentrations to increase accuracy of Ki,R-MP determination (at [R/S-MPA]0 = 100mM, 30°C, pH 7 and 2 g·L-1 Chirazyme L-2, c.-f., C2). Measurements and model are shown by dots and lines, respectively (cR/S-MP(0): closed diamonds: 0M; triangles: 0.25M; open squares: 0.5M; circles: 1.5M).

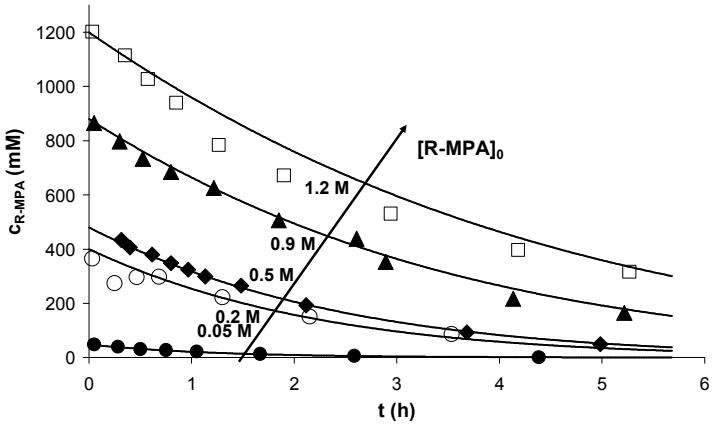

Figure 2.2a Time course plots of R-MPA concentrations at various initial MPA concentrations at 30°C, pH 7 and 2 $g \cdot L^{-1}$ Chirazyme L-2, c.-f., C2. Measurements and model are shown by dots and lines, respectively ($c_{R\text{-}MPA,0}$: closed circles: 0.05M; open circles: 0.2M; diamonds: 0.5M; triangles: 0.9M; open squares: 1.2M).

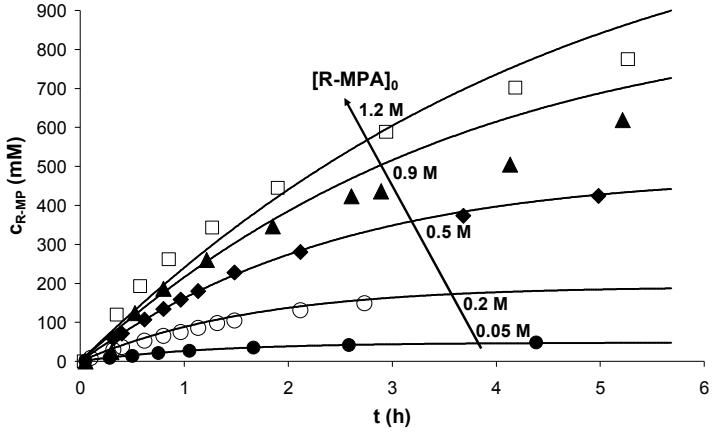

Figure 2.2b Time course plots of R-MP concentrations at various initial MPA concentrations at 30°C, pH 7 and 2 g·L^{-1} Chirazyme L-2, c.-f., C2. Measurements and model are shown by dots and lines, respectively ($c_{R\text{-}MPA,0}$: closed circles: 0.05M; open circles: 0.2M; diamonds: 0.5M; triangles: 0.9M; open squares: 1.2M).

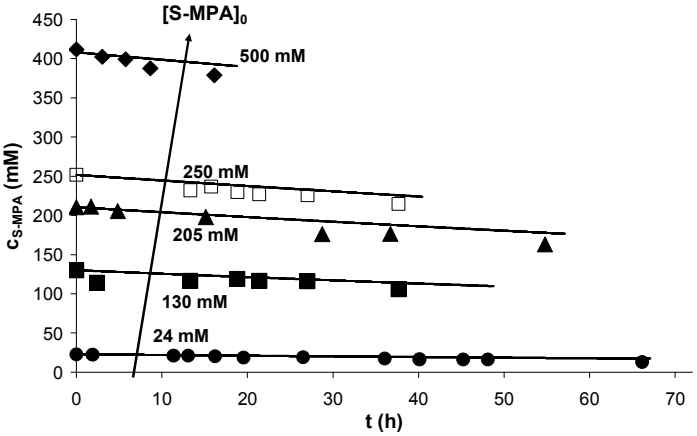

Figure 2.2c Time course plots of S-MPA concentrations at various initial MPA concentrations at 30°C, pH 7 and 2 g·L^{-1} Chirazyme L-2, c.-f., C2. Measurements and model are shown by dots and lines, respectively ($c_{S\text{-}MPA,0}$: circles: 0.024M; closed squares: 0.13M; triangles: 0.205M; open squares: 0.25M; diamonds: 0.5M).

2.2.2 Enantioselectivity and Enantiomeric Ratio

During a typical kinetic resolution, the enantiomeric excess (e.e.) decreases with conversion for a reaction product and increases for a resolved substrate since the kinetic rate of each enantiomer is dependent on its respective substrate concentration. Enantiomeric excess is calculated as follows (Chen et al., 1982):

$$e.e._j = \left| \frac{c_R - c_S}{c_R + c_S} \right| \text{ for both MPA and MP} \tag{2.11}$$

The enantiomeric ratio, or E-value, is generally calculated in order to evaluate a kinetic resolution at different extents of conversion. It is an intrinsic property of an enzyme for a specific acyl donor and alcohol substrate and represents the ratio of the initial reaction rate of both enantiomers (Chen et al., 1982):

$$E = \frac{\dfrac{k_{cat,R}}{K_{m,R-MPA}}}{\dfrac{k_{cat,S}}{K_{m,S-MPA}}} = \frac{\dfrac{k_{cat,R}}{K_{m,R-MPA}}}{k_S} \tag{2.12}$$

As a rule of thumb, an E-value > 30 can be regarded good for practical purposes (Faber, 1997). The kinetic model is used to calculate the typical e.e. vs. conversion plot and the corresponding E-value for kinetic resolutions (Figure 2.3). As is evident from this figure, good e.e.-values at ~ 50% conversion and an excellent E-value is obtained. For production of R-MP or S-MPA, conversions of 45% or 53% respectively should be used to obtain the corresponding products in highest enantiopurity and yield.

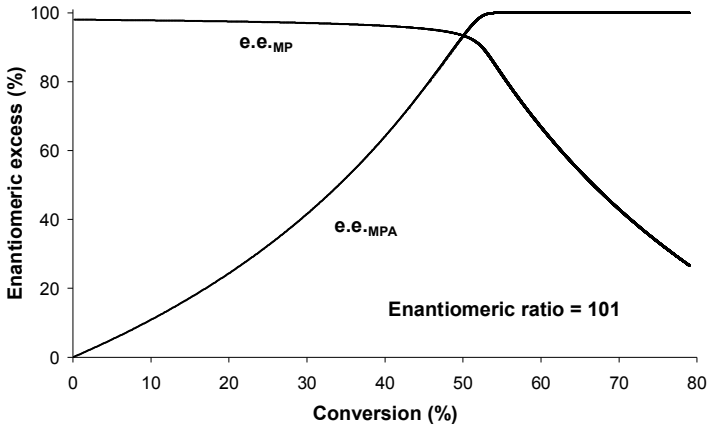

Figure 2.3 Simulation of the enantiomeric excess vs. conversion at 30°C and pH 7.

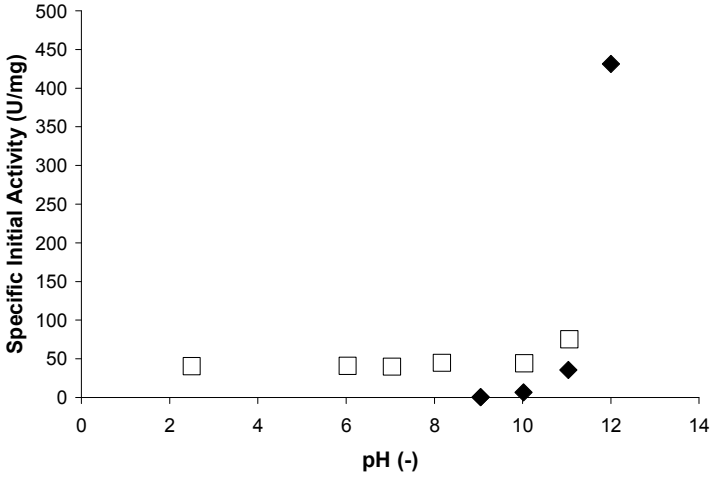

Figure 2.4 The effect of pH on specific initial reaction rate (R/S-MPA_0 = 500mM; 30°C and 2 $g \cdot L^{-1}$ Chirazyme L-2, c.-f., C2; squares: with enzyme; diamonds: without enzyme).

2.2.3 Effect of pH on Enzyme Activity

During kinetic analysis the pH is controlled by addition of NaOH using a potentiometric titrator, thus producing Na-acetate. In industry, continuous processes are preferred. For this purpose, fixed bed reactors are often employed. In such reactors, pH-control is not straight-forward and because of this, the effect of pH on catalytic activity is investigated (Figure 2.4). At pH > 9, chemical hydrolysis of MPA is observed in addition to CAL-B catalysis. Surprisingly, no deactivation is found at very low pH-values. This result exemplifies another interesting property of CAL-B.

2.2.4 The Influence of Temperature on the Enantioselectivity of the Enzyme

In general, each parameter in a kinetic model is temperature dependent. The temperature dependency of rate constants, such as k^f_{cat} or k_S, may be modeled by the absolute rate theory (Chang, 1981). In this theory, the pre-exponential and the exponential factor are also temperature dependent:

$$k'_j = \frac{k_B}{h} T \cdot e^{-\frac{\Delta G^{\ddagger\circ}_j}{R \cdot T}} \quad \text{for j = cat,R; S} \tag{2.13}$$

with: $k'_{cat,R} = \frac{k_{cat,R} \cdot MW_E}{x_E}$ and $k'_S = k_S \cdot m_E$.

where the transition state energy, $\Delta G^{\ddagger\circ}_j$, may be divided in an enthalpic contribution, $\Delta H^{\ddagger\circ}_j$, and an entropic contribution, $\Delta S^{\ddagger\circ}_j$:

$$\Delta G^{\ddagger\circ}_j = \Delta H^{\ddagger\circ}_j - T\Delta S^{\ddagger\circ}_j \quad \text{for j = cat,R; S} \tag{2.14}$$

with:

$\Delta G^{\ddagger\circ}{}_j$	transition state energy	(J·mol^{-1})
h	Planck constant	(J·s)
$\Delta H^{\ddagger\circ}{}_j$	reaction enthalpy	(J·mol^{-1})
k_B	Bolzmann constant	(J·K^{-1})
MW_E	molecular weight of the enzyme	(g·mol^{-1})
R	universal gas constant	(J·mol^{-1}·K^{-1})
$\Delta S^{\ddagger\circ}{}_j$	reaction entropy	(J·mol^{-1}·K^{-1})
T	temperature	(K)

Inserting Equation (2.13) into Equation (2.12) gives:

$$E = e^{-\frac{\Delta G^{\ddagger\circ}{}_R - \Delta G^{\ddagger\circ}{}_S}{R \cdot T}} = e^{-\frac{\Delta_{R-S}\Delta G^{\ddagger\circ}}{R \cdot T}} \tag{2.15}$$

Similar to Equation (2.14), the differential transition state energy, $\Delta_{R-S}\Delta G^{\ddagger\circ}$, may be described using an enthalpic, $\Delta_{R-S}\Delta H^{\ddagger\circ}$, and an entropic part, $\Delta_{R-S}\Delta S^{\ddagger\circ}$:

$$\Delta_{R-S}\Delta G^{\ddagger\circ} = \Delta_{R-S}\Delta H^{\ddagger\circ} - T\Delta_{R-S}\Delta S^{\ddagger\circ} \quad \text{for j = cat,R; S} \tag{2.16}$$

Inserting Equation (2.16) into Equation (2.15) leads to:

$$E = e^{-\frac{\Delta_{R-S}\Delta H^{\ddagger\circ}}{R \cdot T} + \frac{\Delta_{R-S}\Delta S^{\ddagger\circ}}{R}}, \tag{2.17}$$

which may be used to calculate the values of $\Delta_{R-S}\Delta H^{\ddagger\circ}$ and $\Delta_{R-S}\Delta S^{\ddagger\circ}$, if the enantiomeric ratio is plotted in logarithmic form versus the inverse temperature (Figure 2.5).

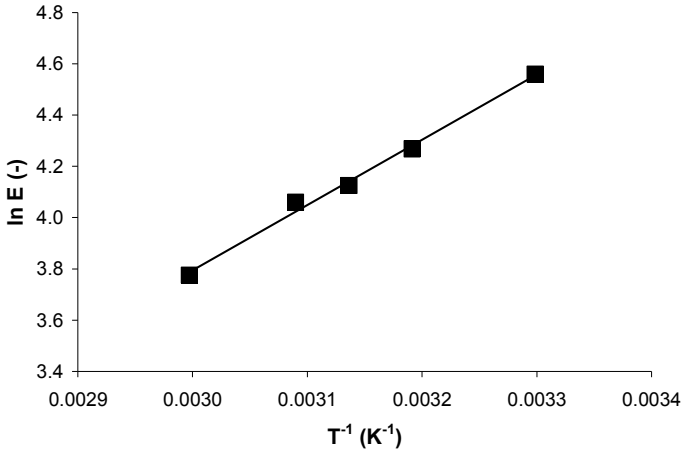

Figure 2.5 Graphical determination of $\Delta_{R-S}\Delta H^{\ddagger\circ}$ and $\Delta_{R-S}\Delta S^{\ddagger\circ}$.

Similar to the kinetic investigation already described above, the kinetic parameters of Equations 2.8 and 2.9 are estimated, but this time using time course measurements at temperatures up to 60°C. At each temperature, the kinetic parameters are estimated (Table 2.1). As may be observed in Figures 2.6a and 2.6b, the model shows a good fit to the experimental data.

The good sensitivity of the estimated parameters allows a mechanistic interpretation of the results. The effect of temperature on enantiomeric ratio is investigated (Figure 2.7). The difference in transition state energy of both enantiomers (e.g. $\Delta_{R-S}\Delta G^{\ddagger\circ}{}_{303\,K}$ = -11.5 kJ·mol^{-1}) causes a strong dependence of the enantiomeric ratio on temperature. This difference is in the same order of magnitude as reported by Orrenius, et al. (1998) for kinetic resolution of several secondary alcohols catalyzed by the same enzyme. A higher temperature results in a faster kinetic resolution, a lower enantioselectivity and a lower long-term stability of the catalyst. From a biochemical engineering point of view, an optimum has to be found between good enantioselectivity and an acceptable conversion rate.

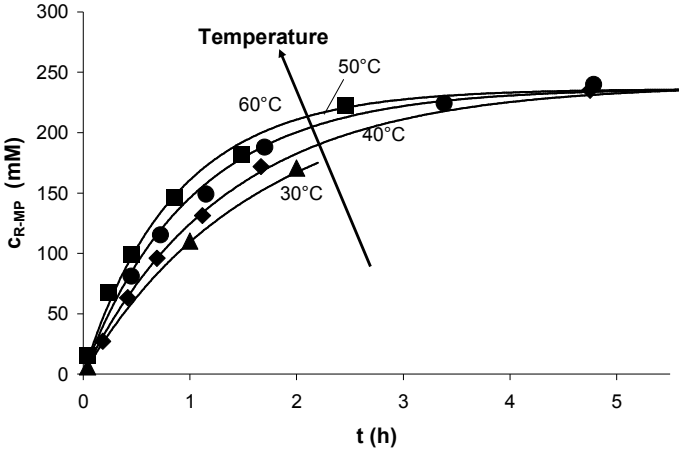

(a)

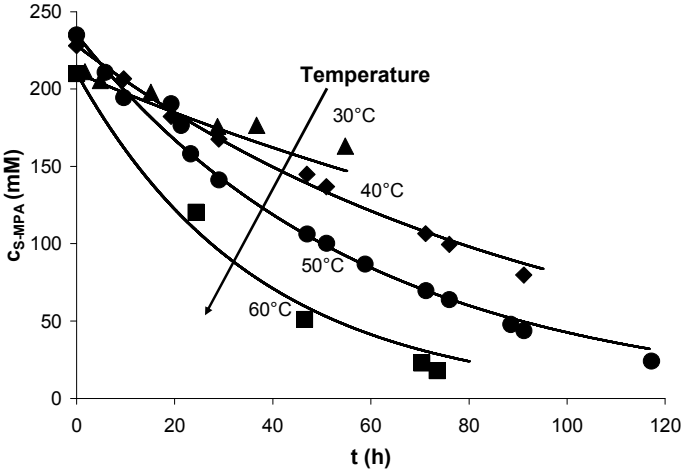

(b)

Figures 2.6a and b The effect of temperature on R-MP and S-MPA dynamic concentration profile in a stirred tank reactor (R/S-MPA_0 ≈ 460mM, pH 7 and 2 $g{\cdot}L^{-1}$ Chirazyme L-2, c.-f., C2). Measurements and model are shown by dots and lines, respectively (triangles: 30°C; diamonds: 40°C; circles: 50°C; squares: 60°C).

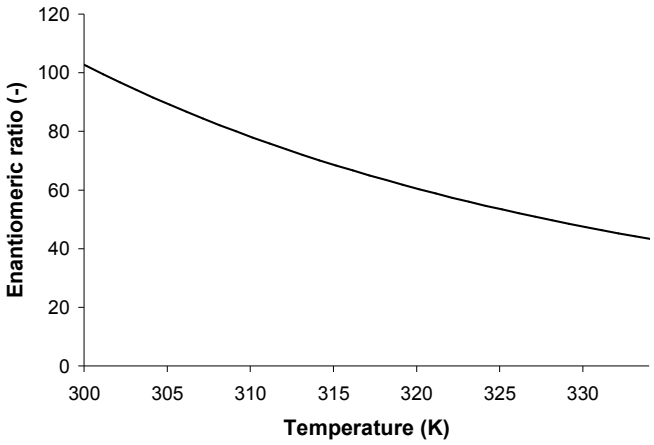

Figure 2.7 The influence of temperature on enantiomeric ratio.

The difference in transition state energy, $\Delta_{R-S}\Delta G^{\ddagger\circ}$ also consists of an entropic and enthalpic part, similar to Equation (2.14). The enthalpic contribution, $\Delta_{R-S}\Delta H^{\ddagger\circ}$ = -21.2 kJ·mol^{-1}, clearly favors the faster R-enantiomer, while the entropic contribution, $-T\cdot\Delta_{R-S}\Delta S^{\ddagger\circ}$ = 9.7 kJ·mol^{-1} at 30°C, counters this (Table 2.2). Hence, the conversion of the slower enantiomer is in favor by entropy. This behavior has been found by several authors as well, as a result of molecular modeling studies of CAL-B catalyzed (trans)-esterification reactions (Ottosson, et al., 2002; Bocola, 2002). The fact that the faster enantiomer is favored by enthalpy, and disfavored by entropy, may be explained biochemically by an improved binding of the substrate to the active site (lower enthalpy) and a concomitant stronger fixation of the enzyme-substrate complex (lower entropy). This should be reflected in the estimated affinity constants as well (i.e. $K_{m,S\text{-}MPA} > K_{m,R\text{-}MPA}$) – unfortunately, the value of $K_{m,S\text{-}MPA}$ could not be accurately determined for this reaction system due to the maximum solubility of MPA in water.

Table 2.2 Parameters related to the temperature dependency of the reaction rate of both enantiomers.

$\Delta H^{\ddagger\circ}_R$ or $E_{act,R}$	18.1	($kJ \cdot mol^{-1}$)	$k^0_{cat,R}$	0.061	($mol \cdot g^{-1} \cdot s^{-1}$)
$\Delta H^{\ddagger\circ}_S$ or $E_{act,S}$	39.2	($kJ \cdot mol^{-1}$)	k^0_S	7.34	($L \cdot g^{-1} \cdot s^{-1}$)
$\Delta_{R-S}\Delta H^{\ddagger\circ}$	-21.2	($kJ \cdot mol^{-1}$)	$\Delta_{R-S}\Delta S^{\ddagger\circ}$	-3.19E-02	($kJ \cdot mol^{-1} \cdot K^{-1}$)
$\Delta_{R-S}\Delta G^{\ddagger\circ}_{303\,K}$	-11.5	($kJ \cdot mol^{-1}$)	T_r	663	($kJ \cdot mol^{-1}$)

From a biochemical and biophysical point of view, one may visualize the decrease in enantioselectivity with temperature by an increased molecular mobility of the catalytic centre at higher temperatures, resulting in more spatial freedom for the substrate as well as a better access into the active site. Overall, the S-enantiomer becomes less sterically hindered and this ultimately leads to a lower enantioselectivity. This correlates with findings of Raza, et al. (2001) and Rotticci et al., (2001b), who observed the increase of the enantioselectivity with increasing size of the acyl moiety for acyl-transfer reactions with the same enzyme.

At the racemic temperature, T_{rac}, where no enantioselectivity is present, $\Delta_{R-S}\Delta G^{\ddagger\circ}_{T_r} = 0$ and E=1. This yields:

$$T_{rac} = \frac{\Delta_{R-S}\Delta H^{\ddagger\circ}}{\Delta_{R-S}\Delta S^{\ddagger\circ}} \tag{2.18}$$

In agreement with values for most secondary alcohols, T_{rac} lies well above applicable temperature (Table 2.2; Ottosson, et al., 2002). In some cases, conversions with T_{rac}-values below ambient temperatures have been found for lipase catalyzed kinetic resolutions (e.g. Watanabe, et al., 2001; Lee et al., 1995). These cases are interesting, since both the enantioselectivity and reaction rate increase with temperature, limited only by the long-term stability of the catalyst.

2.2.5 Estimation of Kinetic Parameters for Reactor Design Studies to Optimize the Operation Temperature

As part of a larger investigation, where different process alternatives are evaluated for the chiral production of secondary alcohols, the impact of temperature on reactor performance and enantioselectivity is studied. For this purpose, the temperature dependency of the kinetic parameters in Equations 2.8 and 2.9 need to be determined. Inserting Equation (2.14) into Equation (2.13) gives:

$$k'_j = \frac{k_B}{h} T \cdot e^{-\frac{\Delta H^{\ddagger\circ}_j}{R \cdot T} + \frac{\Delta S^{\ddagger\circ}_j}{R}}, \text{ j = cat,R; S} \qquad (2.19)$$

Since the enzyme loading, x_E, is not known for this commercial enzyme preparation and the temperature dependency of the pre-exponential term, Equation (2.19), is very small in comparison to $\frac{\Delta H^{\ddagger\circ}_j}{R \cdot T}$, this equation may be simplified to an Arrhenius equation (with $E_{act,R} = \Delta H^{\ddagger\circ}_j$) :

$$k'_j = k'^0_j \cdot e^{-\frac{E_{act,j}}{R \cdot T}}, \text{ j = cat,R; S} \qquad (2.20)$$

with: $k'^0_{cat,R} = \frac{k^0_{cat,R} \cdot MW_E}{x_E}$ and $k'^0_S = k^0_S \cdot m_E$

$E_{act,j}$	activation energy	($J \cdot mol^{-1}$)

The affinity (K_m) and inhibition constants (K_i) should be described using the following Gibbs free energy equation: (Segel, 1993):

$$\Delta G^\circ_{cons} = -R \cdot T \cdot \ln(K_{cons}) \quad \text{for cons = m,R-MPA; i,R-MP} \qquad (2.21)$$

with:

ΔG°_{cons}	Gibbs free energy of K_m or K_i-constants	($J \cdot mol^{-1}$)
K_{cons}	equilibrium constant	(-)

Each parameter is plotted in the logarithmic form versus the inverse temperature, Equations (2.20) and (2.21), resulting in $E_{act,j}$ and ΔG°_{cons}. In the case of $K_{m,R\text{-}MPA}$ and $K_{i,R\text{-}MP}$, the corresponding free energies are too small to be estimated accurately. Therefore, $K_{m,R\text{-}MPA}$ and $K_{i,R\text{-}MP}$ are assumed to be constant over the temperature range studied. The resulting plot and identified parameters are shown in Figure 2.8 and Table 2.2, respectively. The activation energy of both enantiomers at 30°C is of the same order as found by other authors for CAL-B catalyzed kinetic resolutions (Bartling et al., 2001; Raza et al., 2001). The fact, that $E_{act,R}>E_{act,S}$ is in line with the notion, that the slower S-enantiomer requires a higher activation energy for conversion.

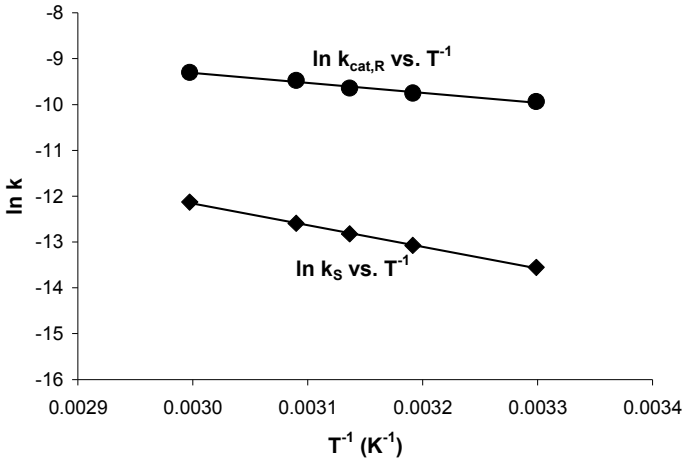

Figure 2.8 Graphical determination of $\Delta H^{\ddagger\circ}_{R}$, $\Delta_{R-S}\Delta S^{\ddagger\circ}$, $k^{0}_{cat,R}$ (mol·g^{-1}·s^{-1}) and k^{0}_{S} (L·g^{-1}·s^{-1}).

2.3 Conclusions

A kinetic model are proposed for CAL-B catalyzed enantioselective hydrolysis of racemic 1-methoxy-2-propyl-acetate in a stirred tank reactor. By model discrimination and parameter identification an irreversible Michaelis-Menten and a first order mechanism including R-MP inhibition, for the R- and S-enantiomer respectively, are shown to successfully predict this conversion at a wide range of reaction conditions. This model is validated at pH 7.0, using time-course measurements at varying initial substrate conditions and temperatures between 30 and 60°C. Also, the effect of pH on the rate of reaction is studied and found to be negligible.

The obtained kinetic model is used for simulation of the enantiomeric ratio at varying temperatures. By making sure the estimated parameters are sensitive, in addition to achieving a good model-fit, this model is used as a solid basis for mechanistic interpretation of the kinetic resolution. The increase of enantioselectivity at lower temperatures, shows that the temperature is an important parameter for process control and design.

With enantiomeric ratio's well above 30, this biotransformation is a promising example for the industrial production of chiral secondary alcohols. The fact, that CAL-B is active at low pH-values, only adds to this.

3

A Kinetic Study of Lipase-Catalyzed Reversible Kinetic Resolution Involving Verification at Miniplant-Scale

Published in:

Berendsen, W. R., Gendrot, G., Resnick, S. M., Reuss, M. (2006b)
Biotechnology and Bioengineering, **95**, 883-892, DOI: 10.1002/bit.21034

Abstract

Lipase catalyzed kinetic resolution of racemates is a popular method for synthesis of chiral synthons. Most of these resolutions are reversible equilibrium limited reactions. For the first time, an extensive kinetic model is proposed for kinetic resolution reactions, which takes into account the full reversibility of the reaction, substrate inhibition by an acyl donor and an acyl acceptor as well as alternative substrate inhibition by each enantiomer. For this purpose, the reversible enantioselective transesterification of (R/S)-1-methoxy-2-propanol with ethyl acetate catalyzed by Candida antarctica lipase B (CAL-B) is investigated. The detailed model presented here is valid for a wide range of substrate and product concentrations.

Following model discrimination and the application of Haldane equations to reduce the degree of freedom in parameter estimation, the eleven free parameters are successfully identified. All parameters are fitted to the complete data set simultaneously. Six types of independent initial rate studies provide a solid data basis for the model. The effect of changes in substrate and product concentration on reaction kinetics is discussed.

The developed model is used for simulations to study the behavior of reaction kinetics in a fixed bed reactor. The typical plot of enantiomeric excess versus conversion of substrate and product is evaluated at various initial substrate mixtures. The model is validated by comparison with experimental results obtained with a fixed bed reactor, which is part of a fully automated state-of-the-art miniplant.

3.1 Introduction

Within biocatalysis, kinetic resolution is a popular method for synthesis of chiral compounds. This method, which represents conversion of primarily one of the two enantiomers of a racemic substrate yielding either the substrate or the product in high enantiomeric purity, is attractive for production of chiral building blocks for pharmaceutical, agricultural and fine-chemical industry. Lipases are the preferred enzymes for this conversion, as they show activity in nearly pure organic solvents as well as long-term stability (Turner and Vulfson, 2000; Lozano, et al., 2003a). In particular, *Candida antarctica* lipase B (CAL-B) is a much used biocatalyst due to its broad substrate specificity and good enantioselectivity (Anderson, et al., 1998; Otto et al., 2000; Resnick et al., 2002).

Kinetic resolution may be achieved via hydrolysis, esterification or transesterification mode (Berendsen, et al., 2006a; Baumann, et al., 2000, Rotticci, et al., 2001b). The reduced solubility of many potential compounds in aqueous solution and the concomitant change in pH during conversion are typical bottlenecks of the hydrolysis mode. This complicates downstream processing through the necessity to extract the products from aqueous solution as well as results in a limiting end-product concentration.

Although a tremendous number of publications deal with biocatalytic kinetic resolutions, only few of them actually provide information in terms of reaction kinetics and parameters. Thorough investigation of the kinetic mechanism involved and the determination of the corresponding parameters is a key step in process development.

Kinetic investigations involving ping-pong bi-bi models have been reported for cases, where only one enantiomer is converted (Shin and Kim, 1998) or where reactions are non-chiral (Kraut, 1977; Martinelle and Hult, 1995; Flores and Halling, 2002; Rizzi et al., 1992). If the formation of the slower enantiomer in a kinetic resolution cannot be neglected, competitive inhibition of one enantiomer's rate by the other enantiomer should be taken into account as well. For irreversible resolution reactions, this was done by considering alternative substrate inhibition by both enantiomers (Indlekofer, et al., 1993; Chang et al., 1999; Berendsen et al., 2006d).

A kinetic study taking into account the reversibility and enantioselectivity of the reaction at the same time has not yet been presented. This is interesting, as most enantioselective esterifications and transesterifications are equilibrium limited reversible reactions.

The detailed model developed here extends existing reversible ping-pong bi-bi models by taking into account both reversibility and competitive inhibition by both enantiomers as well as substrate inhibition by an acyl donor and an acyl acceptor. It enables reliable

prediction of both forward and reverse reactions, accurately describing the experimental data at a wide range of substrate and product concentrations.

This contribution focuses on the transesterification of (R/S)-1-methoxy-2-propanol (MP) with ethyl acetate (EA) into mainly R-1-methoxy-2-propanol acetate (R-MPA) and ethanol (EtOH) catalyzed by *Candida antarctica* lipase B (CAL-B) as a model system for reversible kinetic resolutions (Scheme 3.1).

For demonstration, the developed kinetic model is employed for a fixed bed reactor, which is part of a fully automated state-of-the-art miniplant.

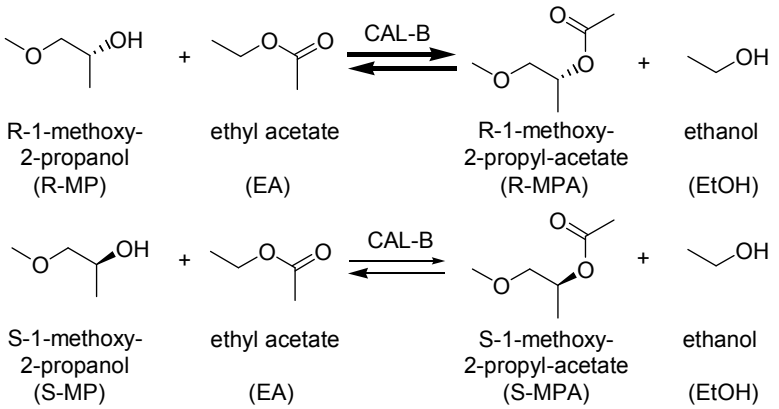

Scheme 3.1 Reversible transesterification of (R/S)-1-methoxy-2-propanol (MP) with ethyl acetate (EA) catalyzed by *Candida antarctica* lipase B.

3.2 Theory

3.2.1 Kinetic Model Development

In case of reactions catalyzed by immobilized enzymes, the occurrence of diffusion limitation needs to be checked. This may be done by determining the General Thiele modulus, $\phi G,a$, for both enantiomers (Bailey and Ollis, 1986). For the transesterification of MP with EA catalyzed by immobilized *Candida antarctica* lipase B, Chirazyme L-2, c.-f. C2 (see Chapter 9: Materials and Methods), a Thiele modulus $\phi G,a << 0.3$ is obtained. Therefore, internal mass transfer limitation does not need to be considered. Since kinetic measurements are performed in a stirred tank reactor, external mass transfer limitation is assumed to be negligible too. Thus, substrate and product concentrations in bulk liquid are directly used for determination of intrinsic kinetics.

For deriving kinetic models, which have not yet been described elsewhere, the King-Altman method may be used. This method considers all possible interactions between substrates, products and enzyme species and derives an equation based on rate constants (k_1, k_{-1}, k_2, k_{-2}, etc.). Then, this equation may be transformed into the final velocity equation containing the usual maximum velocity and affinity constants (V_{max}, $K_{m,i}$) using Cleland's coefficient form. This procedure is described in great detail for various examples by Segel, 1993. This method is applied for the system at hand, i.e. two parallel reversible bimolecular reactions.

Competitive substrate inhibition resulting from the combination of a substrate with the wrong enzyme complex is characteristic of ping-pong bi-bi systems (Segel, 1993). In general, substrate inhibition is only apparent at high substrate concentrations. Both forward and reverse reaction rate may be affected by it. Product inhibition of the rate by the acyl donor and the acyl acceptor has been found for such systems as well (Rizzi et al., 1992). Considering these possible substrate and product inhibition effects in addition to alternative substrate inhibition for both enantiomers, a scheme following Cleland's notation may be derived (Scheme 3.2).

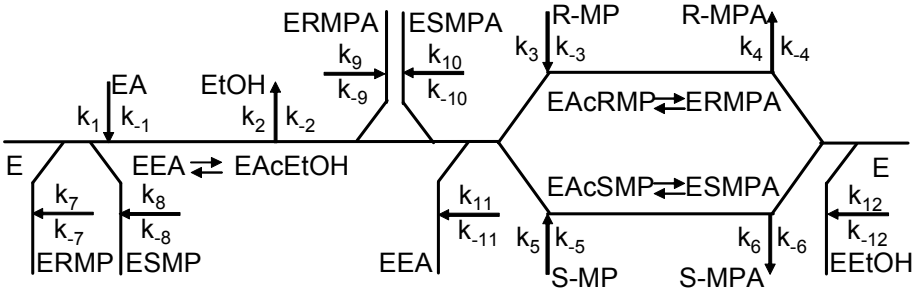

Scheme 3.2 Cleland notation of a ping-pong bi-bi mechanism with alternative substrate inhibition by enantiomers, substrate inhibition by EA and EtOH and product inhibition by all components.

The corresponding volumetric rate of the R-enantiomer, $r_{R\text{-}MP}$, is given by:

$$r_{R-MP} = \frac{dc_{R-MP}}{dt} = -\frac{v^{f}_{\max,R} \cdot v^{r}_{\max,R}\left(c_{R-MP} \cdot c_{EA} - \dfrac{c_{R-MPA} \cdot c_{EtOH}}{K_{eq,R}}\right)}{D_R} \tag{3.1}$$

with:

$$D_R = v^{r}_{\max,R} \cdot \left[K_{m,R-MP} \cdot c_{EA}\left(1 + \frac{c_{S-MP}}{K_{m,S-MP}} + \frac{c_{EA}}{K_{i,EA}} + \frac{c_{EtOH}}{K_{i,EtOH}}\right)\right.$$

$$+ K^{R}_{m,EA} \cdot c_{R-MP}\left(1 + \frac{K_{m,R-MP}}{c_{R-MP}}\left(\frac{K^{S}_{m,EA}}{K^{R}_{m,EA}} \cdot \frac{c_{S-MP}}{K_{m,S-MP}} + \frac{K_{i,EA}}{K_{m,EA}} \cdot \frac{c_{EtOH}}{K_{i,EtOH}}\right)\right.$$

$$\left.\left. + \frac{K_{i,R-MP}}{c_{R-MP}} \cdot \frac{c_{R-MPA}}{K_{i,R-MPA}} + \frac{c_{R-MPA}}{K_{i,R-MPA}} + \frac{K_{i,S-MP}}{c_{S-MP}} \cdot \frac{c_{S-MPA}}{K_{i,S-MPA}} + \frac{c_{S-MPA}}{K_{i,S-MPA}}\right) + c_{R-MP} \cdot c_{EA}\right]$$

$$+ \frac{v^{f}_{\max,R}}{K_{eq,R}}\left[K_{m,R-MPA} \cdot c_{EtOH}\left(1 + \frac{c_{S-MPA}}{K_{m,S-MPA}} + \frac{c_{EtOH}}{K_{j,EtOH}} + \frac{c_{EA}}{K_{j,EA}}\right)\right.$$

$$+ K^{R}_{m,EtOH} \cdot c_{R-MPA}\left(1 + \frac{K_{m,R-MPA}}{c_{R-MPA}}\left(\frac{K^{S}_{m,EtOH}}{K^{R}_{m,EtOH}} \cdot \frac{c_{S-MPA}}{K_{m,S-MPA}} + \frac{K_{j,EtOH}}{K_{m,EtOH}} \cdot \frac{c_{EA}}{K_{j,EA}}\right)\right.$$

$$\left.\left. + \frac{K_{j,R-MPA}}{c_{R-MPA}} \cdot \frac{c_{R-MP}}{K_{j,R-MP}} + \frac{c_{R-MP}}{K_{j,R-MP}} + \frac{K_{j,S-MPA}}{c_{S-MPA}} \cdot \frac{c_{S-MP}}{K_{j,S-MP}} + \frac{c_{S-MP}}{K_{j,S-MP}}\right) + c_{R-MPA} \cdot c_{EtOH}\right]$$

and:

c_i	compound concentration	(mol·L^{-1})
$K_{eq,a}$	equilibrium constant	(-)
$K_{i,i}$; $K_{j,i}$	inhibition constant	(mol·L^{-1})

$K_{m,i}$	affinity constant	$(mol \cdot L^{-1})$
$v_{max,a}$	maximum conversion rate	$(mol \cdot L^{-1} \cdot s^{-1})$

a = R, S; i = R-MP, S-MP, EA, R-MPA, S-MPA, EtOH

The volumetric rate of the S-enantiomer, $r_{S\text{-}MP}$, can be written accordingly by exchanging the R- and S-prefixes.

The terms in both equations can be recognized as parts corresponding to the forward or reverse reaction. In the nominator, $c_{a\text{-}MP} \cdot c_{EA}$ and $c_{a\text{-}MPA} \cdot c_{EtOH}$ belong to the forward and reverse reaction, respectively. In the denominator, the forward reaction is described by the bracket term $v^{r}_{max,a} \cdot [...]$ and the reverse reaction by $v^{f}_{max,a}/K_{eq,a} \cdot [...]$. The forward and reverse part of the denominator consists of the same effects; therefore the representation of these effects is discussed below only for the forward reaction.

K^{R}_{EA} and K^{S}_{EA} are affinity constants of ethyl acetate, when the R- or S-enantiomer of 1-methoxy-2-propanol is second binding substrate, respectively. Due to the presence of affinity constants of both substrates, MP and EA, the kinetic rate describes both limiting MP and EA concentrations. The concentration profile of ethyl acetate may be calculated using a mass balance, just like those of the products R-MPA, S-MPA and EtOH:

$$c_{EA} = c_{EA,0} - c_{R-MPA} - c_{S-MPA}\,; c_{EtOH} = c_{EA,0} - c_{EA}\,; \tag{3.2a}$$

$$c_{R-MPA} = c_{R-MP,0} - c_{R-MP}\,;\; c_{S-MPA} = c_{S-MP,0} - c_{S-MP} \tag{3.2b}$$

Since the equilibrium of both enantiomers is thermodynamically controlled, both equilibrium constants are identical: $K_{eq} = K_{eq,R} = K_{eq,S}$.

The affinity constants of the first substrate are assumed to be independent of the second substrate in both forward and reverse mode ($K^{R}_{m,EA} = K^{S}_{m,EA}$; $K^{R}_{m,EtOH} = K^{S}_{m,EtOH}$). It should be noted, that competitive inhibition of one direction by one component not necessarily means the same component inhibits the reverse direction as well. Hence, the substrate inhibition constant of the acyl donor of the forward rate, $K_{i,EA}$, may be unequal to the product inhibition constant of the same constant, $K_{j,EA}$ of the reverse reaction. This is for example the case in the kinetic model presented by Shin and Kim, 1998. Inhibition constants for the forward and reverse reaction are denoted by K_i and K_j, respectively.

Since the enzyme loading is not known for commercial immobilized enzyme preparations, the concentration of support with enzyme was used for kinetic measurements. The maximum conversion rate was calculated by:

$$v_{\max,a}^{d} = -k_{cat,a}^{d} \cdot m_{E,imm} \quad \text{with a = R,S and d = f,r} \tag{3.3}$$

where $k_{cat,a}$ is the maximum specific conversion rate ($mol \cdot g^{-1} \cdot s^{-1}$) and $m_{E,imm}$ the dry weight of enzyme particles ($g \cdot L^{-1}$) added per unit of reactor volume.

3.3 Results and Discussion

3.3.1 Model Identification and Parameter Estimation

For the two parallel reversible bimolecular reactions studied here, measurements at different initial rate conditions are performed to obtain a solid data basis for parameter estimation and good model validity over a broad range of substrate and product concentrations. The usual procedure to determine kinetic constants of complex kinetic mechanisms, consisting of selecting extreme measurement conditions and reducing the model equations accordingly (e.g. Segel, 1993), cannot easily be applied to kinetic resolutions. In such procedures, formation of reaction products is mostly neglected, allowing model simplification by removing corresponding reverse and inhibition terms and independent determination of a subset of parameters. In general, only the racemate is commercially available for kinetic studies as the chiral ones are very expensive, if available at all. Therefore, both enantiomer rates have to be measured simultaneously. Neglecting product formation in such cases may lead to incorrect parameter results as such measurement is limited on one hand by the analytical detectability of the slow enantiomer and on the other hand by the extend of conversion of the fast enantiomer.

With that many parameters to be estimated (23 in total), it would not be surprising if the model would show a good fit of experimental data. The resulting parameters, however, could not be trusted. Model discrimination and identification of parameters which show significant contribution is important in model development, especially for models with many parameters. Calculation of the relative error between measurement and model is a helpful tool in this analysis. For example, if this error is not improved significantly upon addition of a parameter to the model, this parameter has no added value. The parameter may not play a role at all or the measurement conditions are not correctly selected.

In addition, Haldane equations, which are relationships between kinetic constants, may be obtained for reversible ping-pong bi-bi mechanisms (Segel, 1993). As these equations

can be directly derived from Cleland's definitions, these equations have to be valid. For the current system, some examples are as follows:

$$K_{eq} = \frac{v^f_{\max,R} \cdot K_{m,R-MPA} \cdot K_{i,EtOH}}{v^r_{\max,S} \cdot K_{m,R-MP} \cdot K_{i,EA}} \tag{3.4a}$$

$$K_{eq} = \frac{v^f_{\max,S} \cdot K_{m,S-MPA} \cdot K_{i,EtOH}}{v^r_{\max,S} \cdot K_{m,S-MP} \cdot K_{i,EA}} \tag{3.4b}$$

$$K_{eq} = \frac{\left(v^f_{\max,R}\right)^2 \cdot K_{m,R-MPA} \cdot K_{m,EtOH}}{\left(v^r_{\max,S}\right)^2 \cdot K_{m,R-MP} \cdot K_{m,EA}} \tag{3.4c}$$

$$K_{eq} = \frac{v^r_{\max,R} \cdot K_{m,R-MP} \cdot K_{j,EA}}{v^f_{\max,S} \cdot K_{m,R-MPA} \cdot K_{j,EtOH}} \tag{3.4d}$$

Many more Haldane equations exist, but they have no added value to the current system as their parameters are already part of above equations. This would lead to redundancies. The easiest way to make sure the Haldane equations are met is by reducing the degree of freedom in parameter estimation by replacing some parameters with above equations. This was done for the current system: $K_{m,R\text{-}MP}$ (3.4a); $K_{m,R\text{-}MP}$ (3.4b); $K_{m,EA}$ (3.4c) and $K_{j,EA}$ (3.4d), respectively.

By comparing the relative error between measurement and model, the inhibition constants of the enantiomers were found to have no significant impact on kinetics (i.e. $K_{i,R\text{-}MP}$, $K_{i,,S\text{-}MP}$, $K_{i,,R\text{-}MPA}$, $K_{i,,S\text{-}MPA}$; $K_{j,,R\text{-}MP}$; $K_{j,S\text{-}MP}$; $K_{j,R\text{-}MPA}$ and $K_{j,S\text{-}MPA}$ were $>>10^4$ M). Assuming $K_{eq} = K_{eq,R} = K_{eq,S}$; $K_{m,EA} = K^R_{m,EA} = K^S_{m,EA}$; $K_{m,EtOH} = K^R_{m,EtOH} = K^S_{m,EtOH}$, this allows reduction of the model equation (3.2) to:

$$\frac{dc_{R-MP}}{dt} = -\frac{v^f_{\max,R} \cdot v^r_{\max,R}\left(c_{R-MP} \cdot c_{EA} - \frac{c_{R-MPA} \cdot c_{EtOH}}{K_{eq}}\right)}{D_R} \tag{3.5}$$

with: $D_R = v^r_{\max,R} \cdot \left[K_{m,R-MP} \cdot c_{EA}\left(1 + \frac{c_{S-MP}}{K_{m,S-MP}} + \frac{c_{EA}}{K_{i,EA}} + \frac{c_{EtOH}}{K_{i,EtOH}}\right)\right.$

$\left. + K_{m,EA} \cdot c_{R-MP}\left(1 + \frac{K_{m,R-MP}}{c_{R-MP}}\left(\frac{c_{S-MP}}{K_{m,S-MP}} + \frac{K_{i,EA}}{K_{m,EA}} \cdot \frac{c_{EtOH}}{K_{i,EtOH}}\right) + c_{R-MP} \cdot c_{EA}\right)\right]$

$$+\frac{v^{f}_{\max,R}}{K_{eq}}\left[K_{m,R-MPA}\cdot c_{EtOH}\left(1+\frac{c_{S-MPA}}{K_{m,S-MPA}}+\frac{c_{EtOH}}{K_{j,EtOH}}+\frac{c_{EA}}{K_{j,EA}}\right)\right.$$

$$\left.+K_{m,EtOH}\cdot c_{R-MPA}\left(1+\frac{K_{m,R-MPA}}{c_{R-MPA}}\left(\frac{c_{S-MPA}}{K_{m,S-MPA}}+\frac{K_{j,EtOH}}{K_{m,EtOH}}\cdot\frac{c_{EA}}{K_{j,EA}}\right)+c_{R-MPA}\cdot c_{EtOH}\right)\right]$$

for the R-enantiomer. The rate of the S-enantiomer is obtained similarly by exchanging 'R' for 'S'-indices in Equation (3.5).

This model is schematically shown using a King-Altman plot (Scheme 3.3). By applying the Haldane equations, eleven parameters have to be estimated: $v^{f}_{max,R}$; $v^{f}_{max,S}$; $K_{i,EA}$; $K_{i,EtOH}$; $v^{r}_{max,R}$; $v^{r}_{max,S}$; $K_{m,R-MPA}$; $K_{m,S-MPA}$; $K_{m,EtOH}$; $K_{j,EtOH}$ and K_{eq}. The equilibrium constant K_{eq} is first determined from measurements for t->∞ starting with mixtures of different substrate concentrations of MP - EA as well as MPA - EtOH. The result is 0.1 < Keq < 0.3. In parameter estimation, the equilibrium constant is allowed to vary within this range.

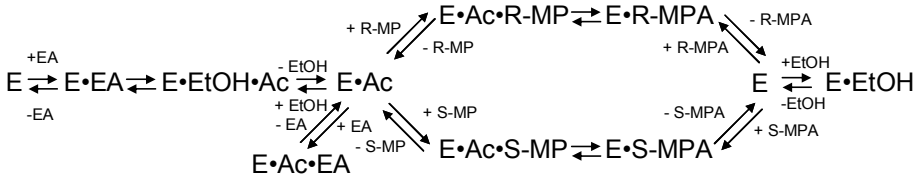

Scheme 3.3 King-Altman plot of an irreversible ping-pong bi-bi mechanism including competitive inhibition by both enantiomers and substrate inhibition by EA and EtOH.

For estimation of the remaining eleven parameters of Equation (3.5), the model is fitted simultaneously to the complete data set presented in Figures 3.1-3.5. In order to identify the global minimum, more than one set of initial guesses of the kinetic constants are used to check if a better fit has not been overlooked. These initial guesses and constraints for the parameter values are selected based on prior experience with kinetic resolution reactions (Berendsen, et al., 2006a; Berendsen, et al., 2006b).

The model describes the different types of independent measurements relatively good with the parameters listed in Tables 3.1 and 3.2. The model equations for the R- and S-enantiomer, Equation (3.5), are highly interrelated due to the presence of the same parameters in both equations. Changes in one parameter thus strongly influence both reaction rates. It makes accurate measurement of both rates crucial, as inaccuracies in the determination of the conversion of one enantiomer impacts modeling of the other also.

Table 3.1 Estimated kinetic parameters (30°C) using the data set presented in Figures 3.5-3.9.

$k^f_{cat,R}$	1.10E-03	$(mol \cdot g^{-1} \cdot s^{-1})$	$k^f_{cat,S}$	8.80E-07	$(mol \cdot g^{-1} \cdot s^{-1})$
$k^r_{cat,R}$	8.30E-05	$(mol \cdot g^{-1} \cdot s^{-1})$	$k^r_{cat,S}$	6.00E-07	$(mol \cdot g^{-1} \cdot s^{-1})$
$K_{i,EA}$	5.00E-02	$(mol \cdot L^{-1})$	$K_{i,EtOH}$	1.20E-03	$(mol \cdot L^{-1})$
$K_{m,R-MPA}$	1.00E-02	$(mol \cdot L^{-1})$	$K_{m,S-MPA}$	5.70E-03	$(mol \cdot L^{-1})$
$K_{m,EtOH}$	1.00E-02	$(mol \cdot L^{-1})$	$K_{j,EtOH}$	1.20E-03	$(mol \cdot L^{-1})$
K_{Eq}	2.50E-01	(-)			

Table 3.2 Calculated parameters using Haldane equations based on the data set shown in Figures 3.5-3.9.

$K_{m,R-MP}$	1.20E-02	$(mol \cdot L^{-1})$
$K_{m,EA}$	5.4	$(mol \cdot L^{-1})$
$K_{m,S-MP}$	8.10E-04	$(mol \cdot L^{-1})$
$K_{j,EA}$	3.10E-03	$(mol \cdot L^{-1})$

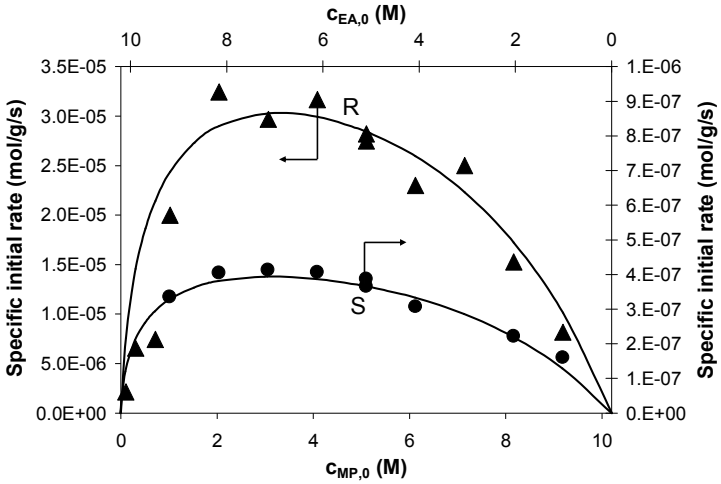

Figure 3.1 Specific initial rate of R- and S-enantiomer in the forward reaction at varying initial MP- and EA- concentrations (solid lines: model, dots: experiments; triangles: R-MPA, circles: S-MPA).

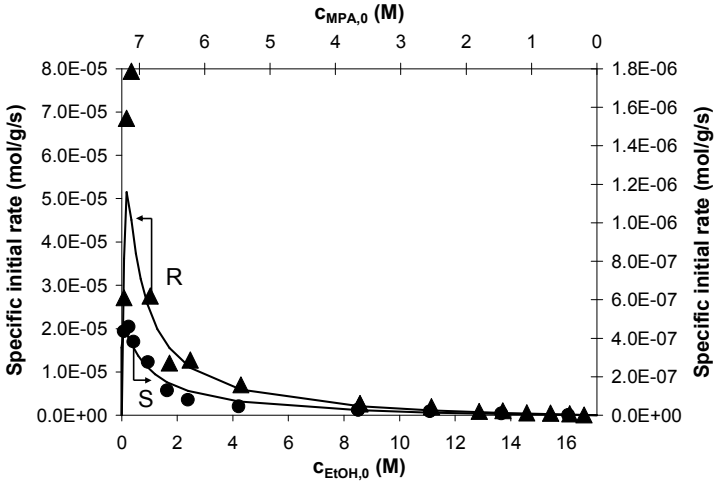

Figure 3.2 Specific initial rate of R- and S-enantiomer in the reverse reaction at varying initial MPA- and EtOH-concentrations (solid lines: model, dots: experiments; triangles: R-MP, circles: S-MP).

When using MP and EA as substrates, the specific initial reaction rate shows a maximum for varying initial concentrations (Figure 3.1). This maximum is located at similar concentrations for both enantiomers. A difference of several orders of magnitude in R- and S-enantiomer rate can be observed, resulting in the enantioselectivity of the reaction.

The influence of EtOH and MPA on the reaction rate is investigated by varying MPA and EtOH concentrations (Figure 3.2). Just like the measurements with EA and MP, the specific initial rate shows a maximum. Here however, this maximum is present at very low EtOH- (or very high MPA-) concentrations. This typical curve progression is mainly caused by a very low value of $K_{j,EtOH}$, i.e. strong substrate inhibition of the reverse reaction rate by ethanol.

In order to improve parameter sensitivity regarding ethanol and ethyl acetate, measurements were performed with varying initial ethanol and ethyl acetate concentrations at constant EA – MP and EtOH-MPA-concentrations, respectively (Figures 3.3 and 3.4). A strong decrease in forward reaction rate is observed with increasing initial ethanol concentrations (Figure 3.3). According to the model, this effect is caused both by product inhibition by ethanol as well as by the reversibility of the reaction. The same causes reduce the reverse rate at increasing ethyl acetate concentrations (Figure 3.4). Ethanol has however a much stronger impact than ethyl acetate.

The effect of variations in product concentrations on forward and reverse reaction rates is studied as well, i.e. changes in MPA on forward rate and variations of MP on reverse reaction rate (Figure 3.5). An increase in product concentration decreases corresponding reaction rates. The effect of MPA on the forward reaction rate is much stronger than the one caused by MP on the reverse reaction rate. According to the model and initial tests of parameter sensitivity, solely the reversibility of the reaction rates but not inhibition appears to be responsible for this behavior.

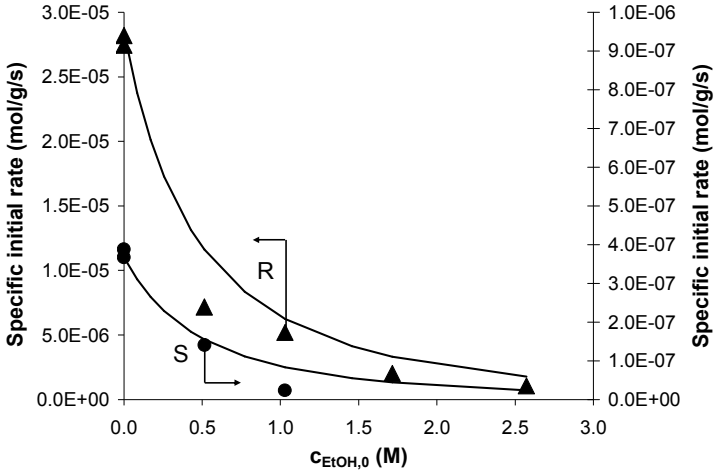

Figure 3.3 Specific initial rate of R- and S-enantiomer in the forward reaction at varying initial EtOH-concentrations (MP_0 : EA_0 = 1 : 1 (v/v), solid lines: model, dots: experiments; triangles: R-MPA, circles: S-MPA).

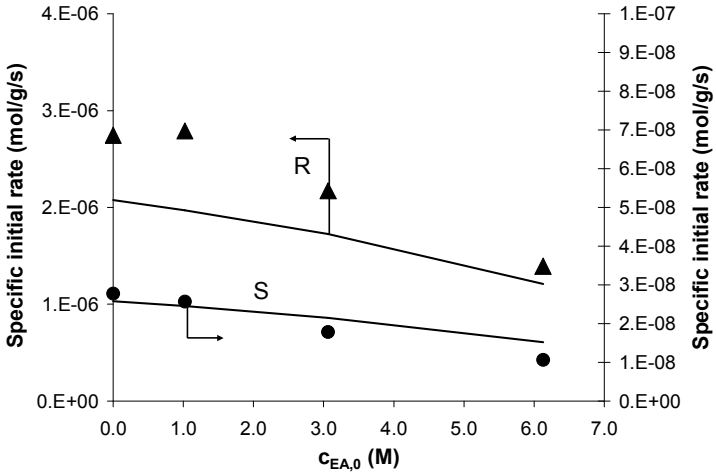

Figure 3.4 Specific initial rate of R- and S-enantiomer in the reverse reaction at varying initial EA-concentrations (MPA_0 : $EtOH_0$ = 1 : 1 (v/v), solid lines: model, dots: experiments; triangles: R-MP, circles: S-MP).

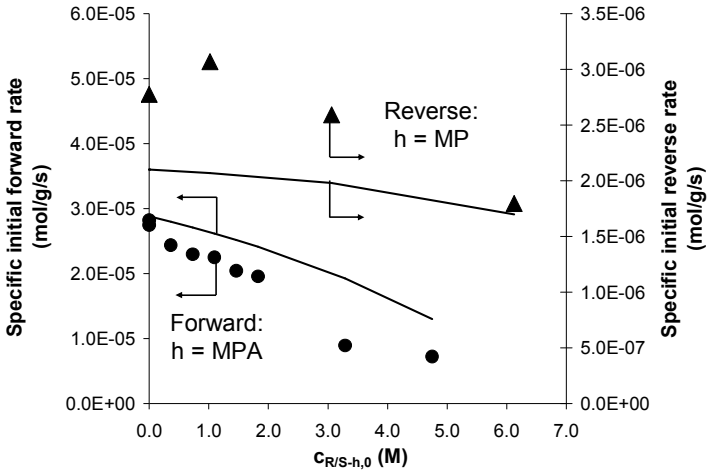

Figure 3.5 Specific initial forward and reverse rate of EtOH and EA at varying initial concentrations of MPA and MP, respectively (forward reaction: i=R/S-MPA, MP_0 : EA_0 = 1 : 1 (v/v); reverse reaction: i=R/S-MP, MPA_0 : $EtOH_0$ = 1 : 1 (v/v); solid lines: model, dots: experiments; triangles: EA, circles: EtOH).

For demonstration, the developed model for this kinetic resolution system is employed for a fixed bed reactor, which is part of a fully-automated miniplant, by comparing experimental results with simulations consisting of a one-dimensional homogeneous reactor model. The mass balance for this system is as follows:

$$\frac{dc_i}{dt} + u_0 \cdot \frac{dc_i}{dx} = -r_i \quad \text{with i = R-MP, S-MP, EA, R-MPA, S-MPA and EtOH.} \tag{3.6}$$

With:

t	time	(s)
u_0	superficial velocity	($m \cdot s^{-1}$)
x	distance from reactor inlet	(m)

Since miniplant experiments are time-intensive, the behavior of the reactor model is investigated first using simulations. Usually, a plot of the enantiomeric excess (e.e.h) versus conversion (ξ_h) is used for evaluation of kinetic resolutions. These quantities are defined by:

$$e.e._h = \left| \frac{c_{R-h} - c_{S-h}}{c_{R-h} + c_{S-h}} \right| \text{ with h = MP, MPA} \tag{3.7}$$

$$\xi_h = \frac{c_{R-h,0} - c_{R-h} + c_{S-h,0} - c_{S-h}}{c_{R-h,0} + c_{S-h,0}} \text{ with cR-h,0>0, cS-h,0>0, h = MP or MPA} \tag{3.8}$$

The impact of enantiomeric excess on conversion is simulated for varying initial substrate concentrations at steady state conditions (Figure 3.6). The e.e. of the product (MPA) starts at a relative high value caused by large differences in initial reaction rates of the R- and S-enantiomer. With increasing conversion, the $e.e._{MPA}$ decreases slowly up to a certain point and then drops quickly. This effect can be explained by the reversibility of the reaction. The faster enantiomer reaches equilibrium sooner. As the faster enantiomer comes closer to equilibrium its conversion is more and more reduced, while the conversion of the slower enantiomer continues. At higher initial MP (and lower EA) concentrations, this effect occurs at lower conversion. This is due to the reduced availability of EA to drive the reaction to the product side and the increase in substrate MP to be converted into enantiopure product.

As the initial substrate mixture is racemic, $e.e._{MP} = 0$ for $\xi_{MP} = 0$. As one enantiomer is converted, the other (here S-MP) remains and the $e.e._{MP}$ increases. This occurs until the faster enantiomer reaches equilibrium after which only the slower enantiomer reacts, resulting in a maximum in $e.e._{MP}$ vs. ξ_{MP}-profile. This maximum is lower for higher initial MP concentrations, due to less available EA for driving the reaction to the product side and more MP substrate to be converted in enantiopure product.

For verification of the reactor model including kinetics, a mixture of 5% mol/mol MP in EA as starting substrates is selected for miniplant studies (Figure 3.7). The typical maximum in e.e. of MP is observed experimentally also. In addition, the complete model describes the experimental data nicely.

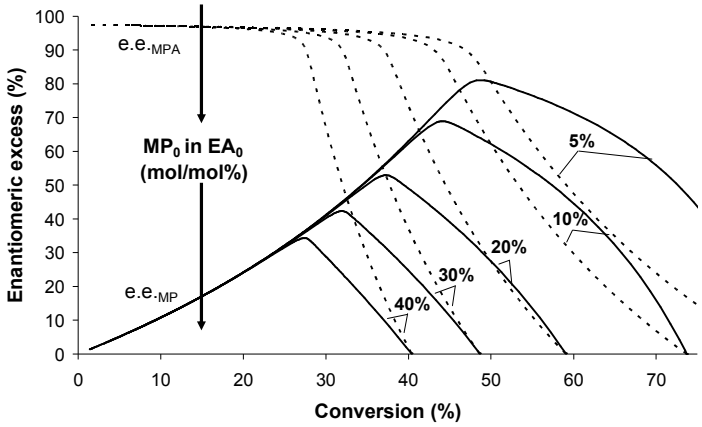

Figure 3.6 Enantiomeric excess versus conversion for substrate MP (solid lines) and product MPA (dotted lines) at different initial MP and EA concentrations.

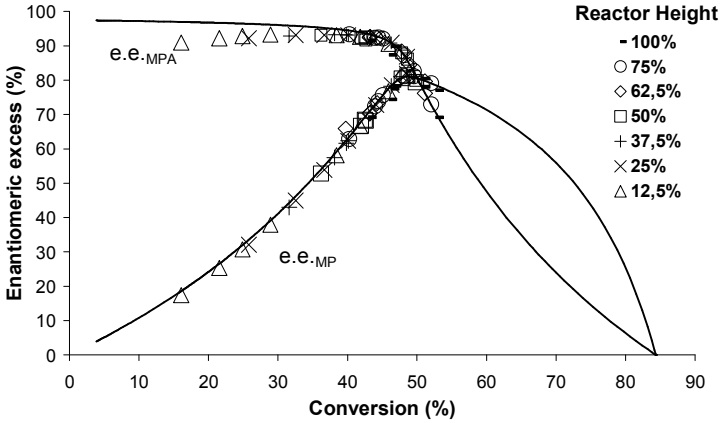

Figure 3.7 Verification of reactor model with experiments in a miniplant fixed bed reactor ($c_{MP,0}$ = 0.5M, $c_{EA,0}$ = 9.7M, solid lines: model, dots: experiments).

3.4 Conclusions

A kinetic model is proposed for the reversible bimolecular kinetic resolution of 1-methoxy-2-propanol with ethyl acetate catalyzed by *Candida antarctica* lipase B. The model takes into account the full reversibility of the reaction, competitive inhibition by both enantiomers and substrate inhibition by an acyl donor and an acyl acceptor. Six types of independent initial rate studies form a solid basis for the model, which has a broad validity regarding substrate and product concentrations. In order to determine sensitive parameters, the model is reduced following model discrimination and the use of Haldane equations.

The independent initial rate studies improve not only the understanding of reaction kinetics; they can be utilized for modeling and simulation as shown in this chapter to allow further interpretation of results. Using the typical plot of the enantiomeric excess ($e.e._i$) versus conversion of racemic substrate the effect of initial substrate concentration on the maximum achievable enantioselectivity is discussed. The position of the reaction equilibrium directly determines the conversion of the faster enantiomer and thus the enantioselectivity of the reaction. While reducing the initial concentration of racemic substrate improves achievable enantiomeric excess, it also significantly impacts the economical viability of the process as the end concentration of the product decreases also. Therefore, the equilibrium constant is a critical parameter in reversible kinetic resolutions and should be among one of the first parameters analyzed during screening of potential substrates for an industrial process. Removing one of the reaction products, such as the byproduct ethanol, from the reaction mixture may overcome the equilibrium limitation and increase end product concentration. The possibility to use pervaporation for this purpose has been investigated (Berendsen et al., 2006c).

The reactor simulations are verified by experiments performed in a fixed bed reactor, which was part of a fully automated state-of-the-art miniplant. The concept of miniplant technology is well-known in chemical industry, but less common in biocatalysis. Next to the ability to provide a solid data basis for model verification as has been applied here, the combination of miniplants, modeling and simulation offers the opportunity to mimic technical processes at the smallest scale. The integrated application of these technologies should accelerate future development of biocatalytic reactions in general towards industrial processes. To ensure its successful application, the use of a modular set-up and standardized components is required to provide plant flexibility towards process changes, ranging from changes in reactor configuration to process alternatives involving different unit operations.

4

Pervaporative Separation of Ethanol from an Alcohol – Ester Quaternary Mixture

Published in:

Berendsen, W. R., Radmer, P., Reuss M. (2006c)

Journal of Membrane Science, **280**, 684-692, DOI:10.1016/j.memsci.2006.02.029.

Abstract

As part of a research project focusing on the development of a sustainable biocatalytic process for production of chiral secondary alcohols, the pervaporative separation of ethanol from ethanol / ethyl acetate / 1-methoxy-2-propanol / 1-methoxy-2-propyl acetate – mixtures through a commercial PVA-based membrane was investigated. Separation behavior of this mixture was studied in a range of mol fractions (10-70%), temperatures relevant for biocatalytic conversions (35-55°C) and downstream pressures (35-200 mbar).

Pervaporation of the non-diluted multicomponent mixture was shown to be strongly influenced by interactions between the permeants and the membrane. Investigation of these interactions contributed to the understanding of the mass transport mechanism of this mixture. Overall, high fluxes were obtained, but small differences between the fastest permeating species were found. The fastest permeating species was ethanol, ethyl acetate or 1-methoxy-2-propanol depending on the feed composition.

4.1 Introduction

Much research has been done in the area of pervaporation, resulting in applications such as removal of organic compounds from aqueous solutions, dehydration of organic – water mixtures and separation of organic – organic mixtures. While the first two are state-of-the-art to date, the latter technology is only recently receiving more attention. Most papers in this area focus on the pervaporation of methanol – methyl *tert*-butyl ether, ethanol – ethyl tert-butyl ether and benzene – cyclohexane mixtures. For a good overview of the latest research activities in this area the reader is referred to the review paper of Smitha et al. (2004).

Most of the work reported up to now deals with the study of binary or pseudo multicomponent systems – i.e. where pervaporation of all but one component is negligible (Ji et al., 1994; Park, 2004). Sometimes, the membrane is also included in this notation, e.g. a ternary or multicomponent system is in such cases in reality a binary mixture with a membrane (Ghoreyshi, et al., 2002; Jonquières et al., 1996; González and Uribe, 2001). While this may be confusing, it points out that research to improve the understanding of real multicomponent pervaporation and the occurrence of coupling effects between the components themselves and the membrane is needed.

The pervaporation of multicomponent mixtures is especially interesting for biochemical kinetic resolution processes, in which the extent of conversion is limited by the reaction equilibrium. For example, in the case of *Candida antarctica* lipase B catalyzed transesterification of 1-methoxy-2-propanol with ethyl acetate into ethanol and 1-methoxy-2-propyl acetate, the equilibrium limitation may be overcome by removal of one of the reaction products. This work reports experimental results on the pervaporative separation of the quaternary system: 1-methoxy-2-propanol (MP) – ethyl acetate (EA) – 1-methoxy-2-propyl acetate (MPA) – ethanol (EtOH) using the commercial membrane Pervap 2256®. This membrane was previously applied for the separation of methanol - methyl *tert*-butyl ether, as well as ethanol – ethyl *tert*-butyl ether mixtures, allowing high alcohol flux values as well as high permeate selectivities Jonquières et al., 1996; González and Uribe, 2001; Sridhar, et al., 2005). The behavior of partial fluxes and mol fractions as a result of changes in feed composition and temperature is investigated. The influence of flow coupling and plasticizing effects on pervaporation is investigated by using a model derived from literature.

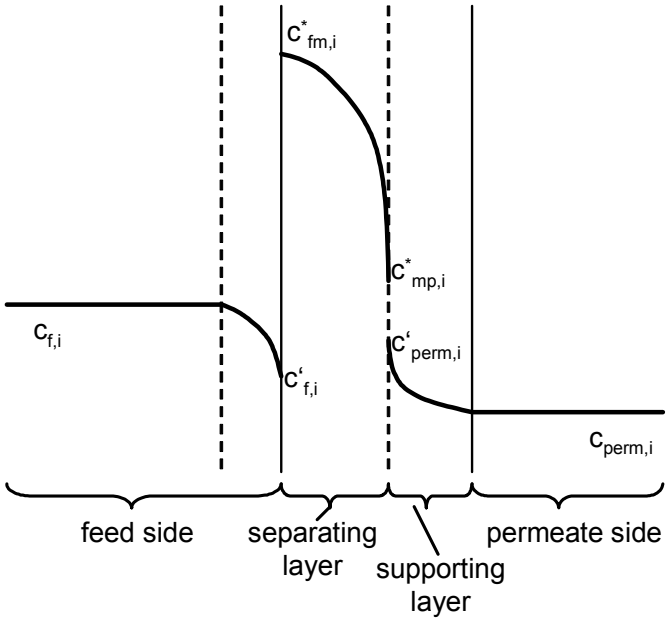

Scheme 4.1 Schematic representation of mass transport through a pervaporation membrane.

4.2 Theory

A five-step mechanism is usually considered to describe mass transfer of a species through a membrane by pervaporation. The species first transfer from the bulk of the liquid into the feed-membrane boundary layer. Then, they sorb into the membrane and diffuse through each layer to the downstream side. In the next step, they desorb from the membrane and diffuse from the membrane-vapor boundary layer into the vapor bulk (see Scheme 1). When the flow on the feed side is turbulent, the first step may be neglected. This is assumed for the stirrer equipped membrane cell used in this study. Because the downstream pressure is very low and the vapor is assumed to be ideal gas, steps four and five may be neglected too. The remaining two-steps are often combined into the “solution-diffusion-theory”.

4.2.1 Models Based on the Concentration Gradient as the Driving Force for Mass Transport

Many different approaches for modeling mass transfer by pervaporation have been used. Very often, these models are based on Fick's first law, which describes the diffusion of a component along its concentration gradient over a certain length, z, while assuming thermodynamic ideality:

$$J_i = -D_i \cdot \frac{dc_i}{dz} \tag{4.1}$$

c_i	concentration of component i inside the membrane	(mol·m^{-3})
D_i	Fick diffusion coefficient of component i	(m^2·s^{-1})
J_i	pervaporation flux of component i	(mol·m^{-2}·s^{-1})
z	distance of diffusion	(m)

In case of diffusion of a component i through a quaternary mixture, the flux of component i may depend on the sorption of the other components in the mixture, and their corresponding concentrations:

$$J_i = -\sum_{j=1}^{4} D_{i,j} \cdot \frac{dc_j}{dz} \text{ with i = 1 – 4.} \tag{4.2}$$

In addition, diffusion coefficients themselves depend strongly on the concentration of the components. Various empirical relationships have been described in the literature to take this effect into account. One of the first was Greenlaw's model (Greenlaw et al., 1977), who described the pervaporation of the binary hexane/heptane mixture through polyethylene films with the equation:

$$D_i = B_i \cdot \left(c_i + B_{ij} \cdot c_j\right) \text{ with i = 1,2} \tag{4.3}$$

B_i, B_{ij}	adjustable parameters	(L·mol^{-1})

Extending this model for a multicomponent mixture with n components results in the following equation, which describes the diffusion coefficient of component i by means of m·n adjustable parameters:

$$D_i = B_i \cdot \left(c_i + \sum_{j=1}^{n} B_{ij} \cdot c_j \right) \text{ with i = 1, 2, 3, ...m} \qquad (4.4)$$

Another empirical equation often used to describe the diffusion coefficient in a multicomponent mass transfer, is the exponential relationship originally introduced by Brun et al. (1985).

$$D_i = D_{0,i} \cdot \exp\left(\sum_{j=1}^{n} B_{ij} \cdot c_j \right) \text{ with i = 1, 2, 3, ...m} \qquad (4.5)$$

$D_{0,i}$ Pure component Fick diffusion coefficient in membrane ($m^2 \cdot s^{-1}$)

This equation offers the opportunity to analyze the effect of coupling between permeants, i.e. a negative or positive value of the interaction constants means the presence of one component hampers or improves mass transport of another component. This phenomenon is called flow coupling and may be divided into two parts: thermodynamic and kinetic flow coupling. The thermodynamic part, the change in concentration of one component due to the presence of another, is caused by non-ideality of the mixture in the membrane. The kinetic part resembles the interaction of the individual compounds between the membrane polymer, resulting in structural changes of the polymer and ultimately in concentration dependent diffusion. While the empirical equations (4.3) and (4.4) do not specifically take thermodynamic flow coupling into account, these equations have been applied with good success, even for cases which deviate strongly from ideality.

4.2.2 The Challenge of Choosing the Right Boundary Conditions

For composite membranes, which consist of more than one layer, all layers may impact diffusion of the permeants. Assuming the rate-limiting step of diffusion is the separating layer, Equation (4.2) can be solved numerically using the following expression:

$$J_i = -\frac{1}{l}\sum_{j=1}^{4}\int_{c^*_{fm,j}}^{c^*_{mp,j}} D_{i,j}\cdot dc_j \quad \text{with i = 1 – 4.} \tag{4.6}$$

l	membrane thickness of separating layer	(m)

Since Equation (4.6) describes the concentration profile inside a membrane, boundary conditions are needed to relate the concentration at the feed – membrane surface, $c^*_{fm,i}$, and the membrane – permeate surface, $c^*_{mp,i}$, with measurable quantities in feed and permeate. Different approaches have been reported, but their application may not be suited for multicomponent pervaporation with commercial membranes. The most straightforward solution is to assume the feed-membrane and membrane-permeate interface concentrations are equal to the bulk feed and permeate concentrations, respectively (Nagy, 2004) and to use the measured concentrations in the condensate for $c_{p,i}$:

$$c^*_{fm,i} = c_{f,i} \;;\; c^*_{mp,i} = c_{perm,i} \tag{4.7}$$

$c_{k,i}$	concentration of component i	(mol·m^{-3})

Subscripts k: fm = feed – membrane interface; f = feed; mp = membrane-permeate; perm = permeate

Marx et al. (2002) used this assumption to obtain a very rough estimate of the diffusion coefficients of methanol and tert-amyl methyl ether for pervaporation through a Pervap 2256® membrane. This only works if $c_{perm,i} > c_{f,i}$, because otherwise negative diffusion coefficients are needed to obtain a positive flux for a certain component. Multicomponent diffusion may cause uphill diffusion, the diffusion of a component up its own concentration gradient (Nishiyama, 1998), which would cause the diffusion coefficient to become negative. On one hand, this effect may occur in pervaporation to a certain extent. On the other hand, negative diffusion coefficients are not very likely, since the concentration of the permeants on the vapor downstream side should be very low due to the low pressure. This leads to another boundary condition for the permeate side (Urtiaga, et al., 2002):

$$c^*_{mp,i} = 0 \tag{4.8}$$

Other authors have solved the challenge of choosing the right boundary conditions by considering the difference in activity of as driving force and extending the classic Fick laws to thermodynamic ones (González and Uribe, 2001; Meuleman, 1999):

$$J_i = -\sum_{j=1}^{4} D_{i,j} \cdot \frac{d\mu_j}{dz} = -\frac{1}{l}\sum_{j=1}^{4} \int_{a^*_{fm,j}}^{a^*_{mp,j}} D_{i,j} \cdot d \ln a_j \tag{4.9}$$

a_j	activity of component j	(-)
μ_j	chemical potential of component i	(-)

At thermodynamic equilibrium, the activity of the feed-membrane and membrane-permeate interfaces are equal to the activity of the liquid feed and permeate, respectively:

$$a^*_{fm,i} = a_{f,i} = \gamma_{f,i} \cdot c_{f,i} \tag{4.10}$$

$$a^*_{mp,i} = a_{p,i} = \frac{p_{perm} \cdot y_{perm,i}}{p^s_{f,i}} \tag{4.11}$$

p_{perm}	downstream pressure in the permeate	(Pa)
$p^s_{f,i}$	saturated partial pressure of component i in the feed	(Pa)
$y_{perm,i}$	mole fraction of component i in the permeate	(mol·mol^{-1})
$\gamma_{f,i}$	activity coefficient of component i in the feed	(-)

In general, the activities of the components inside the membrane will be a function of the permeant volumes, resulting in the following equation:

$$J_i = -\sum_{j=1}^{4} \int_0^l \phi_j \cdot D_{i,j} \cdot \left(\frac{d \ln a_j}{d\phi_j} \right) \frac{d\phi_{v,j}}{dz} \tag{4.12}$$

$\phi_{v,i}$:	permeant volume fraction in the membrane polymer	(m^3/m^3)

In order to apply Equations (4.10)-(4.12), the volume fraction of the permeants in the membrane need to be known, which is dependent on sorption behavior of the components. This may be done by using the ENSIC model, which describes polymer swelling as a result of changes in composition across the membrane (Favre et al., 1996):

$$\phi_i = \frac{k_2}{k_1 - k_2} \cdot \left(e^{a_i \cdot (k_1 - k_2)} - 1 \right) \tag{4.13}$$

Hence, this requires the preliminary determination of sorption thermodynamics. For a commercial composite pervaporation membrane, such sorption studies are difficult to analyze, as it is impossible to separate the sorption characteristics of the permeants in each layer. More specifically, sorption of the components in supporting layers will overshadow the sorption behavior occurring in the separation layer, as the latter layer is usually as small as possible to obtain good fluxes.

4.2.3 Models Based on the Pressure Gradient as the Driving Force for Mass Transport

Next to the activity and concentration gradients in the membrane, other driving forces play an important role during pervaporation, such as the transmembrane pressure difference. Emanating from this driving force, the expression for the permeation flux of compound i through a membrane can be derived as:

$$J_i = \frac{P_i}{l} \cdot \left(p_{f,i} - p_{perm,i} \right) \tag{4.14}$$

with:

$p_{f,i}$:	partial pressure of component i in the liquid feed	(Pa)
P_i:	permeability coefficient of component i	($mol \cdot m^{-1} \cdot s^{-1} \cdot Pa^{-1}$)
$p_{perm,i}$:	partial pressure of component i in the vapor permeate	(Pa)

As has been reported by numerous authors, the permeance of a component generally exhibits a linear relationship between the logarithmized permeance versus the reciprocal temperature, i.e. (e.g. Feng and Huang, 1996):

$$J_i = \frac{P_{0,i}}{l} \cdot e^{-\frac{E_{a,i}}{R \cdot T}} \cdot \left(p_{f,i} - p_{perm,i}\right) \tag{4.15}$$

with:

$E_{act,i}$	activation energy of pervaporation	($J \cdot mol^{-1}$)
$P_{0,i}$	permeability constant of component i	($mol \cdot m^{-1} \cdot s^{-1} \cdot Pa^{-1}$)
R	gas constant	($J \cdot mol^{-1} \cdot K^{-1}$)
T	temperature	(K)

Since both the permeability constant, $P_{0,i}$, and the membrane thickness, l, do not change for any given membrane, they may be lumped together in one permeance constant, P':

$$\frac{P_{0,i}}{l} = P'_{0,i} \tag{4.16}$$

$P'_{0,i}$:	lumped permeance constant of component i	($mol \cdot m^{-2} \cdot s^{-1} \cdot Pa^{-1}$)

When the partial saturation pressure of each compound is determined with an Antoine equation and the activity coefficients are approximated by e.g. the UNIFAC method, the difference in partial pressure across the membrane , ($p_{f,i}$ - $p_{p,i}$), may be calculated as follows:

$$\left(p_{f,i} - p_{perm,i}\right) = x_{f,i} \cdot \gamma_{f,i} \cdot p^s_{f,i} - y_{perm,i} \cdot p_{perm} \tag{4.17}$$

with:

$x_{f,i}$:	mole fraction of component i in the feed	($mol \cdot mol^{-1}$)

4.3 Results and Discussion

4.3.1 Dynamic Behavior of Mass Transport Through Pervap 2256® Membranes

When a membrane is used for the first time in a pervaporation system, a certain period is generally needed for adaptation of mass transfer through the membrane, before the operation reaches a steady state. This is often referred to as conditioning behavior. Conditioning behavior can last from minutes to several days, depending on the membrane material, feed conditions and initial state of the polymer (i.e. dry or preswollen) (Neel, 1991). While the dynamic adaptation of initial dry membranes may be interesting from an academic point of view, as it gives information about the interactions between the polymer and the permeating species, it is not important for an industrial process as it occurs only once: at plant start-up. Instead, the dynamic response of a pervaporation membrane to changes in feed conditions during operation is more interesting, especially when the separation step is integrated with a (bio)-chemical reaction or distillation unit operation. A slow membrane adaptation may in such cases hamper the stability of such integrated systems (Jacobsen and Skogestad, 1994).

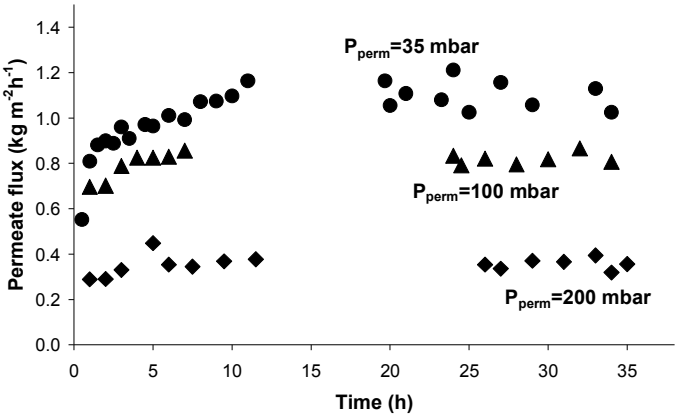

Figure 4.1 Dynamic behavior of the permeate flux through a Pervap 2256® membrane at P_{perm} = 35 mbar (circles), P_p = 100 mbar (triangles) and P_{perm} = 200 bar (diamonds) at 40°C and x_{EtOH} = 8 %, x_{EA} = 40 %; x_{MP} = 39 %; x_{MPA} = 13 %.

In case of Pervap 2256® membranes, both kinds of dynamic behavior were found to be significant for the separation of methanol / methyl *tert* butyl ether - and ethanol / ethyl *tert* butyl ether – mixtures (González and Uribe, 2001; Ortiz et al., 2002). For the EtOH/EA/MP/MPA-mixture, the adaptation of the membrane is presented in Figure 4.1, exemplary showing typical dynamic measurements at various downstream pressures. Although the first time adaptation is significant (12h), it is not as high as found for other separations with the same membrane (Ortiz et al., 2002). After the membrane is conditioned for the first time, shorter times are needed to reach steady state for subsequent changes in feed composition, system temperature or downstream pressure. Although the times needed for pervaporation stabilization are more significant for drastic changes, like decreasing the downstream pressure from 200 to 100 mbar, than reported by Rautenbach and Hömmerich (1998) for polyvinyl alcohol membranes (5h), they were barely or not noticeable for smaller changes, such as changes in feed composition (<1h). Therefore, these dynamic effects are not important for industrial process design considerations, but they should be carefully checked for each application to ensure that pervaporation measurements are really performed at steady state conditions.

4.3.2 Effect of Feed Composition on Permeation Behavior

The effect of changes in feed composition on pervaporative separation is studied by varying the mol fraction of component i in the feed, while keeping the others at equal ratio at fixed feed temperature and permeate pressure. From the Figures 4.2a and 4.2b, it is evident that an increase in mol fraction of component i results in an increase in permeate mol fraction of the same component. At $x_{f,i}$=0.25, all components are present at equal mol fraction. The mol fraction of the components in the permeate increases in the order of ethanol > ethyl acetate > 1-methoxy-2-propanol > 1-methoxy-2-propyl acetate (i.e. 0.42, 0.3, 0.17, 0.05, respectively). Thus, at this condition, the compound which should be removed from the reaction mixture to drive the reaction equilibrium is separated most. To our knowledge, no papers exist up to now about pervaporation of ethanol from binary ethanol - ethyl acetate mixtures. The separation of ethyl acetate from the same binary mixture has been reported by Ozdemir et al. using polyethylene- and polyethylene terepathalate membranes and by Hasanoğlu et al through polydimethylsiloxane membranes (Ozdemir, et al., 1999; Hasanoğlu, et al., 2005). Low values in separation factors are found by these authors, indicating that the separation of this mixture is not yet state-of-the-art and offers potential for further research.

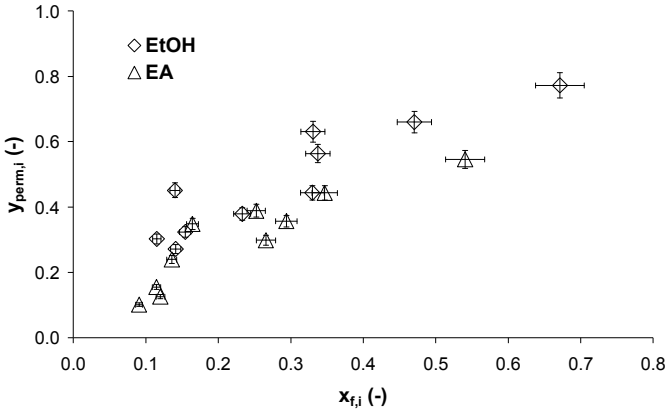

(a)

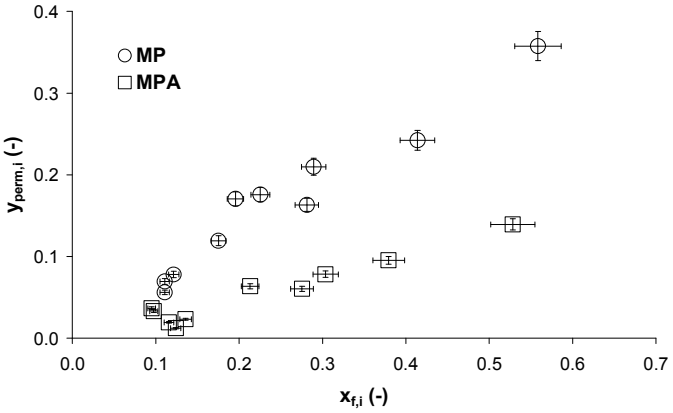

(b)

Figures 4.2a and b Experimental values of permeate vs. feed mole fraction of EtOH, EA, MP and MPA at steady state conditions (T=35°C; Pperm = 35 mbar; error bars: 5%).

The mass transfer mechanism through the membrane is complex because of the high number of interactions between the liquid feed components themselves and the membrane polymer. By combining the flux equations, which are based on pressure as driving force, Equations (4.15)-(4.17), the following equation may be obtained for the molar flux in a multicomponent mixture:

$$J_i = P'_{0,i} \cdot e^{-\frac{E_{a,i}}{R \cdot T}} \cdot \left(x_{f,i} \cdot \gamma_{f,i} \cdot p^s_{f,i} - y_{perm,i} \cdot p_{perm} \right) \tag{4.18}$$

whereas the permeability constant may be defined as a function of coupling and plasticizing effects similar to Equations (4.3)-(4.5):

$$P'_{0,i} = P''_{0,i} \cdot \exp\left(\sum_{j=1}^{n} B_{ij} \cdot c_j \right) \tag{4.19}$$

The presence of a component in the membrane may cause membrane swelling. This phenomenon is also called the plasticizing effect. This effect is represented by interaction parameters, B_{ij}, when i = j (Jiraratananon et al., 2002). Positive interaction parameters correspond to a positive plasticizing effect. For $i \neq j$, the interaction parameters represent the influence of the components on mass transport of each other. A positive value here means a positive effect of the component on the flux of another.

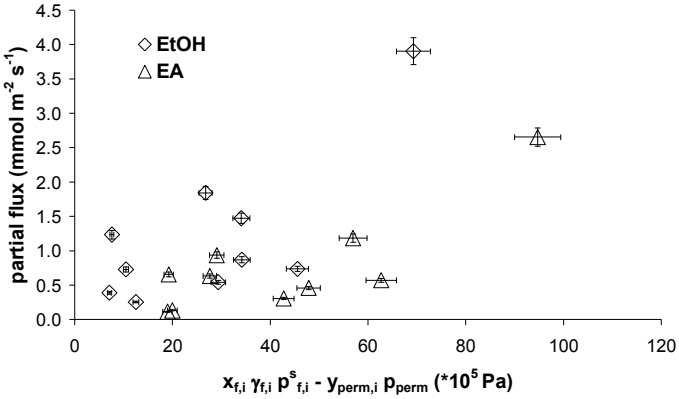

(a)

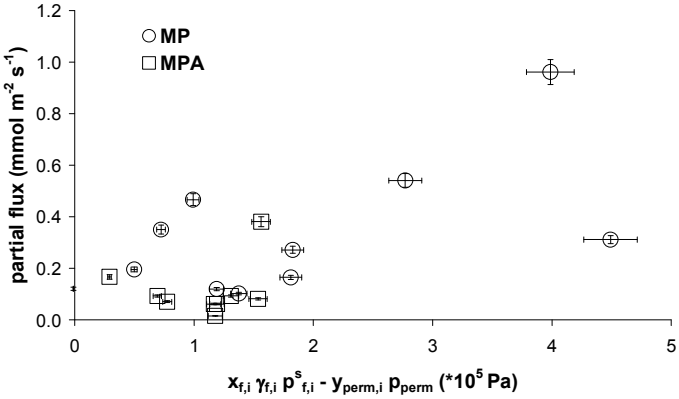

(b)

Figures 4.3a and b Checking if a linear relationship exists for EtOH, EA, MP and MPA.

Equations (4.18) and (4.19) can be used to determine if flow coupling and plasticizing effects play a role during pervaporation of the quaternary mixture through the Pervap 2256 membrane. This is evident from a plot showing individual fluxes versus $\left(x_{f,i} \cdot \gamma_{f,i} \cdot p^{s}_{f,i} - y_{perm,i} \cdot p_{perm}\right)$ at fixed temperature and downstream pressure. If this plot shows a straight line, these effects may be considered negligible and each component only permeates because of its own driving force. The activity coefficients, $\gamma_{f,,i}$, and the saturated partial pressure, $p^{s}_{f,,i}$, of each permeating compound is calculated using the UNIFAC method and Antoine equations, respectively. As is evident from Figures 4.3a and 4.3b, the partial flux of each component does not show a linear relationship versus $\left(x_{f,i} \cdot \gamma_{f,i} \cdot p^{s}_{f,i} - y_{perm,i} \cdot p_{perm}\right)$, i.e. the flux is strongly influenced by the presence of the other components through flow coupling and plasticizing effects. The activity coefficient is close to unity for used mol fractions (1 - 1.3). This indicates that thermodynamic flow coupling does not play a significant role in this multicomponent system.

The exact quantification of kinetic flow coupling and plasticizing effects would require the estimation of the individual interaction parameters, B_{ij}. Estimation of these parameters for pervaporation of a quaternary system through a commercial membrane involves an extensive number of experiments, which is out of the scope of this research.

By comparison of partial fluxes at various mol fractions in the feed, however, the importance of flow coupling and plasticizing effects for pervaporation of this multicomponent mixture can be assessed. For example, if $x_{f,1} \neq x_{f,2}$ and $x_{f,3}=x_{f,4}$ in a quaternary system, a change in J_3 or J_4 can only be explained by component interactions. The same is true if partial fluxes J_1 or J_2 change in the opposite direction as $x_{f,1}$ or $x_{f,2}$.

Comparing mix A and B in Table 4.1 shows the effect of $x_{f,MP}$- and $_{xf,MPA}$- changes at constant $x_{f,EtOH}$ and $x_{f,EA}$. Partial fluxes J_{MP} and J_{MPA} vary according to their changes in mol fraction, i.e. the mol fraction change is their prevailing driving force, but partial fluxes of EtOH and EA change also. An example for changes in partial flux in opposite direction as their mol fractions is mix E vs. F, here J_{MPA} increases at decreasing $x_{f,MPA}$ and increasing $x_{f,MP}$. An other possibility to study component interactions, is to follow changes in J_i at different $x_{f,i}$ and equal ratio in mol fraction, $x_{f,i+1}=x_{f,i+2}=x_{f,i+3}$. Like mix C and G, where changes in $x_{f,EtOH}$ at $x_{f,EA}=x_{f,MP}=x_{f,MPA}$ result in an increase of J_{EA}, J_{MP} and J_{MPA}, while their corresponding mol fractions decrease. In other words, an increase in $x_{f,EtOH}$ has an enhancing effect on the flux of the other components here. In Table 4.1 examples can be found for each component mol fraction influencing the others partial flux.

Quantitive interpretation of these results, however, is not trivial as changes in partial flux of one component may be caused by absolute variations in multiple $x_{f,i}$, which is typical for non-diluted multicomponent systems.

Table 4.1 shows, that the order of the partial fluxes is not always similar at varying mol fractions. At high ethanol mol fractions $x_{f,EtOH}$, its flux $J_{EtOH}>J_{EA}$, but at higher $x_{f,EA}$ it is the other way around. Also, $x_{f,MP}$ plays a role in the order of fluxes, as high $x_{f,MP}$ makes MP the best permeating compound (mix B).

Table 4.1 Changes in partial flux, Ji, caused by changes in feed composition, xf,i at 35 mbar and 35°C (gray fields highlight values, which are approximately equal in a row, to facilitate comparison).

mix	$x_{f,EtOH}$	$x_{f,EA}$	$x_{f,MP}$	$x_{f,MPA}$	J_{EtOH}	J_{EA}	J_{MP}	J_{MPA}	J_{Total}
	(-)				(mmol m^{-2} s^{-1})				
A	0.14	0.14	0.2	0.53	1.24	0.66	0.47	0.38	2.74
B	0.14	0.16	0.56	0.14	0.73	0.94	0.96	0.06	2.69
C	0.15	0.25	0.29	0.3	0.25	0.31	0.17	0.06	0.79
D	0.23	0.54	0.11	0.12	1.84	2.65	0.27	0.09	4.86
E	0.33	0.29	0.28	0.1	1.47	1.18	0.54	0.12	3.32
F	0.34	0.27	0.12	0.28	0.87	0.46	0.12	0.09	1.54
G	0.67	0.12	0.11	0.1	3.9	0.63	0.35	0.17	5.05

4.3.3 Effect of Temperature on Permeate Flow

The effect of temperature on pervaporation performance was investigated by varying the feed temperature from 30 to 55°C. This temperature window is selected to enable integration of pervaporation and biocatalytic reaction at optimal conditions for the process. In an enzyme catalyzed kinetic resolution, the long-term stability of the catalyst and the enantioselectivity of the reaction products decrease with temperature (Berendsen, et al., 2006a), but pervaporation flux is generally less with lower temperature and therefore, it is a trade-off between process quality and separation.

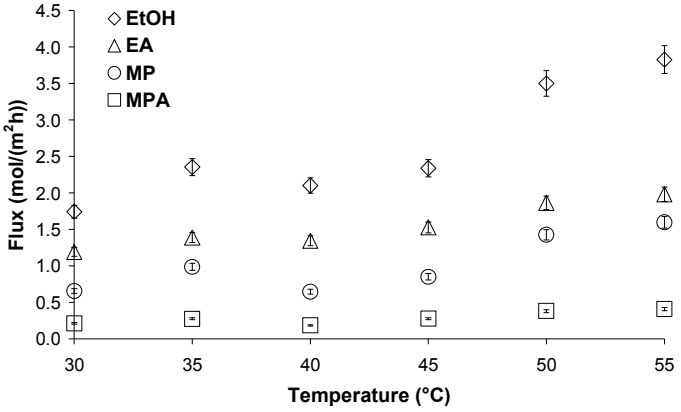

Figure 4.4 Dependency of temperature on partial flux (Pp = 35 mbar, xEtOH = 25 %, xEA = 25 %; xMP = 30 %; xMPA = 20 %).

In Figure 4.4 the flux of the permeants is shown for varying temperatures at approximately equal mol fractions in feed. At these conditions, the flux of the components is in the same order as the boiling points of the permeants, except for the azeotrope forming Ethanol and Ethyl acetate, showing the characteristic opportunity of pervaporation to separate mixtures with close boiling points ($T_{b,EtOH}$ = 78-80 °C; $T_{b,EA}$ = 77 °C; $T_{b,MP}$ = 90.12 °C and $T_{b,MPA}$ = 120 °C). Each partial flux increases with temperature, leading to an increase of total flux also.

By measuring both mole fractions ($x_{f,i}$, $y_{perm,i}$) at various temperatures and fixed downstream pressure (p_{perm}) and logarithmizing Equation (4.18) into:

$$\ln \frac{J}{\left(x_{f,i} \cdot \gamma_{f,i} \cdot p^{s}_{f,i} - y_{perm,i} \cdot p_{perm}\right)_i} = \ln\left(P'_{0,i}\right) - \frac{E_{act,i}}{R} \cdot \frac{1}{T} \tag{4.20}$$

the activation energy, $E_{act,i}$, and the permeability constant, $P'_{0,i}$, can be determined by plotting the permeance, the left side of Equation (4.20), on the y-axis versus the inverse temperature (Figure 4.5). As the measure of 'goodness of fit' of the linear regression model is quite low (0.84, 0.93, 0.82, 0.77 for EtOH, EA, MP, MPA, respectively), the absolute values of $E_{act,i}$ and $P'_{0,i}$ should be interpreted with caution. This inaccuracy follows from the fact, that the quality of experimental data of each component is dependent on the analytics of all components, as mol fractions are used at several occasions in Equations (4.18) and (4.19). These are calculated by dividing the measured

concentrations of each component by the sum of all concentrations. The average of the relative standard deviation of each species is 5-7%.

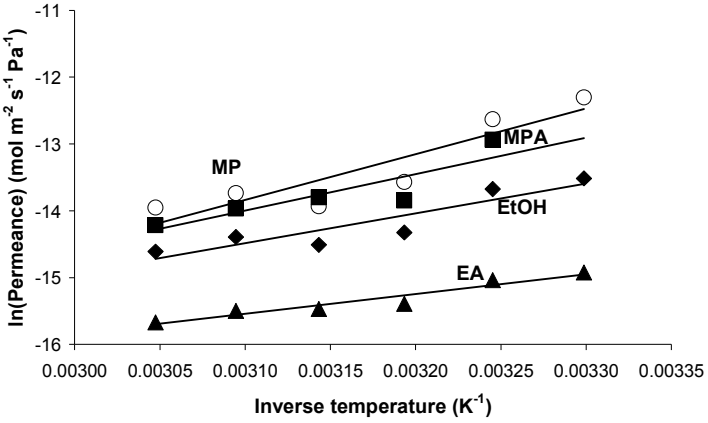

Figure 4.5 The activation energy of permeation was determined by plotting the logarithmized permeance versus the inverse temperature at steady state conditions (Pperm = 35 mbar, xEtOH = 25 %, xEA = 25 %; xMP = 30 %; xMPA = 20 %).

As is shown in Table 4.2, the values for the activation energy of pervaporation, $E_{act,i}$, obtained by plotting the logarithmized permeance versus the inverse temperature, are negative for all components. This suggests that the permeance of the components decreases with temperature, while the partial flux increases with temperature. This can be explained as follows. The activation energy of pervaporation is in fact the sum of the activation energy of diffusion and the enthalpy of sorption (Feng and Huang, 1996):

$$E_{act,i} = E_{D,i} + \Delta H_{s,i} \tag{4.21}$$

$E_{D,i}$	Energy of diffusion	($J \cdot mol^{-1}$)
$\Delta H_{s,i}$	Enthalpy of sorption	($J \cdot mol^{-1}$)

The first term is usually positive and the latter generally negative corresponding to the exothermic sorption process. Apparently, the energy of diffusion is more negative than the enthalpy of sorption is positive, and negative activation energy of pervaporation is the result. The flux still increases with temperature, because the effect of temperature on saturated vapor pressure is more significant.

Table 4.2 Determined activation energies of permeation and pre-exponential factors of permeating compounds.

		EtOH	EA	MP	MPA
$E_{a,i}$	$(kJ \cdot mol^{-1})$	-37.2	-24.7	-59.7	-45.4
$P'_{0,i}$	$(mol \cdot m^{-2} \cdot s^{-1} \cdot Pa^{-1})$	4.9 E-13	1.80E-11	2.10E-16	3.80E-14

4.4 Conclusions

This study reports on pervaporative separation of the mixture, ethanol – ethyl acetate – 1-methoxy-2-propanol – 1-methoxy-2-propyl acetate through a commercial Pervap2256® membrane. While high partial flux values are obtained, small differences in partial fluxes limit the industrial application of this membrane for the separation of this mixture. At best, ethanol has a twice higher flux than ethyl acetate, while fluxes of MP and MPA cannot be neglected. In particular, a typical biocatalytic reaction with EA and MP as substrates requires an initial feed composition, which is contra productive for pervaporative separation of EtOH: high $x_{f,MP}$ and $x_{f,EA}$ and low $x_{f,MPA}$ and $x_{f,EtOH}$.

Up to now, pervaporation of ethanol from binary ethanol – ethyl acetate mixtures has not been reported. Pervaporation of ethyl acetate from the same binary mixture has been reported recently (Ozdemir, et al, 1999; Hasanoğlu, et al., 2005), describing similar differences in separation. Clearly, the pervaporative separation of ethanol or ethyl acetate from ethanol – ethyl acetate mixtures offers much potential for further research, especially in the area of membrane development.

The interactions between the permeants themselves and the membrane are shown to play a major role in pervaporation of this multicomponent mixture. Analysis of the involved interaction phenomena improves the understanding of the mass transport mechanism occurring in pervaporation of the EtOH/EA/MP/MPA- mixture through a commercial membrane. We are convinced that further investigation of flow coupling and plasticizing effects will improve insight enhancing membrane development for such multicomponent organic-organic mixtures.

5

Investigations of Reaction Kinetics for Immobilized Enzymes – Identification of Parameters in the Presence of Diffusion Limitation

Published in:

Berendsen, W. R., Lapin, A., Reuss M. (2006d)

Biotechnology Progress, **22**, 1305-1312, DOI: 10.1021/bp060062e

Abstract

A method is proposed for identification of kinetic parameters, when diffusion of substrates is limiting in reactions catalyzed by immobilized enzymes. This method overcomes conventional sequential procedures, which assume immobilization does not affect the conformation of the enzyme and thus consider intrinsic and inherent kinetics to be the same. The coupled equations describing intraparticle mass transport are solved simultaneously using numerical methods and used for direct estimation of kinetic parameters by fitting modeling results to time-course measurements in a stirred tank reactor. While most traditional procedures were based on Michaelis-Menten kinetics, the method presented here is applicable to more complex kinetic mechanisms involving multiple state-variables, such as ping-pong bi-bi.

The method is applied to the kinetic resolution of (R/S)-1-methoxy-2-propanol with vinyl acetate catalyzed by Candida antarctica lipase B. A mathematical model is developed consisting of irreversible ping-pong bi-bi kinetics including competitive inhibition of both enantiomers. The kinetic model, which fits to experimental data over a wide range of both substrates (5-95%) and temperatures (5-56°C), is used for simulations to study typical behavior of immobilized enzyme systems.

5.1 Introduction

The technology of enzyme immobilization is widely accepted in biocatalysis due to their advantages over soluble enzymes and the increasing number of applications in this field. Immobilization offers the benefit of enzyme reuse providing cost advantages and enabling continuous reactor operation. In some cases, improved temperature stability upon immobilization has been reported (Santano, et al., 2002; Roy and Gupta, 2004; Pereira et al., 2001). Different immobilization methods are known, for example adsorptive, ionic or covalent binding, chemical crosslinking and matrix entrapment or microencapsulation.

In order to improve the understanding of a typical reaction system involving immobilized enzymes, modeling and simulation may be applied as an effective tool. Prior to application of this technology, the model needs to be identified and its parameters determined.

In the simplest case, when the rate of reaction is much lower than the rate of diffusion inside the particle, the inherent kinetic parameters may be determined by using measurements with immobilized enzymes. Most frequently, this method has been applied in combination with irreversible Michaelis-Menten models (e.g. Ayhan, et al., 2002; Yu et al., 2004; Masoud et al., 2002). In order to check if internal mass transfer may be considered negligible, the dimensionless observable modulus, Φ_i may be calculated (Bailey and Ollis, 1986):

$$\Phi_i = \frac{v_{app,i,0}}{D_{ep,i} \cdot c_{l,i,0}} \left(\frac{V_p}{A_p} \right)^2 \quad \text{with i = R,S} \tag{5.1}$$

with:

A_p	particle surface area	(m^2)
$c_{l,i,0}$	initial substrate concentration in liquid bulk	($mol \cdot L^{-1}$)
$D_{ep,i}$	effective diffusion coefficient in particle	($m^2 \cdot s^{-1}$)
$v_{app,i,0}$	initial apparent reaction velocity	($mol \cdot L^{-1} \cdot s^{-1}$)
V_p	particle volume	(m^2)

If $\Phi_i < 0.3$, substrate diffusion is fast in comparison to its conversion and the measured changes in bulk concentration can be used directly as input for the kinetic model. For $\Phi_i > 0.3$, substrate conversion is diffusion-limited and estimation of kinetic parameters at these conditions would result in apparent parameters.

High specific activity is desired for industrial relevant enzymes. Depending on the enzyme loading and the substrate to be converted, biocatalysis with immobilized preparations of such enzymes may become diffusion limited. The classic methodology to identify kinetic parameters of highly active immobilized enzyme preparations consists of (e.g. Atkinson and Lester, 1974; Gonçalves et al., 2001; Indlekofer, et al., 1993):

1. Determination of the intrinsic parameters on the basis of experiments with free soluble enzyme;

2. Adjusting the maximum catalytic velocity (v_{max}) to compensate for the loss of enzyme activity upon immobilization and the extent of enzyme loading.

Immobilization may however, also impact the binding affinity of substrates, products and inhibitors to the active site of the enzyme (K_m, K_i). This may be caused by interactions of these compounds with the immobilization support, i.e. the enzyme experiences a locally different concentration, or by changes in the three dimensional structure of the protein. Thus, in order to identify the kinetic parameters, which are relevant for process design studies, measurements with immobilized enzymes should be used as basis for modeling.

Various approaches have been used for determination of such kinetics, most of them focusing on Michaelis-Menten models. For example, Giordano et al. used a three-step procedure: First, they measured the specific activity at different particle diameters in order to discriminate which particle size was small enough to rule out intraparticle diffusion limitation. Then they used only those particles with small enough diameters for parameter determination and validated the model by running experiments where intraparticle diffusion is significant (Giordano, et al., 2000). The approach to vary particle diameters was also used by Chen et al., who determined the parameters of the Michaelis-Menten model by using Lineweaver-Burk plots (Chen, et al., 2003). Guisán et al. varied enzyme loading and applied Eadie-Hofstee plots (Guisán et al., 1981). Such graphical methods require extrapolation to abscissa or ordinate axes and may therefore lead to inaccurate parameter results.

In this chapter, a one-step method is presented to estimate the kinetic parameters of reactions catalyzed by immobilized biocatalysts in the presence of diffusion limitation, which are relevant for process design studies, by simultaneously solving coupled mathematical equations describing reaction and diffusion inside the particle. In addition, a kinetic model more complex than Michaelis-Menten is applied.

As a model reaction, the enantioselective transesterification of (R/S)-1-methoxy-2-propanol (MP) with vinyl acetate (VA) catalyzed by *Candida antarctica* lipase B (CAL-B) is selected, which yields mainly enantiopure (R)-1-methoxy-2-propyl acetate (R-MPA), (S)-1-methoxy-2-propanol (S-MP) and acetaldehyde (Ac) (Scheme 1). R-MPA and S-MP are potential chiral synthons, interesting as building blocks for pharmaceutical, agricultural or fine-chemical industry. *Candida antarctica* lipase B is known to exhibit high activity and good enantioselectivity for a wide range of substrates (Anderson, et al., 1998, Rotticci, et al., 2001b) and to perform well in organic solvents (e.g. Lozano, et al., 2003a).

The kinetic model is used for simulations to assess the impact of diffusion limitation on kinetics of this particular conversion and to study systems behavior of diffusion limited immobilized enzyme reactions.

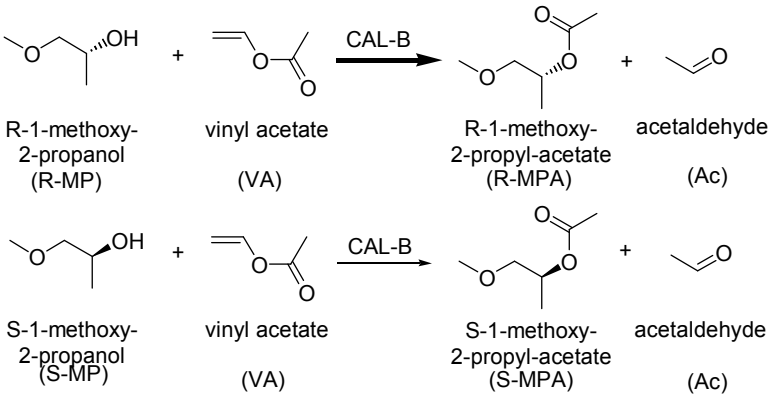

Scheme 5.1 Transesterification of (R/S)-1-methoxy-2-propanol with vinyl acetate catalyzed by *Candida antarctica* lipase B.

5.2 Theoretical Analysis

5.2.1 Coupled Reaction and Diffusion Model

The system under investigation consists of *Candida antarctica* lipase B immobilized on a porous acrylic carrier, which is suspended in a stirred tank reactor. The reactor initially contains only MP and VA, serving as organic solvents and substrates at the same time. Conversion of MP and VA into MPA and AC takes place inside the particles only. A kinetic resolution may be written as two parallel occurring reactions (Scheme 5.1).

The following assumptions are made in model development:

- The enzyme is equally distributed within the particles, i.e. enzyme adsorption during enzyme immobilization occurs inside the whole particle, as the surface of the enzyme (3x4x5 nm, i.e. 12-20 nm^2; Uppenberg, et al., 1994) is much smaller than the pores in the support (300-1200 nm^2; Eigtved, 1992).
- Particles are spherical (Eigtved, 1992);
- No enzyme deactivation occurs during course of measurement. This assumption is realistic, since CAL-B is known to be extremely thermally stable. Not only did it not lose any activity during 250-350h of operation at 65°C in organic solvents (Fishman et al., 2001; Bousquet, et al., 2000), it even showed activity for a considerable time at 130°C (Turner and Vulfson, 2000).
- Diffusion of substrates and products inside the particles can be described by Fick's law;
- External mass transfer resistance between bulk liquid and particle was neglected as the Damköhler number (Bailey and Ollis, 1986), which represents the ratio of reaction velocity to mass transfer rate, was much less than unity.
- Adsorption is considered negligible. This assumption is reasonable, since the mathematical model developed here accurately describes the dynamic experiments, which would not be the case if adsorption would be significant.

In view of these assumptions, mass balance equations of the bulk liquid and particle phases are given by:

Bulk:

$$V_l \cdot \frac{\partial c_{l,i}}{\partial t} = k_l \cdot A_p \cdot \left(c_{s,i} - c_{l,i}\right) \tag{5.2}$$

Particle:

$$\frac{\partial c_{s,i}}{\partial t} = D_{ep,i} \cdot \frac{1}{r_p^{\,2}} \cdot \frac{\partial}{\partial r}\left(r_p^{\,2} \frac{\partial c_{s,i}}{\partial r_p} \right) - v_i \tag{5.3}$$

with the following initial and boundary conditions, where Equation (5.4) is given by the symmetry condition at the center of the particle:

r_p=0:

$$\frac{\partial c_{s,i}}{\partial r_p} = 0 \tag{5.4}$$

r_p=R_p:

$$D_{ep,i} \cdot \frac{\partial c_{s,i}}{\partial r_p} = k_l \cdot \left(c_{l,i} - c_{s,i}\right) \tag{5.5}$$

t=0:

$$c_{l,i} = c_{l,i,0} \tag{5.6}$$

t=0:

$$c_{s,i} = c_{s,i,0} \tag{5.7}$$

with:

$c_{s,i}$	concentration inside particle	(mol·L^{-1})
$c_{l,i}$	concentration in liquid bulk	(mol·L^{-1})
k_l	mass transfer coefficient	(m·s^{-1})
r_p	distance from particle center	(m)
R_p	particle radius	(m)
t	time	(s)
V_l	specific bulk volume	(L)
v_i	volumetric reaction rate	(mol·L^{-1}·s^{-1})

i = R-MP, S-MP and VA

5.2.2 Kinetics

Candida antarctica lipase B is a serine hydrolase and its reaction mechanism has been characterized as ping-pong bi-bi (Martinelle and Hult, 1995, Hu, et al., 1998). In the first step, VA binds to the enzyme, forming an enzyme-acyl complex as well as the intermediary product, vinyl alcohol. Deacylation of this complex may occur via two parallel pathways: either by binding of R-MP and conversion to R-MPA or by binding of the opposite enantiomer, yielding S-MPA. Due to the complete tautomerization of the resulting vinyl alcohol to acetaldehyde (AC), the reaction may be considered irreversible (Degueil-Castaing, et al., 1987). The King-Altman plot in Scheme 5.2 shows the interconversion patterns of enzyme, substrate and product species for such a system. Both enantiomers can be considered alternative substrates for the same active site.

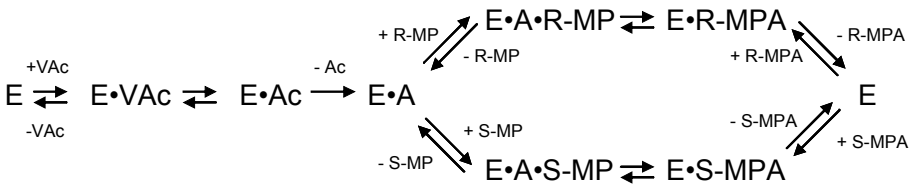

Scheme 5.2 King-Altman plot of an irreversible ping-pong bi-bi mechanism, taking into account competitive inhibition by both enantiomers.

The reaction rate may hence be written as (Segel, 1993):

$$v_{R-MP} = \frac{v_{\max,R} \cdot c_{s,R-MP} \cdot c_{s,VA}}{K_{m,R-MP} \cdot c_{s,VA} \cdot \left(1 + \frac{c_{s,S-MP}}{K_{m,S-MP}}\left(1 + \frac{K^S_{m,VA}}{c_{s,VA}}\right)\right) + K^R_{m,VA} \cdot c_{s,R-MP} + c_{s,R-MP} \cdot c_{s,VA}} \tag{5.8}$$

$$v_{S-MP} = \frac{v_{\max,S} \cdot c_{s,S-MP} \cdot c_{s,VA}}{K_{m,S-MP} \cdot c_{s,VA} \cdot \left(1 + \frac{c_{s,R-MP}}{K_{m,R-MP}}\left(1 + \frac{K^R_{m,VA}}{c_{s,VA}}\right)\right) + K^S_{m,VA} \cdot c_{s,S-MP} + c_{s,S-MP} \cdot c_{s,VA}} \tag{5.9}$$

$$v_{VA} = v_{R-MP} + v_{S-MP} \tag{5.10}$$

with: $v_{\max,a} = k_{cat,a}\left(\frac{1}{1-\varepsilon_l}\right) \cdot \rho_p$ with a = R,S (5.11)

and:

$k_{cat,a}$	maximum specific conversion rate	($mol \cdot g^{-1} \cdot s^{-1}$)
$K_{m,b}$	affinity constant	($mol \cdot L^{-1}$)
$v_{max,a}$	maximum volumetric reaction rate	($mol \cdot L^{-1} \cdot s^{-1}$)
ρ_p	particle density in liquid bulk	($g \cdot L^{-1}$)

$K^R_{m,\,VA}$ and $K^S_{m,VA}$, represent the affinity constant of the enzyme for VA in the reaction rate of one enantiomer, when the other enantiomer is the second substrate. These two parameters can only determined sensitively if separate measurements with either R-MP or S-MP are performed. Since these enantiomers are not available in sufficient quantities, these parameters are lumped and assumed to be identical ($K_{m,VA} = K^R_{m,\,VA} = K^S_{m,VA}$).

By introducing typical dimensionless numbers, Equations (5.2)-(5.10) can be normalized into dimensionless equations, where a prime indicates a dimensionless variable or parameter (i.e. $c'_{s,i} = \frac{c_{s,i}}{c_{s,i,0}}$; $c'_{l,i} = \frac{c_{l,i}}{c_{l,i,0}}$; $K'_{m,i} = \frac{K_{m,i}}{c_{i,0}}$; $r_p' = \frac{r_p}{R_p}$):

Bulk:

$$\frac{\partial c'_{l,i}}{\partial Fo_i} = Bi_i \cdot \frac{3 \cdot \varepsilon_l}{1-\varepsilon_l} \cdot \left(c'_{s,i} - c'_{l,i}\right) \tag{5.12}$$

Particle: $$\frac{\partial c'_{s,i}}{\partial Fo_i} = \frac{1}{r_p'^2} \cdot \frac{\partial}{\partial r_p'}\left(r_p'^2 \frac{\partial c'_{s,i}}{\partial r_p}\right) - \phi_i^2 \cdot v'_i \tag{5.13}$$

$$v'_{R-MP} = \frac{c'_{s,R-MP} \cdot c'_{VA}}{c'_{s,VA} \cdot \left(1 + \frac{c'_{s,S-MP}}{K'_{m,S-MP}}\left(1 + \frac{K'_{m,VA}}{c'_{s,VA}}\right)\right) + \frac{K'_{m,VA} \cdot c'_{s,R-MP}}{K'_{m,R-MP}}\left(1 + \cdot c'_{s,VA}\right)} \tag{5.14}$$

$$v'_{S-MP} = \frac{c'_{s,S-MP} \cdot c'_{s,VA}}{c'_{s,VA} \cdot \left(1 + \frac{c'_{s,R-MP}}{K'_{m,R-MP}}\left(1 + \frac{K'_{m,VA}}{c'_{s,VA}}\right)\right) + \frac{K'_{m,VA} \cdot c'_{s,S-MP}}{K'_{m,S-MP}}\left(1 + \cdot c'_{s,VA}\right)} \tag{5.15}$$

r_p'=0:

$$\frac{\partial c'_{s,i}}{\partial r_p'} = 0 \tag{5.16}$$

r_p'=1:

$$\frac{\partial c'_{s,i}}{\partial r_p'} = Bi_i \cdot \left(c'_{l,i} - c'_{s,i}\right) \tag{5.17}$$

The general Thiele modulus, ϕ_i, Biot number, Bi_i, and the Fourier number, Fo_i are given by:

$$\phi_i^2 = \frac{R_p \cdot v_{\max,i}}{D_{ep,i} \cdot K_{m,i}} \tag{5.18}$$

$$Bi_i = \frac{k_{l,i} \cdot R_p}{D_{ep,i}} \tag{5.19}$$

$$Fo_i = \frac{t \cdot D_{ep,i}}{R_p^{\,2}} \tag{5.20}$$

The effective diffusion coefficient was calculated using empirical relationships available in literature (see Appendix). For 28°C, effective diffusion coefficients of R-MP, S-MP and VA were calculated as $1.65 \cdot 10^{-10}$ $m^2 \cdot s^{-1}$; $1.65 \cdot 10^{-10}$ $m^2 \cdot s^{-1}$ and $1.67 \cdot 10^{-10}$ $m^2 \cdot s^{-1}$, respectively.

5.3 Results and Discussion

5.3.1 Kinetic Measurements and Modeling

In this kinetic investigation, the mass balances describing intraparticle diffusion and reaction are solved simultaneously (Equations (5.12)-(5.17)). The kinetic parameters are estimated directly using implicit numerical methods with iterations and minimizing the relative error between experimentally determined and calculated time course of concentrations in the liquid bulk[1]:

$$\min_{\{k_{cat,i};K_{m,i}\}} F = \frac{1}{n}\sum_{j=1}^{n} \frac{\left(c_{l,i,m}\left(k_{cat,a};K_{m,i}\right) - c_{l,i,\exp}\right)^2}{c_{l,i,\exp}^{\,2}} \text{ with a = R,S} \tag{5.25}$$

[1] Numerical calculations were performed by Alexei Lapin at the IBVT, University of Stuttgart

One of the advantages of using time course instead of initial rate measurements is that there is no need for transformation of the data (e.g. when using Lineweaver-Burk or Eadie-Hofstee plots) and thus there is no distortion in error distribution (Rakels, et al., 1993).

Model selection and discrimination is an important step in a kinetic investigation. Not only the reversibility of the reaction but also possible inhibition effects have to be considered. Reactions catalyzed by *Candida antarctica* lipase B are typically characterized by a ping-pong bi-bi mechanism, which may include inhibitions of first and/or second substrates as well as products (e.g. Chulalaksananukul, et al., 1992; Shin et al., 1998). As discussed in 'theoretical analysis', the kinetic resolution of MP and VA catalyzed by this enzyme may be considered an irreversible reaction. Because of this and because no inhibition effects are found to play a role, an irreversible ping-pong bi-bi model, Equations (5.14) and (5.15), is selected for the current reaction system. The parameters are estimated by focusing on measurements of time course profiles at different initial conditions and constant temperature (28°C). The resulting model fit is shown in Figures 5.1a, b and 5.2a, b. The corresponding kinetic parameters are listed in Table 5.1. A very good model description is achieved for the conversion of the R-enantiomer, both at low and high initial substrate concentrations ($4.5 < c_{l,MP,0} < 95$ % mol/mol in VA). For the S-enantiomer, an additional measurement at high enzyme concentrations ($\varepsilon_l = 0.65$) was performed to improve parameter sensitivity ($K_{m,S\text{-}MP}$; $k_{cat,S}$). Overall, the model of S-enantiomer conversion describes the experimental data good; only at high MP-concentrations deviations occur.

The fact that experimental results of both enantiomers are accurately described by the model during the full time-course at a broad range of both substrate concentrations ($5\% <= c_{l,MP} <= 95\%$, $5\% <= c_{l,VA} <= 95\%$), proves the model assumptions mentioned in the 'theoretical analysis' to be reasonable as their influence on this reaction system are not significant enough to cause lack of model prediction.

Table 5.1 Estimated kinetic parameters at 28°C ($k_l \to \infty$; $R_p = 3 \cdot 10^{-4}$m; $\rho_p = 200$ g·L^{-1}).

$\mathbf{k_{cat,R}}$	$1.4 \cdot 10^{-6}$	(mol·g^{-1}·s^{-1})
$\mathbf{K_{m,R\text{-}MP}}$	1.4	(mol·L^{-1})
$\mathbf{k_{cat,S}}$	$9.4 \cdot 10^{-9}$	(mol·g^{-1}·s^{-1})
$\mathbf{K_{m,S\text{-}MP}}$	0.72	(mol·L^{-1})
$\mathbf{K_{m,VA}}$	0.28	(mol·L^{-1})

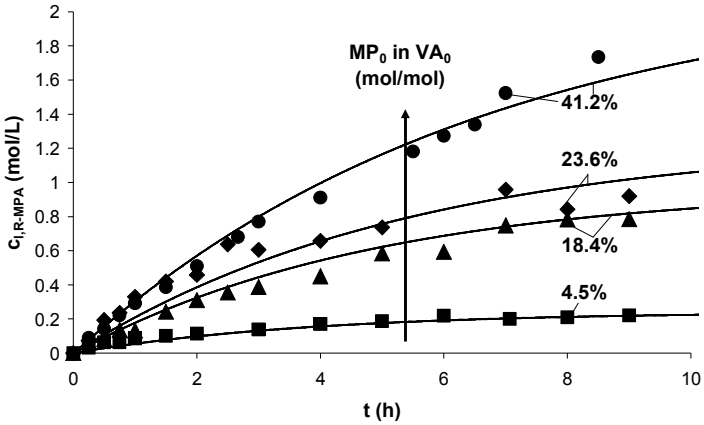

(a)

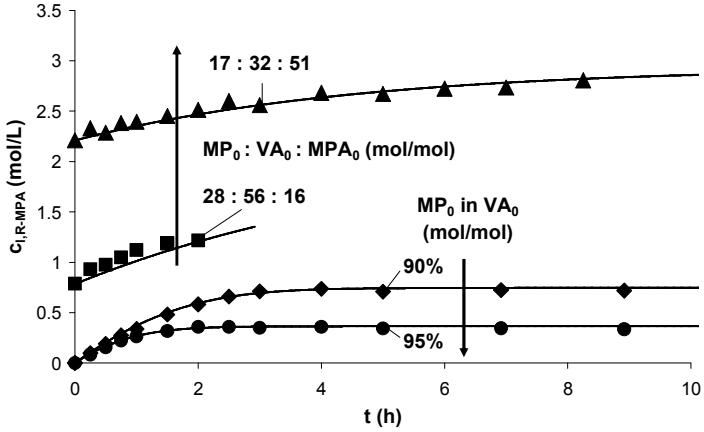

(b)

Figure 5.1 a and b Time course profiles of R-MPA-concentrations for different initial substrate and product ratio's (ε_l = 0.99, T = 28°C; k_l -> ∞; $R_p = 3 \cdot 10^{-4}$m; ρ_p = 200 g·L^{-1}).

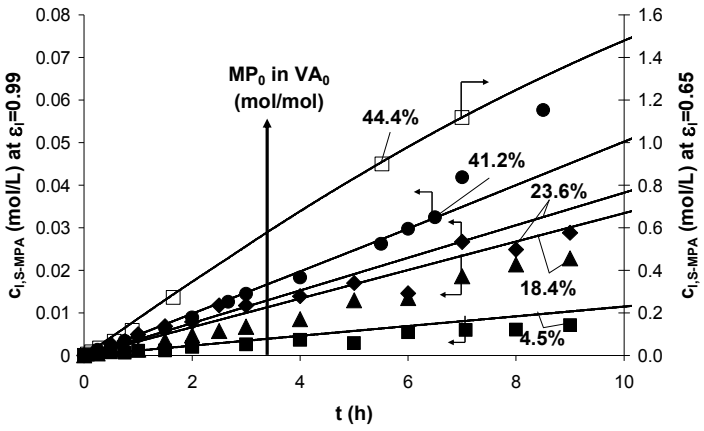

(a)

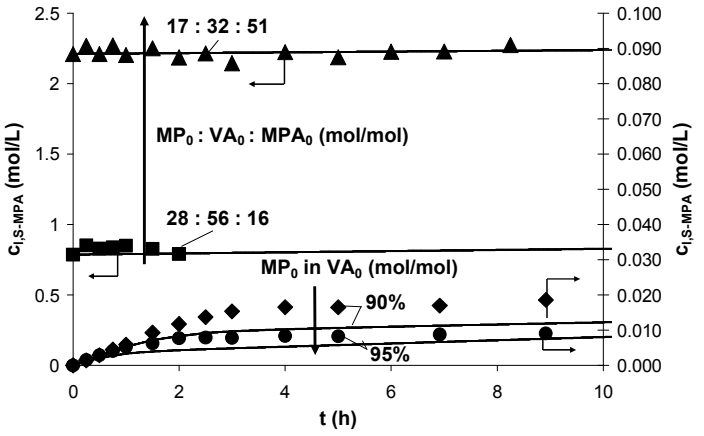

(b)

Figures 5.2 a and b Time course profile of S-MPA-concentrations for different initial substrate and product ratio's (ε_l = 0.99; T = 28°C; k_l -> ∞; $R_p = 3 \cdot 10^{-4}$m; ρ_p = 200 g·L^{-1}).

In general, each parameter in a kinetic model is temperature dependent. While the temperature dependency of rate constants, such as v_{max}, may be modeled by Arrhenius equations assuming the active enzyme concentration is constant with temperature, affinity constants may be described by the Van 't Hoff equation (Segel, 1993):

$$v_{\max,i} = v^{\circ}_{\max,i} \cdot e^{-\frac{E_{act,a}}{R \cdot T}} \quad \text{with i = R; S} \tag{5.26}$$

$$\frac{d \ln\left(K_{m,i}\right)}{dT} = \frac{\Delta H^{\ddagger\circ}{}_{i}}{R \cdot T^2} \quad \text{with i = R-MP; S-MP; VA} \tag{5.27}$$

$v^{\circ}_{max,a}$	maximum volumetric rate at T->∞	($mol \cdot L^{-1} \cdot s^{-1}$)
$E_{act,a}$	activation energy	($J \cdot mol^{-1}$)
$\Delta H^{\ddagger\circ}{}_{i}$	reaction enthalpy	($J \cdot mol^{-1}$)
R	universal gas constant	($J \cdot mol^{-1} \cdot K^{-1}$)
T	temperature	(K)

The already estimated kinetic parameters at 28°C may be used for the determination of the relevant temperature parameters. Rearranging Equation (5.22) and integrating the Van 't Hoff equation between the limits of $K^{28}_{m,i}$ and $K^{T}_{m,i}$ at 301.15 K and T gives:

$$v^{T}_{\max,i} = v^{28}_{\max,i} \cdot e^{-\frac{E_{act,a}}{R}\left(\frac{1}{T}-\frac{1}{301.15}\right)} \quad \text{with i = R; S} \tag{5.28}$$

$$K^{T}_{m,i} = K^{28}_{m,i} \cdot e^{\frac{\Delta H^{\ddagger\circ}{}_{i}}{R}\left(\frac{T-301.15}{301.15 \cdot T}\right)} \quad \text{with i = R-MP; S-MP; VA} \tag{5.29}$$

The activation energy, $E_{act,a}$ and the reaction enthalpy, $\Delta H^{\ddagger\circ}{}_{i}$, may be estimated by fitting Equations (5.12)-(5.17) to time course measurements at various temperatures and calculating the kinetic constants with Equations (5.28) and (5.29). Estimation of $E_{act,a}$ and $\Delta H^{\ddagger\circ}{}_{i}$ simultaneously resulted in very low values of $\Delta H^{\ddagger\circ}{}_{i}$.

Also, no significant increase in relative error is observed when the effect of temperature on Michaelis-Menten constants is neglected. Therefore, $K_{m,i}$ is assumed to be constant over the temperature range studied. The resulting model fit to experimental data is shown in Figures 5.3a and 5.3b and the corresponding parameters in Table 5.2. The model describes the conversion of both enantiomers satisfactorily. Both activation energies are in the same order of magnitude as found previously (Berendsen et al., 2006a).

The difference in reaction enthalpy, $\Delta_{R-S}\Delta H^{\ddagger\circ}{}_{i}$, is a characteristic value of kinetic resolutions and has been used as one of the key values for analyzing molecular modeling of *Candida antarctica* lipase catalyzed reactions (Ottosson, et al., 2002; Bocola, 2002). They report values in the same order of magnitude as the -8 kJ·mol^{-1} found here.

Table 5.2 Estimated parameters related to the temperature dependency of the reaction rate of both enantiomers (k_l -> ∞; R_p = 3·10^{-4}m; ρ_p = 200 g·L^{-1}).

$E_{act,R}$	37	(kJ·mol^{-1})
$E_{act,S}$	45	(kJ·mol^{-1})
$\Delta_{R-S}\Delta H^{\ddagger\circ}{}_{j}$	15	(kJ·mol^{-1})
E-value$_{303K}$	74	(-)

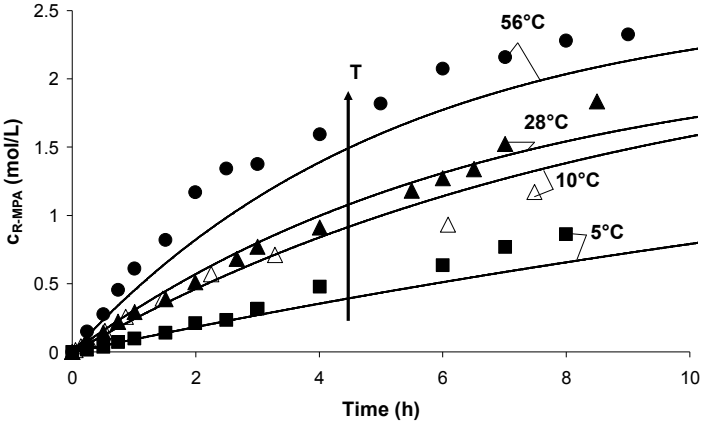

(a)

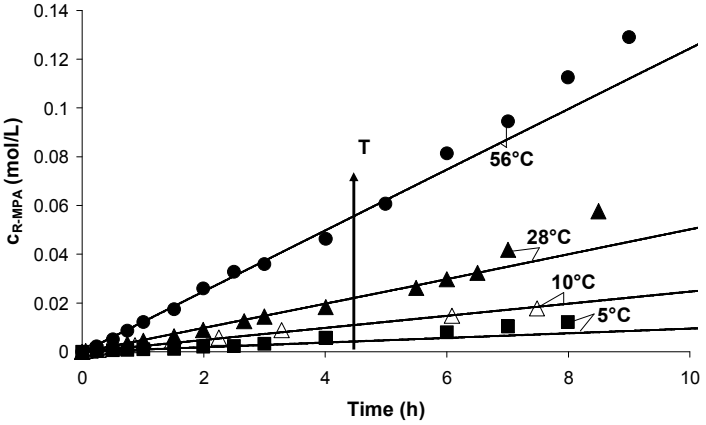

(b)

Figures 5.5 a and b R-MPA concentration profiles at varying temperatures at $[MP]_0$ = 2.3 M and $[VA]_0$ = 6 M (ε_l = 0.99; k_l -> ∞; $R_p = 3 \cdot 10^{-4}$m; ρ_p = 200 g·L^{-1}).

5.3.2 The Impact of Diffusion Limitation

The quantification and analysis of the effect of diffusion limitation on the conversion rate of a kinetic resolution is greatly facilitated by introduction of effectiveness factors. They are defined for immobilized enzymes as the ratio of actual reaction rate $\left(v_{eff,a}\left(c_{s,i}\right)\right)$ to the rate without diffusion limitation $\left(v_a\left(c_{l,i}\right)\right)$, i.e. the observed reaction rate at r=d/2 vs. the reaction rate at bulk conditions with no concentration gradient in the particle, $c_{s,i} = c_{l,i}$:

$$\eta_a = \frac{v_{eff,a}\left(c_{s,i}\right)}{v_i\left(c_{l,i}\right)} \text{ with a = R; S} \tag{5.30}$$

If the conversion is purely reaction controlled, $\eta_a = 1$. By plotting the effectiveness factors versus time for typical initial substrate concentrations, the effect of diffusion limitation on the current reaction system can be evaluated (Figure 5.4a and b). For the R-enantiomer, this factor is below unity for the complete time-course at 28°C, i.e. the effect of internal diffusion limitation is present. This effect is higher at lower MP bulk substrate concentrations for $c_{MP}(0)$<=60 % mol/mol. If the initial MP-concentration, however, is increased above 60% mol/mol the effectiveness factor decreases also. This is due to limitation of the other substrate, vinyl alcohol. The conversion of MP with VA catalyzed by CAL-B is thus an example for a reaction system, where diffusion of both substrates plays a role.

In case of the S-enantiomer, effectiveness factors close to unity are obtained for $c_{l,MP}(0)$<=60 % mol/mol, indicating the conversion is reaction-controlled at these conditions (Figure 5.4b). For $c_{l,MP}(0)$>60 % mol/mol, diffusion limitation is caused by decreasing VA-concentrations, in accordance with the findings for the R-enantiomer. These simulations show the necessity of taking intraparticle mass transport as well as reaction into account.

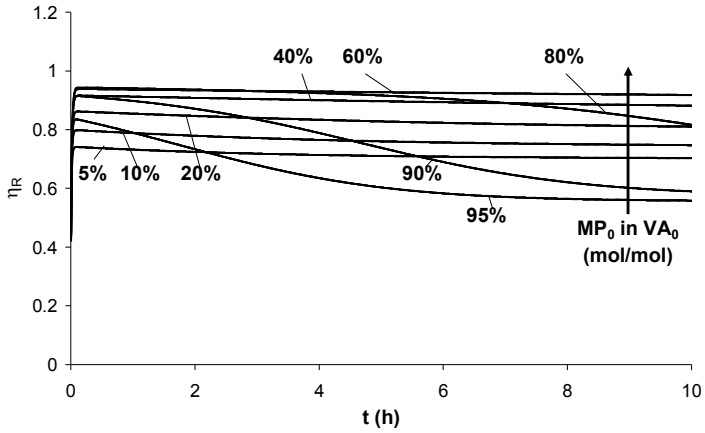

(a)

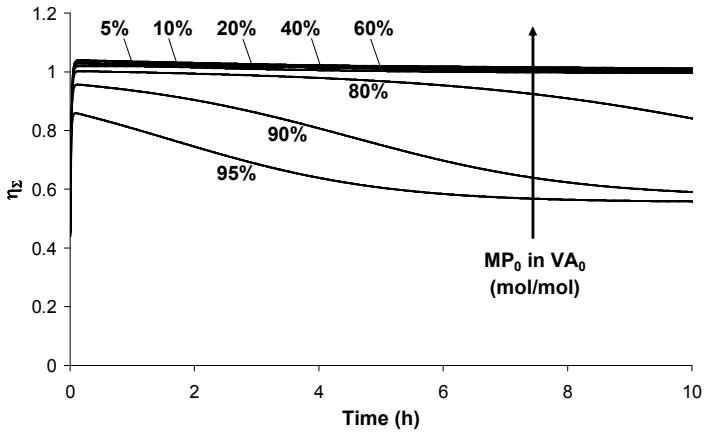

(b)

Figures 5.4 a and b. Simulated dynamic profile of effectiveness factor of R-enantiomer and S-enantiomer at various initial MP-VA concentrations (ε_l =0.99; T=28°C; k_l -> ∞; R_p = $3 \cdot 10^{-4}$m; ρ_p = 200 g·L^{-1}).

One of the most frequently used parameters to quantify the quality of a kinetic resolution reaction is the enantiomeric ratio, also named E-value. It represents the ratio of specificity constants ($v_{max,i}$ / $K_{m,i}$) between both enantiomers and is the only parameter in the ratio of reaction velocities (Ferscht, 1985). Dividing the rate of the faster enantiomer, Equation (5.8), by the rate of the slower enantiomer, Equation (5.9), when $c_{s,i}(r) = c_{l,i}$, gives:

$$\frac{v_R}{v_S} = \frac{\frac{k_{cat,R}}{K_{m,R-MP}} c_{l,R-MP}}{\frac{k_{cat,S}}{K_{m,S-MP}} c_{l,S-MP}} = E \cdot \frac{c_{l,R-MP}}{c_{l,S-MP}} \tag{5.31}$$

The enantiomeric ratio for the current reaction system is 74 at 28°C, which indicates the kinetic resolution is well suitable for industrial purposes (Faber, 1997). As is evident from Figures 5.4a and b, diffusion limitation influences conversion of each enantiomer differently. Thus, diffusion limitation should have an effect on the enantiomeric ratio. Similar to Equation (5.31) an effective enantiomeric ratio, E_{eff}, may be defined:

$$E_{Eff} = \frac{v_{R,Eff} \cdot c_{l,S-MP}}{v_{S,Eff} \cdot c_{l,R-MP}} = \frac{\eta_R \cdot v_R \cdot c_{l,S-MP}}{\eta_S \cdot v_S \cdot c_{l,R-MP}} = \frac{\eta_R}{\eta_S} \cdot E \tag{5.32}$$

Hence, by plotting the ratio of effectiveness factors directly versus time the impact of diffusion limitation on the enantiomeric performance of the current model system (E_{Eff}/E) can be studied (Figure 5.5). Clearly, diffusion limitation of the R-enantiomer is strongest at lowest R-MP concentrations, yielding E_{Eff}/E-values far below unity, which is in agreement with expectations. Interestingly, the dynamic profile of E_{eff}/E initially decreases and then increases for $c_{l,MP}(0)$ >= 80 % mol/mol. The decrease of E_{eff}/E is due to the reduction of the rate velocity of the R-enantiomer caused by the diffusion of its own substrate. An additional lack of VA supply into the particle lowers the rate velocity of both enantiomers, simultaneously diminishing the limitation caused by R-MP. This ultimately leads to no difference between in enantiomeric ratio's: E_{Eff}/E =1.

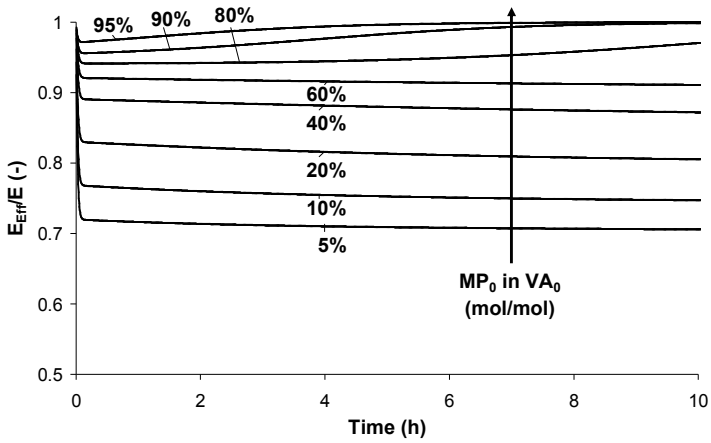

Figure 5.5 Simulated dynamic profile of enantiomeric performance, E_{Eff}/E, at various initial MP-VA concentrations (ε_l =0.99; T=28°C; k_l -> ∞; $R_p = 3 \cdot 10^{-4}$m; ρ_p = 200 g·L^{-1}).

5.3.3 Investigation of Systems Behavior

The effect of parameter changes on model behavior was studied in order to evaluate coupled mass transport and reaction of immobilized enzymes. For this purpose, the effectiveness factors and enantiomeric performance (E_{Eff}/E) are simulated at varying squared general Thiele moduli for different E-values (Figure 5.6 and 5.7).

For $c_{l,VA}$ -> ∞, limitation of the locally available faster R-enantiomer causes a decrease in η_R, which is independent of the enantioselectivity of the enzyme. At the same time, this leads to an increase of η_S, resulting in values larger than unity, which is more pronounced for higher enantiospecific enzymes. Effectiveness factors larger than unity have been found previously for competitive Michaelis-Menten kinetics at steady state conditions (Indlekofer, et al., 1996). The increase of η_S above unity is due to the reduced competition of the R-enantiomer on S-enantiomer conversion. The fact that enzymes with higher E-values suffer more from diffusion limitation is also evident from the E_{Eff}/E - ϕ^2 – plot (Figure 5.7), which corresponds to findings of Xiu et al. for first-order and Michaelis-Menten kinetics (Xiu et al., 2001).

For $c_{l,VA}$ -> $K_{m,VA}$, diffusion of the acyl donor dominates the E_{Eff}/E - ϕ^2 – plot canceling out almost completely the difference in effectiveness factors, which both decrease with increasing squared general Thiele moduli (Figure 5.6). The nullification of this difference leads to E_{Eff}/E-values close to unity (Figure 5.7). Hence, diffusion limitation may actually improve the enantiomeric performance of a kinetic resolution.

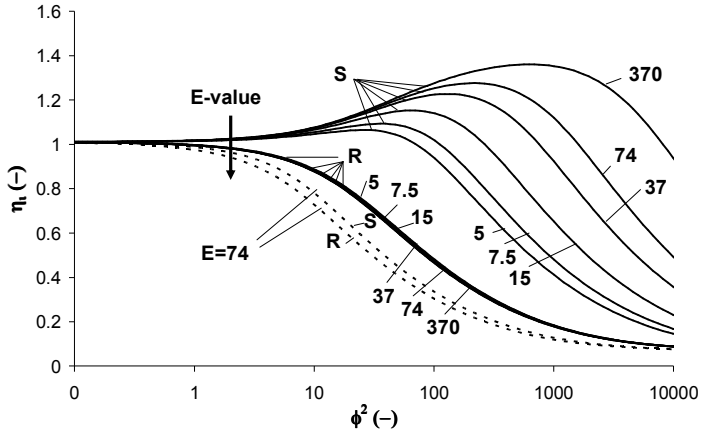

Figure 5.6 Simulated effectiveness factor profile versus the square of the general Thiele modulus for various E-values ($c_{l,R\text{-}MP} = K_{m,R\text{-}MP}$; $c_{l,\text{-}MP} = K_{m,S\text{-}MP}$; ε_l =0.99; T=28°C; k_L -> ∞; $R_p = 3{\cdot}10^{-4}$m; ρ_p = 200 g·L^{-1}; solid lines $c_{l,VA}$->∞; dotted lines: $c_{l,VA}=K_{m,VA}$).

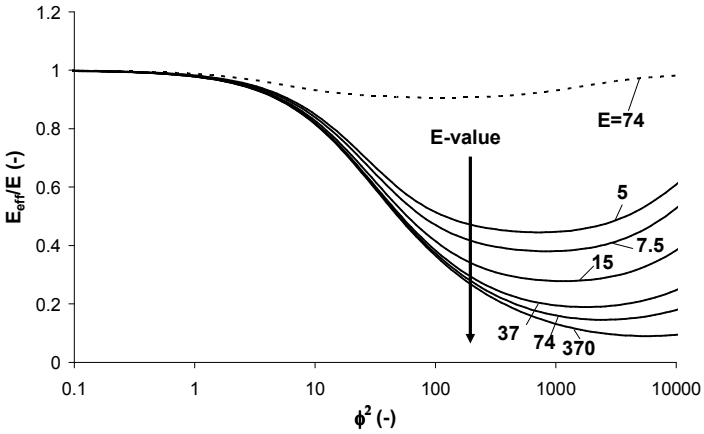

Figure 5.7. Simulated enantiomeric performance, E_{Eff}/E, versus the square of the general Thiele modulus for various E-values. ($c_{l,R\text{-}MP} = K_{m,R\text{-}MP}$; $c_{l,S\text{-}MP} = K_{m,S\text{-}MP}$; ε_l =0.99; T=28°C; k_l -> ∞; $R_p = 3{\cdot}10^{-4}$m; ρ_p = 200 g·L^{-1}; solid lines $c_{l,VA}$->∞; dotted lines: $c_{l,VA}=K_{m,VA}$).

5.4 Conclusions

In this chapter, a one-step method for estimation of kinetic parameters of diffusion limited immobilized enzymes is reported. This method involves simultaneously solving coupled equations describing mass transport and reaction inside immobilization particles using numerical methods and estimating the kinetic parameters.

This method is successfully applied to the kinetic resolution of 1-methoxy-2-propanol and vinyl acetate catalyzed by *Candida antarctica* lipase B. Following model identification and discrimination, a kinetic model is developed consisting of an irreversible ping-pong bi-bi mechanism and taking competitive inhibition by both enantiomers into account. The resulting model provides a good fit at broad substrate (5% <=$c_{l,MP}$<=95%; 5% <=$c_{l,VA}$<=95%) and temperatures (5-56°C).

The simulations in this chapter point out, that the immobilized preparation of *Candida antarctica* lipase B, Chirazyme L-2, c.-f. C2, is highly active and enantioselective for the current reaction system. It is an example for a reaction system, which is not only hampered by diffusion limitation of the faster enantiomer, but also by the acyl donor. While diffusion limitation of the faster enantiomer reduces the enantioselectivity, the limitation of the locally available acyl donor slows conversion of both enantiomers. This ultimately leads to an enantiomeric performance (E_{Eff}/E) of reaction-controlled enzymes.

In particular, such kinetic models may be used as basis for process engineering studies to improve understanding of biocatalytic reactions and to accelerate their development and implementation for industrial applications.

6

Nonisothermal Lipase-Catalyzed Kinetic Resolution in a Packed Bed Reactor: Modeling, Simulation and Miniplant Studies

Published in:

Berendsen, W. R., Lapin, A., Reuss M. (2007)

Chemical Engineering Science, **62**, 2375-2385, DOI: 10.1016/j.ces.2007.01.006

Abstract

A rigorous model is developed for the exothermic kinetic resolution of 1-methoxy-2-propanol with vinyl acetate catalyzed by immobilized Candida antarctica lipase B in a packed bed reactor. The non-isothermal two-dimensional heterogeneous model takes into account the coupled mass and energy balances, the uneven flow distribution and irreversible ping-pong bi-bi kinetics with alternative substrate inhibition by both enantiomers. This model is based on kinetic parameters, which were estimated in Chapter 5. The model simulation is validated with experimental results obtained in a fully automated modular miniplant and is shown to be capable of predicting the key parameters needed for process design of a kinetic resolution, the enantiomeric excess and the extent of conversion at a given superficial velocity.

6.1 Introduction

Due to recent advancements in enzyme production, purification and immobilization technology, packed bed reactors are becoming more and more the reactor of choice for biochemical reactions. They offer higher enantioselectivity in case of kinetic resolutions (Indlekofer, et al., 1993), higher substrate conversion (Lin, 1991) and easier catalyst retainment in comparison with stirred tank reactors. Hence, it is industrially interesting for biocatalytic conversions.

The transport mechanisms in such a wall-cooled fixed bed reactor consist of convective and dispersive mass transport as well as convective and conductive energy transport in the bulk phase, mass and heat transfer between the solid and fluid phase, heat transfer between the reaction mixture and the cooling agent, dispersive mass and conductive energy transport and biocatalytic conversion in the solid phase (Figure 6.1).

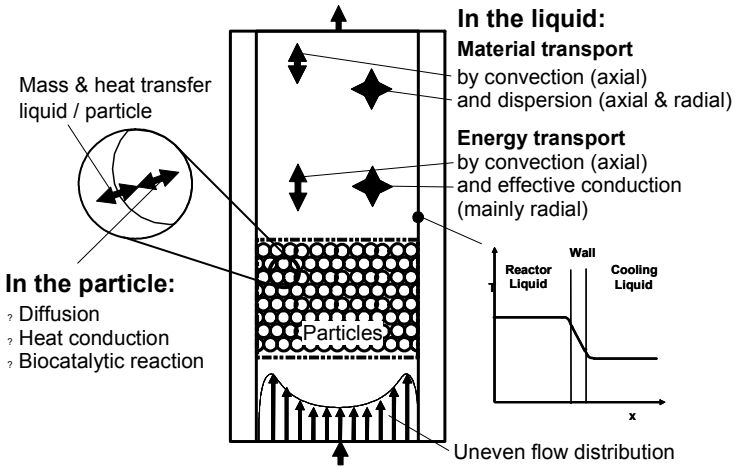

Figure 6.1 Transport mechanisms in a fixed bed reactor packed with immobilized enzymes.

Models of enzymatic reactions in packed bed reactors have been built by considering one or more of these phenomena in various combinations and for various reactions. An overview of activities in this field is presented in Table 6.1. As is evident from this table, most studies apply simple models based on one-dimensional pseudo-homogeneous or heterogeneous models. While all give insight through modeling and/or simulation, only a few studies actually provide experimental data for verification of these results. The

majority of them apply a simple kinetic model, such as the irreversible or a reversible Michaelis-Menten mechanism.

Table 6.1 Non-exclusive overview of scientific publications focusing on modeling of immobilized enzyme reactions in packed bed reactors (1D, 2D = one-, two-dimensional model; [1] Michaelis-Menten kinetics, [2] through effectiveness factor correlation).

Authors	1D	2D	mass & energy balances	intraparticle	experimental verification	M.-M.[1] kinetics
Carrara. et al., 2003	x				x	x
Ching and Chu, 1988	x			x	x	x
Faqir and Attarakih, 2002	x					x
Faqir, 2004						
Gonzalez, et al., 1989	x				x	
Hassan et al., 1995	x		x	x		x
Hassan et al., 1996	x		x	x		x
Indlekofer et al., 1996	x			x	x	
Jung and Bauer, 1992	x			x	x	
Kim et al., 1982	x					x
Kobayashi and Moo-Young, 1971	x					x
Lin, 1972		x	x			x
Lin, 1991	x		x			x
Lortie, 1994	x					x
Lortie and Thomas, 1986	x					x
Marrazzo and Merson, 1975	x				x	x
Marsh and Tsao, 1976a	x		x		x	x
Marsh and Tsao, 1976b	x			[2]		x
Moynihan, et al., 1989	x			[2]	x	
Patwardhan and Karanth, 1982	x				x	x
Stadler, 2005	x			x	x	
Xiu, et al., 2001	x			x		x

In general, isothermal conditions are assumed, thus no energy balances are needed (e.g. Indlekofer, et al., 1996; Jung and Bauer, 1992; Xiu, et al., 2001), neglecting the heat of reaction and its potential consequences on reactor performance. This is justified for most enzymatic reactions, as their heat of reaction and productivity are usually low.

Some examples, however, exist of biocatalytic conversions with a considerable heat of reaction and productivity, such as the decomposition of hydrogen peroxide catalyzed by catalase from beef liver ($\Delta H_{m(25°C,1atm)} = -93 \pm 3$ kJ·mol^{-1}; Liang et al., 1997; Tran-Minh, et al., 1976). Lipase-catalyzed transesterification with the acyl donor vinyl acetate is another example, where the major contribution to the heat of reaction originates from tautomerization of vinyl alcohol to acetaldehyde (-42 ± 13 kJ·mol^{-1}; Holmes and Lossing, 1982; Toullec, 1990).

The use of vinyl esters, such as vinyl acetate, in *Candida antarctica* lipase B catalyzed transesterifications is popular for kinetic resolution of secondary alcohols, since the tautomerization causes the reaction to be irreversible (Degueil-Castaing, et al., 1987), which results in high conversion and enantioselectivity values (e.g. Kazlauskas and Bornscheuer, 1998; Resnick, et al., 2002, Rottici, 2000).

In this chapter, the enantioselective conversion of (R/S)-1-methoxy-2-propanol with vinyl acetate catalyzed by immobilized *Candida antarctica* lipase B is investigated as a model system for the application of exothermic kinetic resolution reactions in packed bed reactors. A non-isothermal two-dimensional heterogeneous model is developed and used for simulations, which are validated with experimental results obtained in a fully automated modular miniplant. In addition to intraparticle mass transport, which plays a role in this system (Berendsen, et al., 2006d), uneven flow distribution is taken into account, as this effect significantly improved modeling of a wall-cooled reactor (Hein and Vortmeyer, 1995). As kinetic mechanism, an irreversible ping-pong bi-bi mechanism with alternative substrate inhibition by both enantiomers is applied. The coupled mathematical model is solved numerically using the control volume technique (Patankar, 1982; Lapin et al., 2004; Lapin et al., 2006).

6.2 Mathematical Model Development

The following assumptions are made in model development for the fixed bed reactor system involving immobilized *Candida antarctica* lipase B (CAL-B) catalyzed kinetic resolution of (R/S)-1-methoxy-2-propanol (MP) with vinyl acetate (VA):

- All physical and transport properties are independent of temperature, except rate constants;
- Catalyst particles are spherical (Eigtved, 1992) and randomly packed inside the reactor;
- Enzyme molecules are uniformly distributed inside even-sized particles. Of course, this is a simplification of reality, as the particle radius ranges from 0.15 to 0.45 mm (Eigtved, 1992) and the enzyme is highly unevenly distributed in an external shell of 0.1 mm (Mei et al., 2003). This assumption is reasonable however, as determination of the exact enzyme location in each applied particle is beyond the scope of this research.
- Diffusion of substrates and products inside the particles can be described by Fick's law;

- Adsorption is assumed to be negligible, as the model simulations presented within describe the fixed bed reactor measurements accurately, using prior estimated kinetic parameters (Berendsen, et al., 2006d) and parameters using empirical relationships. This would not be the case if adsorption would be significant, since the kinetic parameters were estimated on the basis of dynamic experiments.
- Enzyme deactivation is not taken into account. CAL-B is known to exhibit good stability at high temperatures (compared to other enzymes). For example, it did not lose any activity at all during 250-300 hours of operation at 65°C in organic solvents (Fishman et al., 2001; Bousquet et al., 2000) and it showed prolonged activity at 130°C (Turner and Vulfson, 2000).

6.2.1 Mass and Energy Balances

The mass balance equations for the substrates (i = R-MP, S-MP, VA) and energy balance equations in the bulk liquid phase can be written as:

$$\varepsilon_l \frac{\partial c_{l,i}}{\partial t} = D_{ax,l} \frac{\partial^2 c_{l,i}}{\partial x^2} + \frac{1}{r_r} \cdot \frac{\partial}{\partial r_r}\left(D_{er,l} \cdot r_r \frac{\partial c_{l,i}}{\partial r_r} \right) - u_{0,l} \frac{\partial c_{l,i}}{\partial x} + k_l \cdot a_p \cdot \left(c_{s,i} - c_{l,i} \right), \tag{6.1}$$

$$\varepsilon_l \rho_l c_{p,l} \frac{\partial T_l}{\partial t} = \Lambda_{ax,l} \frac{\partial^2 T_l}{\partial x^2} + \frac{1}{r_r} \cdot \frac{\partial}{\partial r_r}\left(\Lambda_{er,l} \cdot r_r \frac{\partial T_l}{\partial r_r} \right) - u_{0,l} \rho_l c_{p,l} \frac{\partial T_l}{\partial x} + \alpha_{lp} \cdot a_p \cdot \left(T_s - T_l \right). \tag{6.2}$$

The boundary conditions at the entry (x=0), exit (x=X), center (r_r=0) and wall (r_r=R_r) of the reactor are given by:

x=0: $$u_{0,l} \cdot c_{l,i} - D_{ax,l} \frac{\partial c_{l,i}}{\partial x} = u_{0,l} \cdot c_{l,inlet,i}\,, \tag{6.3a}$$

x=0: $$u_{0,l} \rho_l c_{p,l} T_l - \Lambda_{ax,l} \frac{\partial T_l}{\partial x} = u_{0,l} \rho_l c_{p,l} T_{l,inlet}\,, \tag{6.3b}$$

x=X: $$\frac{\partial c_{l,i}}{\partial x} = 0\,, \qquad \frac{\partial T_l}{\partial x} = 0\,, \tag{6.4}$$

r_r=0: $$\frac{\partial c_{l,i}}{\partial r_r} = 0\,, \qquad \frac{\partial T_l}{\partial r_r} = 0\,, \tag{6.5}$$

r_r=R_r: $$\frac{\partial c_{l,i}}{\partial r_r} = 0\,,\ \Lambda_{er,l} \cdot \frac{\partial T_l}{\partial r_r} = k_h \cdot \left(T_c - T_l\right). \tag{6.6}$$

The initial conditions pertaining to Equations (6.1) and (6.2) are as follows:

t=0: $$c_{l,inlet,i} = c_{l,inlet,i,0}\,,\ T_{l,inlet} = T_{l,inlet,0}\,. \tag{6.7}$$

where :

a_p	specific external particle surface area per unit reactor volume	(m^{-1})
$c_{l,i}$, $c_{s,i}$	concentration in liquid and solid phase, respectively	($mol \cdot L^{-1}$)
$c_{p,l}$	specific heat capacity of liquid	($J \cdot kg^{-1} \cdot K^{-1}$)
$D_{ax,l}$, $D_{er,l}$	effective axial / radial dispersion coefficient in liquid phase	($m^2 \cdot s^{-1}$)
k_L	mass transfer coefficient	($m \cdot s^{-1}$)
k_h	lumped heat transfer coefficient	($m \cdot s^{-1}$)
r_r	distance from reactor center	(m)
R_r	inner reactor radius	(m)
t	time	(s)
T_l, T_c	temperature of liquid and cooling medium, respectively	(K)
$u_{0,l}$	superficial velocity	($m \cdot s^{-1}$)
x	distance from reactor inlet	(m)
X	reactor height	(m)
α_{lp}	heat transfer coefficient between liquid and particle	($W \cdot m^{-2} \cdot K^{-1}$)
ε_l	reactor porosity	(-)
$\Lambda_{ax,l}$, $\Lambda_{er,l}$	effective axial and radial heat conduction in liquid phase	($W \cdot m^{-1} \cdot K^{-1}$)
ρ_l	liquid density	($kg \cdot L^{-1}$)

The internal mass and energy balance for a representative particle must be simultaneously simulated at every position in the reactor. The mass (i=R-MP, S-MP, VA) and energy balances for the immobilized enzyme particle are represented by the following equations:

$$\frac{\partial c_{s,i}}{\partial t} = D_{ep,l} \cdot \frac{1}{r_p^{\,2}} \cdot \frac{\partial}{\partial r_p}\left(r_p^{\,2} \frac{\partial c_{s,i}}{\partial r_p} \right) - v_i \,, \tag{6.8}$$

$$\rho_p c_{p,p} \frac{\partial T_s}{\partial t} = \Lambda_{ep,l} \cdot \frac{1}{r_p^{\,2}} \cdot \frac{\partial}{\partial r_p}\left(r_p^{\,2} \frac{\partial T_s}{\partial r_p} \right) - \Delta H_m \cdot \left(v_{R-MP} + v_{S-MP} \right), \tag{6.9}$$

which are subject to the following initial and boundary conditions at the center (r_p=0) and surface (r_p=R_p) of the particle:

r_p=0: $$\frac{\partial c_{s,i}}{\partial r_p} = 0 \,, \quad \frac{\partial T_s}{\partial r_p} = 0 \tag{6.10}$$

r_p=R_p: $$D_{ep,l} \cdot \frac{\partial c_{s,i}}{\partial r_p} = k_l \cdot \left(c_{l,i} - c_{s,i} \right), \quad \Lambda_{ep,l} \cdot \frac{\partial T_s}{\partial r_p} = k_h \cdot \left(T_l - T_s \right) \tag{6.11}$$

t=0: $$c_{s,i} = c_{s,i,0} \,, \quad T_s = T_{s,0} \tag{6.12}$$

where:

$$k_h = \left(\frac{1}{\alpha_{wl}} + \frac{\delta_w}{\lambda_w} + \frac{1}{\alpha_{wc}} \right)^{-1} \tag{6.13}$$

with:

$D_{ep,l}$	effective diffusion coefficient in particle	($m^2 \cdot s^{-1}$)
r_p	distance from particle center	(m)
R_p	particle radius	(m)
v_R, v_S	volumetric reaction rate of R or S-enantiospecific substrate	($mol \cdot L^{-1} \cdot s^{-1}$)
α_{wc}	heat transfer coefficient between wall and cooling medium	($W \cdot m^{-2} \cdot K^{-1}$)
α_{wl}	heat transfer coefficient between wall and liquid	($W \cdot m^{-2} \cdot K^{-1}$)
δ_w	thickness of glass wall between cooling medium and mixture	(m)
ΔH_m	enthalpy of reaction	($J \cdot mol^{-1}$)
λ_w	thermal conductivity of the glass reactor wall	($W \cdot m^{-1} \cdot K^{-1}$)
$\Lambda_{ep,l}$	effective heat conduction in particle	($W \cdot m^{-1} \cdot K^{-1}$)

For the cooling liquid, the energy balance may be written as:

$$\rho_c c_{p,c} \frac{\partial T_c}{\partial t} = -u_{0,c} \rho_c c_{p,c} \frac{\partial T_c}{\partial x} - \frac{k_h}{\delta_c}\left(T_c - T_l\right). \tag{6.14}$$

with the following initial and boundery conditions:

x=0: $T_c = T_{c,inlet}$, (6.15)

t=0: $T_c = T_{c,inlet,0}$, (6.16)

where:

$c_{p,c}$	specific heat capacity of cooling medium	($J \cdot kg^{-1} \cdot K^{-1}$)
δ_c	cooling jacket width	(m)
ρ_c	density of cooling medium	($kg \cdot L^{-1}$)

6.2.2 Kinetics

The biocatalytic reaction, the enantioselective conversion of 1-methoxy-2-propanol (MP) with vinylacetate (VA) into R- and S-1-methoxy-2-propyl-acetate (R- and S-MPA) and acetaldehyde (Ac), may be modeled using an irreversible ping-pong bi-bi mechanism taking into account competitive substrate inhibition by both enantiomers (Berendsen, et al, 2006d). The corresponding equations for the volumetric rate of both enantiomers of MP and VA, v_i, are:

$$v_{R-MP} = \frac{v_{\max,R} \cdot c_{s,R-MP} \cdot c_{s,VA}}{K_{m,R-MP} \cdot c_{s,VA} \cdot \left(1 + \frac{c_{s,S-MP}}{K_{m,S-MP}}\left(1 + \frac{K_{m,VA}}{c_{s,VA}}\right)\right) + K_{m,VA} \cdot c_{s,R-MP} + c_{s,R-MP} \cdot c_{s,VA}} \tag{6.17}$$

$$v_{S-MP} = \frac{v_{\max,S} \cdot c_{s,S-MP} \cdot c_{s,VA}}{K_{m,S-MP} \cdot c_{s,VA} \cdot \left(1 + \frac{c_{s,R-MP}}{K_{m,R-MP}}\left(1 + \frac{K_{m,VA}}{c_{s,VA}}\right)\right) + K_{m,VA} \cdot c_{s,S-MP} + c_{s,S-MP} \cdot c_{s,VA}} \tag{6.18}$$

$$v_{VA} = v_{R-MP} + v_{S-MP} \tag{6.19}$$

with: $v_{\max,a} = k_{cat,a}\left(\frac{1}{1-\varepsilon_l}\right)\cdot\rho_p$ with a = R,S (6.20)

and $v^T_{\max,a} = v_{\max,a}\cdot e^{-\frac{\Delta H_{act,a}}{R}\left(\frac{1}{T}-\frac{1}{301.15}\right)}$ with a = R; S (6.21)

$k_{cat,a}$	maximum specific conversion rate	(mol·L^{-1}·s^{-1})
$K_{m,i}$	affinity constant	(mol·L^{-1})
ρ_p	particle density	(kg·L^{-1})
$\Delta H_{act,a}$	activation energy	(J·mol^{-1})

6.2.3 Calculation of Radial Porosity and Superficial Velocity Profile

The porosity in a fixed bed reactor may be considered constant, assuming it is an unlimited wide bed (ε_∞), however, in doing so, the increase in porosity close to the reactor wall is neglected. This porosity profile results in a radially uneven flow distribution. By taking this effect into account, a significantly improved model prediction of a wall-cooled reactor was obtained by Hein and Vortmeyer (1995). The radial porosity profile is calculated with the exponential function (Tsotsas, 2002):

$$\varepsilon_l = \varepsilon_\infty\left(1 + a_1\cdot\exp\left[-b_1\frac{R_r - r_r}{R_p}\right]\right),\ a_1=1.36,\ b_1=2.5,\ \varepsilon_\infty=0.4 \quad (6.22)$$

The dependency of the superficial velocity in radial direction can be obtained by applying iterative methods for numerically solving the enhanced Brinkmann equation (Tsotsas, 2002):

$$\frac{\partial p}{\partial x} = -f_1 u_0 - f_2 {u_0}^2 + \frac{\eta_{eff}}{r_r}\cdot\frac{\partial}{\partial r_r}\left(r\frac{\partial u_0}{\partial r}\right), \quad (6.23)$$

with: $f_1 = a_2\cdot\frac{(1-\varepsilon_l)^2}{\varepsilon_l^3}\frac{\eta_l}{{R_p}^2}$, $f_2 = b_2\cdot\frac{(1-\varepsilon_l)}{\varepsilon_l^3}\frac{\rho_l}{R_p}$, $\eta_{eff} = c_2\eta_l\cdot\exp\left(d_2\,\mathrm{Re}_p\right)$,

a_2=37.5, b_2=0.875, c_2=2, d_2=2.0·10^{-3},

with the boundary conditions:

r_r=0: $$\frac{\partial u_0}{\partial r_r} = 0\,, \tag{6.24}$$

r_r=R_r: $$u_0 = 0\,. \tag{6.25}$$

where p (Pa), Re_p (-) and η_l (Pa·s) are pressure, particle Reynolds and viscosity of the liquid phase, respectively.

The following condition is used to determine the pressure gradient: the cross-section integrated fluid velocity equals the given flow rate.

6.3 Results and Discussion

While investigating the kinetic resolution of 1-methoxy-2-propanol with vinyl acetate catalyzed by immobilized *Candida antarctica* lipase B in a fixed bed reactor, a significant temperature gradient is observed in axial direction (Figure 6.2). While a temperature gradient is common in chemical engineering, it is rare in biocatalysis, as the heat of the reaction is usually low and/or the applied biocatalysts exhibit low productivity. Since transesterification with vinyl esters is an attractive means for production of chiral intermediates for pharmaceutical, agricultural and fine-chemical industry, the kinetic resolution of MP in a fixed bed reactor is investigated here and the performance of the developed model discussed.

Although the miniplant set-up used for obtaining the results displayed in Figure 6.2 clearly shows the axial temperature gradient in the reactor, it is not practical for additional experimental investigations, as the time needed to reach steady state is very long. Due to the limited cooling capacity available in the miniplant, a reactor with smaller diameter is used from now on (1.4 cm instead of 3 cm).

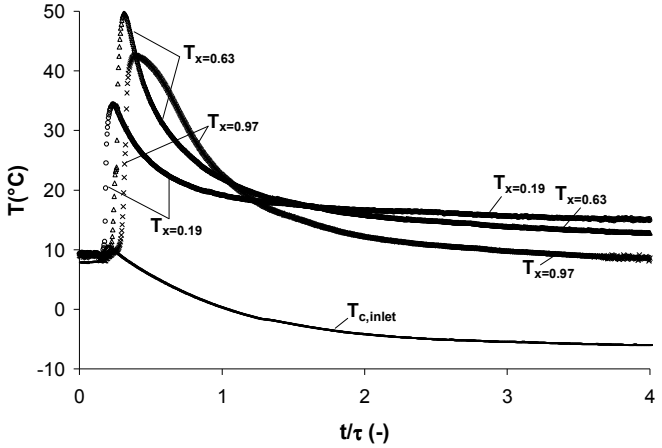

Figure 6.2 Dynamic temperature profile in a fixed bed reactor during kinetic resolution of 1-methoxy-2-propanol by immobilized *Candida antarctica* lipase B ($\overline{u_{0,l}} = 322$ cm·h^{-1}, $T_{setpoint,x=0.63}$=10°C; $T_{l,inlet}$=10°C; R_R=0.015 m; X = 0.3 m; $c_{l,inlet,MP}$ = 4.4 M, $c_{l,inlet,VA}$ = 6.2 M).

In this investigation, the radial porosity and superficial velocity profiles are determined for each mass flow, Equations (6.22)-(6.25), before the coupled mass and energy balances, Equations (6.1)-(6.16), and kinetic equations, Equations (6.17)-(6.21), are solved simultaneously using implicit numerical methods with iterations[2], as described by Patankar, 1982. Model verification with experimental results obtained with the miniplant is show in Figures 6.5 to 6.8.

[2] Numerical calculations were performed by Alexei Lapin at the IBVT, University of Stuttgart

The first figure, Figure 6.3, shows the steady state axial product concentration profile of both enantiomers in the reactor. As is typical for a kinetic resolution reaction, the conversion of one of the enantiomers (here the R-enantiomer) progresses faster than the other one. In biocatalysis, this characteristic property is usually analyzed using the enantiomeric excess, e.e.$_h$, and total enantiomer conversion, ξ_{MP}, defined as (Chen et al., 1982):

$$e.e._h = \left| \frac{c_{R-h} - c_{S-h}}{c_{R-h} + c_{S-h}} \right|, \; h=MP,\; MPA, \tag{6.26}$$

$$\xi_{MP} = \frac{c_{R-MP,0} - c_{R-MP} + c_{S-MP,0} - c_{S-MP}}{c_{R-MP,0} + c_{S-MP,0}}, \tag{6.27}$$

whereas an enantiopure compound has an e.e. of 100%.

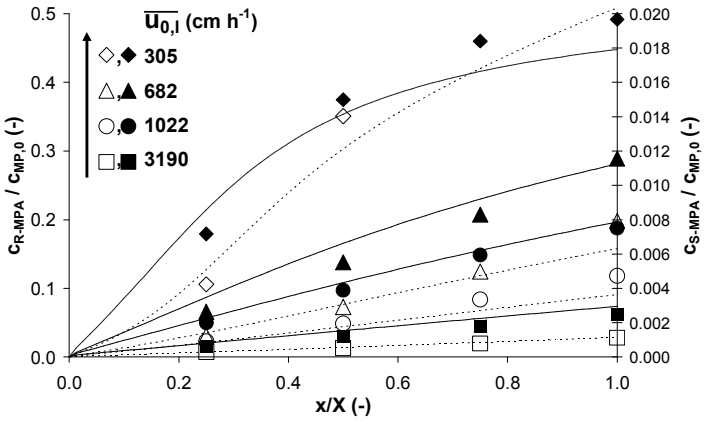

Figure 6.3 Measured and simulated axial concentration profile of R- and S-enantiomer in the packed bed reactor at several average superficial velocities, $\overline{u_{0,l}}$ (lines: model, dots: experiments; solid lines and closed symbols: R-MPA; dotted lines and open symbols: S-MPA; R_R=0.007 m; X = 0.8 m; $c_{l,inlet,MP}$ = 4.4 M, $c_{l,inlet,VA}$ = 6.2 M, $T_{setpoint,x=0.63}$=30°C; $T_{c,inlet}$=24°C; $T_{l,inlet}$=23°C).

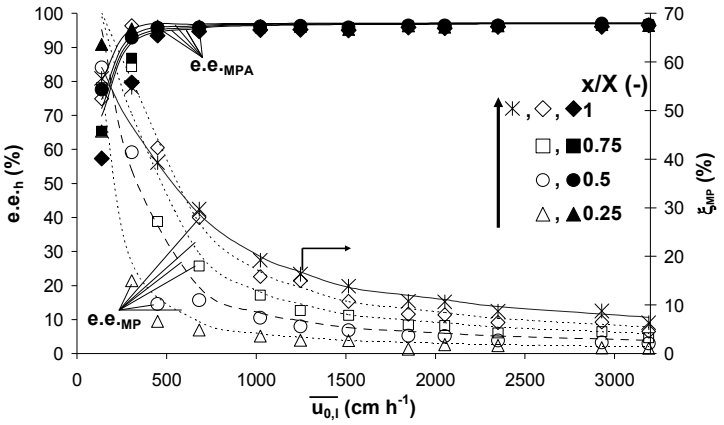

Figure 6.4 Verification of non-isothermal heterogeneous model by experiments in a miniplant reactor: enantiomeric excess ($e.e._h$) versus average superficial velocity ($\overline{u_{0,l}}$) at different dimensionless axial positions. The profile of the total enantiomer conversion (ξ_{MP}) versus superficial velocity is shown exemplary for x=1 (lines: model, dots: experiments, R_R=0.007 m; X = 0.8 m, $c_{l,inlet,MP}$ = 4.4 M, $c_{l,inlet,VA}$ = 6.2 M, $T_{setpoint,x=0.63}$=30°C; $T_{c,inlet}$=24°C; $T_{l,inlet}$=23°C).

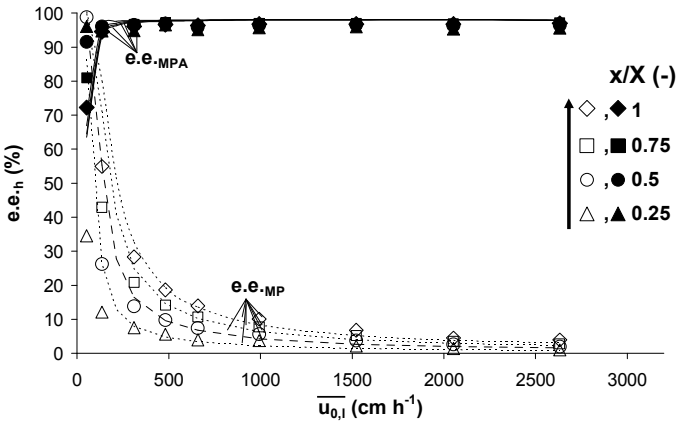

Figure 6.5 Verification of non-isothermal heterogeneous model by experiments in a miniplant reactor: enantiomeric excess ($e.e._h$) versus average superficial velocity ($\overline{u_{0,l}}$) at different dimensionless axial positions (lines: model, dots: experiments, R_R=0.007 m; X = 0.8 m, $c_{l,inlet,MP}$ = 4.4 M, $c_{l,inlet,VA}$ = 6.2 M, $T_{setpoint,x=0.63}$=10°C; $T_{c,inlet}$=4°C; $T_{l,inlet}$=6°C).

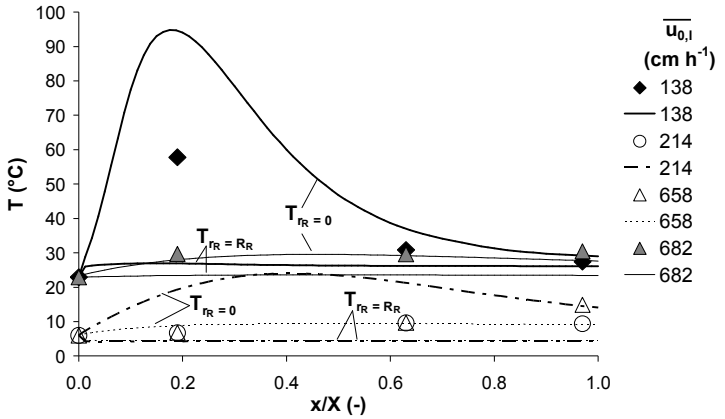

Figure 6.6 Measured and simulated axial temperature profile in the packed bed reactor at several average superficial velocities and set point temperatures (lines: model, dots: experiments; R_R=0.007 m; X = 0.8 m; $c_{l,inlet,MP}$ = 4.4 M, $c_{l,inlet,VA}$ = 6.2 M; closed symbols and solid lines: $T_{setpoint,x=0.63}$=30°C, $T_{c,inlet}$=24°C, $T_{l,inlet}$=23°C; open symbols and dotted lines: $T_{setpoint,x=0.63}$=10°C, $T_{c,inlet}$=4°C, $T_{l,inlet}$=6°C).

The dependency of the enantiomeric excess on superficial velocity and axial position in the reactor is illustrated in Figures 6.4 and 6.5 for two set point temperatures at dimensionless axial position x/X=0.5 and steady state conditions (10°C, 30°C). These setpoint temperatures correspond to the temperature, which is used as input for temperature control of the cryostat. As is evident from both graphs, enantiomeric values close to 95-98% can be achieved depending on the conditions applied. Finding the right superficial velocity is a trade-off between having a high endproduct concentration of the respective enantiomer and obtaining a high enantiopurity. At high superficial velocity, the conversion of both enantiomers,ξ_{MP}, is lower (shown exemplary for x/X=1 in Figure 6.4) than at low superficial velocity, resulting in good e.e.-values for the product (e.e.$_{MPA}$). By lowering the superficial velocity, the conversion increases, just like the e.e. of the substrate (e.e.$_{MP}$). At one point, however, when the R-enantiomer is nearly fully converted, its reaction rate drops in comparison to the rate of the S-enantiomer causing a decrease in product e.e. As soon as the faster enantiomer is converted, the process may yield the S-enantiomer of the reaction substrate in high enantiopurity. Hence, it is crucial to adjust the superficial velocity accurately in fixed bed reactor operated kinetic resolutions.

While this behavior of enantioselectivity and conversion is typical for kinetic resolutions and is usually shown in plots of e.e. versus conversion (e.g. Berendsen, et al., 2006a; Berendsen, et al., 2006b), such plots do not give information about the the relationship of these parameters with the reaction velocity, i.e. the way the reactor needs to be operated, and thus are not suited for complete validation of the reactor model. Figures 6.4 and 6.5 offer this possibility, while giving insight into process behavior.

Overall, the model applied in Figures 6.3 to 6.6 describes the experimental findings relatively well considering the fact, that all parameters needed for model simulations are calculated using in literature available correlations (Table 6.2) and, in case of kinetic parameters, are previously estimated using a set of dynamic experiments in a stirred tank reactor (Berendsen, et al., 2006d, Table 6.3). In particular, the dependency of enantiomeric excess on superficial velocity, which is crucial for kinetic resolution reactions, is nicely predicted by the model. The simulated axial temperature profile is presented in Figure 6.8 for the reactor center (r_r=0) and wall (r_r=R_r). Unfortunately, it is unclear which spot in radial direction the temperature sensors in the miniplant reactor actually measure. Therefore an accurate comparison between predicted and measured temperatures is not possible. However, the measured temperatures are well within the simulated temperatures at r_r=0 and r_r=R_r. Since the mass and energy balances are coupled, the prediction of the temperature appears to be correct also, as otherwise the concentration profiles would not be correctly described either.

Table 6.2 Applied parameters in model simulations shown in Figure 6.5-6.8. The empirical calculation methods summarized by Koning (2002) were used for determination of heat and mass transport parameters.

Parameters	Value	Unit
$c_{p,c}$	2440	$J \cdot kg^{-1} \cdot K^{-1}$
$c_{p,l}$	2130	$J \cdot kg^{-1} \cdot K^{-1}$
$c_{p,p}$	1460	$J \cdot kg^{-1} \cdot K^{-1}$
$D_{ax,l}$	$1.1 \cdot 10^{-5}$	$m^2 \cdot s^{-1}$
$D_{er,l}$	$2.5 \cdot 10^{-8}$	$m^2 \cdot s^{-1}$
$D_{ep,l}$	$1.66 \cdot 10^{-10}$	$m^2 \cdot s^{-1}$
k_l	$1 \cdot 10^{-4}$	$m \cdot s^{-1}$
Re_p	0.5-6	-
R_p	$3.0 \cdot 10^{-4}$	m
R_r	$7.0 \cdot 10^{-3}$	m
$u_{0,c}$	$9.9 \cdot 10^{-2}$	$m \cdot s^{-1}$
X	0.8	m
α_{lp}	2300	$W \cdot m^{-2} \cdot K^{-1}$
α_{wc}	300	$W \cdot m^{-2} \cdot K^{-1}$
α_{wl}	970	$W \cdot m^{-2} \cdot K^{-1}$
δ_c	$8 \cdot 10^{-3}$	m
δ_w	$1 \cdot 10^{-3}$	m
ΔH_m	-68700	$J \cdot mol^{-1}$
η_l	$1 \cdot 10^{-3}$	Pa·s
$\Lambda_{ax,l}$	11.5	$W \cdot m^{-1} \cdot K^{-1}$
$\Lambda_{ep,l}$	0.186	$W \cdot m^{-1} \cdot K^{-1}$
$\Lambda_{er,l}$	0.2	$W \cdot m^{-1} \cdot K^{-1}$
λ_w	1.05	$W \cdot m^{-1} \cdot K^{-1}$
ρ_c	789	$kg \cdot m^{-3}$
ρ_l	900	$kg \cdot m^{-3}$
ρ_p	200	$kg \cdot m^{-3}$

Table 6.3 Previously estimated kinetic parameters (Berendsen, et al., 2006c).

Parameters	Value	Unit
$k_{cat,R}$	$1.4 \cdot 10^{-6}$	$mol \cdot g^{-1} \cdot s^{-1}$
$k_{cat,S}$	$9.4 \cdot 10^{-9}$	$mol \cdot g^{-1} \cdot s^{-1}$
$K_{m,R\text{-}MP}$	0.28	$mol \cdot L^{-1}$
$K_{m,S\text{-}MP}$	0.72	$mol \cdot L^{-1}$
$K_{m,VA}$	1.4	$mol \cdot L^{-1}$
$\Delta H_{act,R}$	37000	$J \cdot mol^{-1}$
$\Delta H_{act,S}$	45000	$J \cdot mol^{-1}$

6.4 Conclusions

The presented comprehensive mathematical model is capable of predicting accurately the critical parameters needed for fixed bed reactor operation of an exothermic kinetic resolution reaction without additional estimation of parameters.

The *Candida antarctica* lipase B catalyzed transesterification of 1-methoxy-2-propanol with vinyl acetate in a fixed bed reactor is shown to be influenced by axial and radial temperature gradients. If the temperature is appropriately controlled, however, the reaction yields high enantioselectivity values at nearly complete conversion of the faster enantiomer. This demonstrates the technological feasibility of this reaction and indicates the importance of iterating reactor design improvements though the combination of modeling, simulation and miniplant experiments to optimize selectivity and productivity.

In chemical industry, the application of miniplant technology, modeling and simulation plays a major role in fast development of new products and processes (Behr et al., 2004; Heimann, 2003). This technology is especially suited for mimicking technical operations at the smallest scale. While state-of-the-art in chemical industry, its application in biocatalysis is rare. Only one case has been reported previously (Stadler, 2005). This technology offers also much potential for the field of biocatalysis. The verified model and the learnings presented in this chapter are an example for this.

By application of such miniplant validated models early in development, the gained knowledge and experience may be utilized for sustainable decision making or rationally controlled improvement of the complete process and biocatalyst. This will be reported in future.

7

Applications of Integrated Miniplant Technology and their Opportunity for Process Development of Enzymatic Reactions

Parts of this chapter are published in:

Berendsen, W. R. and Samorski, M. (2006e)

Chemie Ingenieur Technik, **78**, 1013-1021, DOI: 10.1002/cite.200600057

Abstract

The application of integrated miniplant technology, which is the combination of miniplant-technique, modeling and simulation, is state-of-the-art in chemical engineering. This integrated technology offers also enormous potentials for process development of enzyme catalyzed reactions. This chapter provides an overview of the area of application and the potential of this technology for the field of enzyme catalysis.

7.1 Introduction

The high number of biochemical reactions, which are described in scientific literature, show the enormeous potential of enzymes for the production of compounds for the chemical, pharmaceutical and agricultural industry. Often, however, the industrialization of such an enzymatic process fails, due to the considerable development time needed and the concomitant costs involved. The integrated miniplant technology, which is a combination of miniplant-technology, modeling and simulation, enables the integrated analysis of single process units or complete processes to speed up process development (Greß, et al., 1979; Buschulte and Heimann, 1995). Enzymatic processes for the production of medicines, fine- and agrochemicals could benefit significantly by these technologies. Next to the opportunity to evaluate alternative process configurations, this combination of tools allows for fast realization of biocatalytic processes.
In this chapter, an overview of the potential applications of miniplant-technology is presented and their opportunity for biocatalysis highlighted. Next, the miniplant developed at the Institute of Biochemical Engineering is presented, which is the source of many experimental results reported in this thesis.

7.2 Miniplant-Technology

The concept of miniplant-technology was first mentioned in scientific literature in the late seventies (Greß, et al., 1979; Robbins, 1979), which is used for equipment, which is able to mimic technical operation at the smallest scale. Planning, construction and operation of a miniplant needs much less resources than a pilot plant, which results in less cost-intensive process development. In combination with modeling and simulation, the results obtained at miniplant level may be extrapolated to industrial scale. As a result, the intermediary step pilot plant can often be skipped in the development process (Orsat et al., 1999) and the time-to-market reduced significantly.
Hence, trials at miniplant scale deliver know-how about the technical and commercial feasibility of the process (*proof of concept*) at an early stage of the project, especially with regard to product quality, product yield and process stability. Furthermore, they offer the opportunity to study processes continuously (Wörz, 1995), to produce sample amounts for market tests (Wörz, 1995) and to test the stability of used materials (Maier et al., 1990). Next to their application for research and development purposes, they can be applied for production of small product quantities (Behr et al., 2004). For production of

toxic compounds, continuously operated miniplants offer reduced safety risks compared to batch-wise operated production plants (Behr et al., 2000).
Next to the determination of the degree of miniaturization and the acurate design of process units (Steude et al., 1997), measurement technology is key in miniplants. Since the operation of such plants is more cost-intensive than their construction (Greß et al., 1979), each trial should deliver as much information as possible. The precision of measurement and dosing technology are success determining factors (Appelhaus, 1998), just like the significance and reproducibility of obtained data.

7.3 Miniplant Used for Studying Biocatalytic Synthesis of Chiral Glycolethers

The fully-automated miniplant (Figures 7.1-7.7), which was planned, constructed and operated at the Institute of Biochemical Engineering, features complete modularity and flexibility, which is ensured by the use of rapid available components and standardized connections. This allows systematic evaluation of different process alternatives, substrates and biocatalysts at near-industrial conditions. The design and construction of this miniplant was successfully completed through the combination of in-house expertise, outsourcing and technology transfer with Dow Chemical, Midland, MI, USA. Detailed information about the used components and applied methods are available in Chapter 9: Materials and Methods.

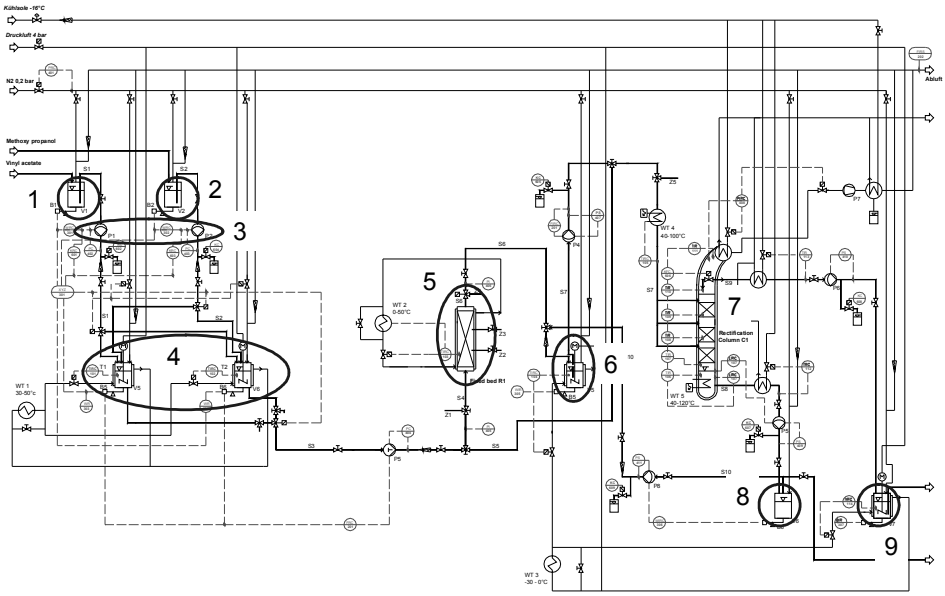

Figure 7.1 Miniplant process information diagram (1, 2: substrate vessels, 3: substrate pumps, 4: mixing vessels, 5: reactor, 6: intermediary vessel, 7: distillation column, 8: bottom product, 9: top product, B: balance, P: pressure sensor, S: stream, T: temperature sensor, V: vessel, WT: cryostat, X, XWT: automatic valve, Z: sampling valve).

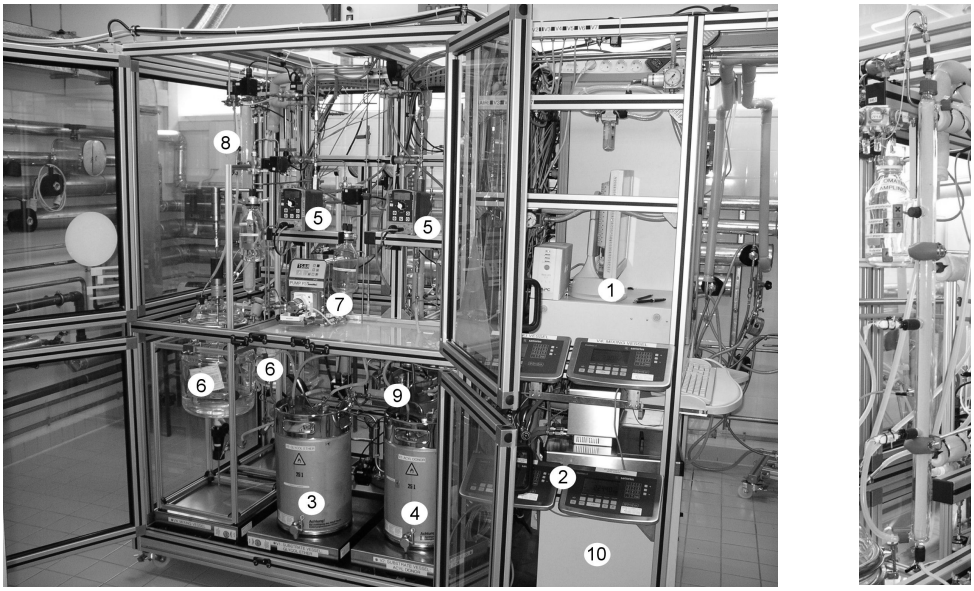

Figure 7.2 left: Reaction part of fully automated miniplant (1: PC for process control, 2: balances, 3: MP substrate vessel, 4: VA substrate vessel, 5: substrate pumps, 6: mixing vessels, 7: pump, 8: fixed bed reactor, 9: intermediate vessel between reaction and distillation part of miniplant, 10: cryostats for temperature control), **right:** fixed bed reactor.

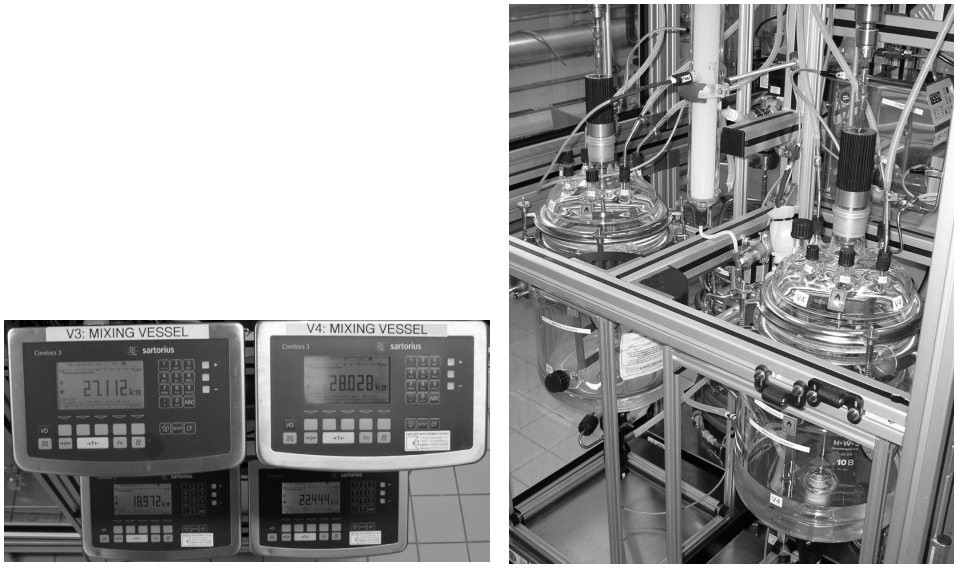

Figure 7.3 left: Balance displays; **right:** mixing vessels and reactor.

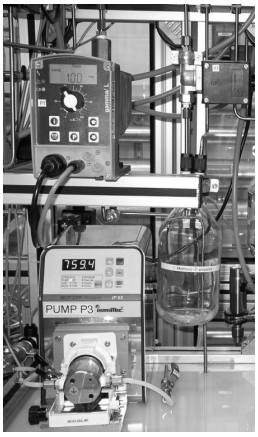

Figure 7.4 left: Substrate tanks on balances; **right:** dosing pumps.

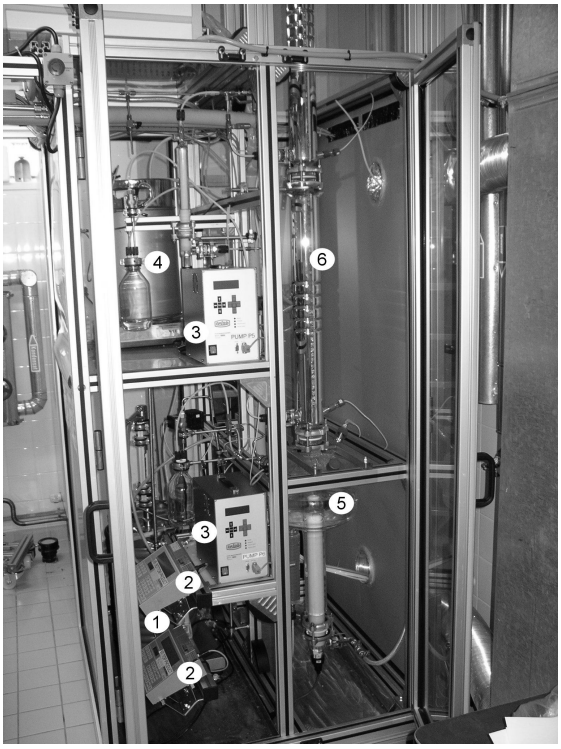

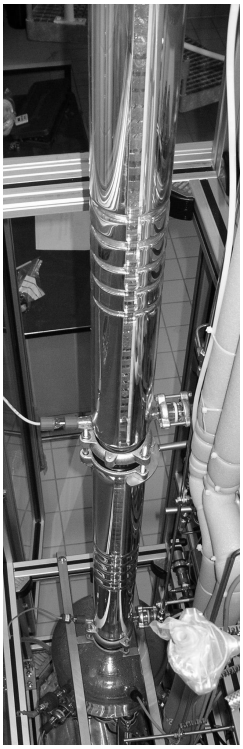

Figure 7.5 left: Distillation part of fully automated miniplant (1: top product vessel, 2: balances, 3: pumps, 5: boiler, 6: packed column with silvered vacuum jacket with approximately 30 theoretical stages); **right:** distillation column viewed from above.

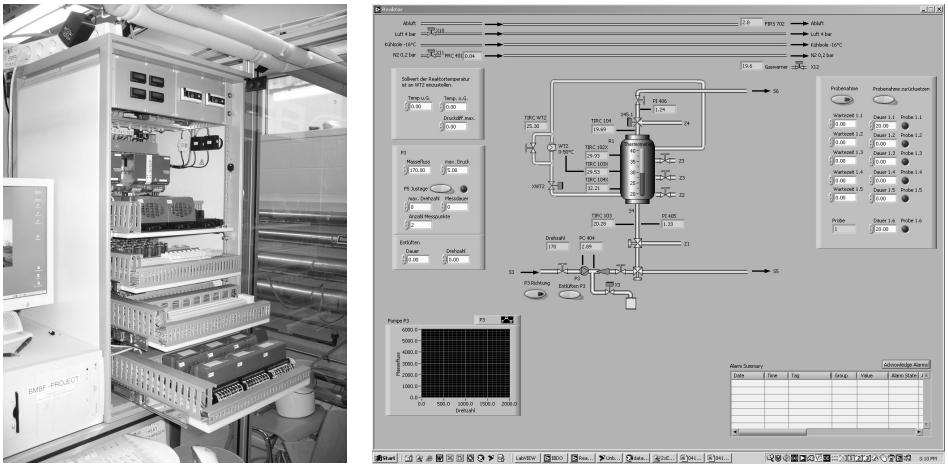

Figure 7.6 left: Electrical switching cabinet and pc; **right:** Labview-based process control software showing the section involving the reaction.

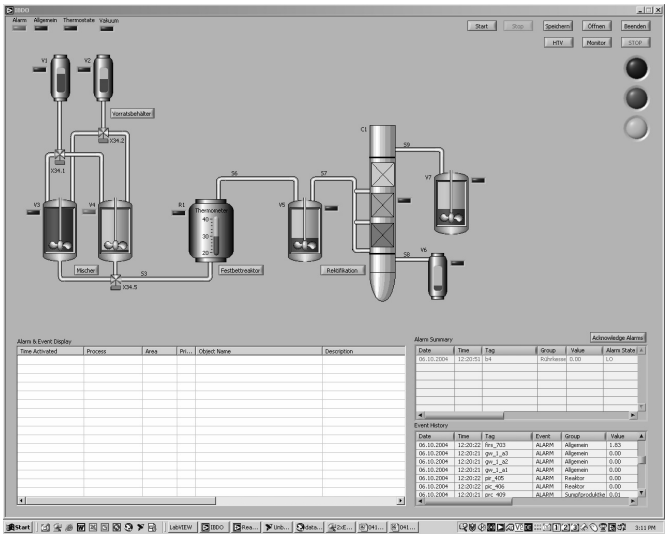

Figure 7.7 Process control software for the miniplant.

8

Concluding Remarks and Outlook

8. Concluding Remarks and Outlook

This study shows how the combination of modeling, simulation and experimental investigations in terms of reaction kinetics and miniplant studies offers much potential for process development of enzyme catalyzed reactions. The combination of these technologies allows mimicking technical operation at the smallest scale.

For this purpose, a fully-automated miniplant was operated following in-house design and construction. The modular concept, which is an integral part of the developed miniplant, enables systematic investigation of different reaction chemistries, various operational modes and/ or alternative routes.

Three reaction alternatives were studied for the kinetic resolution of racemic glycol ethers as a model system for production of chiral secondary alcohols. They are catalyzed by *Candida antarctica* lipase B:

A) The hydrolysis of (R/S)-1-methoxy-2-propyl-acetate with water into (R/S)-1-methoxy-2-propanol and acetate;
B) The irreversible transesterification of (R/S)-1-methoxy-2-propanol with ethyl acetate into (R/S)-1-methoxy-2-propyl-acetate and ethanol;
C) The reversible transesterification of (R/S)-1-methoxy-2-propanol with vinyl acetate into (R/S)-1-methoxy-2-propyl-acetate and acetaldehyde.

Usually, a sustainability analysis consists of three aspects, the economical, ecological and social ones. The social apects are mostly not considered, just like in this study. For quantification of economical and ecological aspects, indicators are defined such as technical feasibility, capital investment or environmental impact. The required supply of raw materials and energy is calculated using mass and energy balances and is based on the mathematical models described in this thesis. For estimation of the impact of the reaction components on the environment, several life cycle analysis (LCA-) methods are available, like for example, Ecoindicator 99 (Europe; Goedkoop and Spriensma, 2000), TRACI (USA; Bare et al., 2003) and EPS 2000 (global; Steen, 2000). Here, the LCA-method EPS 2000 was applied.

The result of this sustainability study is presented in Figure 8.1. From this figure, it can be concluded that two of these alternatives are presently suited for industrialization; Reaction A and C. Reaction C, the *Candida antarctica* lipase B catalyzed transesterification of (R/S)-1-methoxy-propanol with vinyl acetate, is most sustainable.

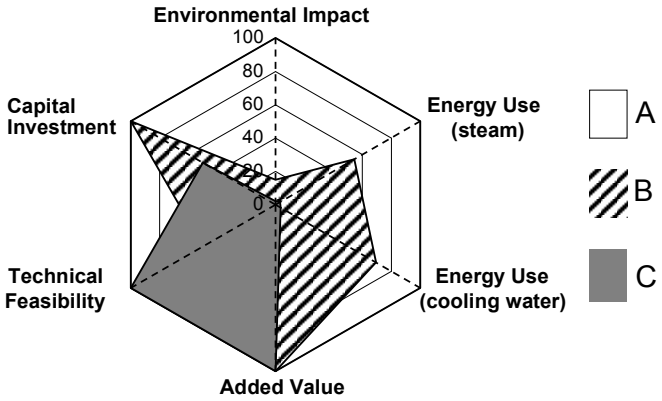

Figure 8.1 Result of sustainability analysis of the three reaction alternatives (A, B and C; in %).

The remaining alternative, Reaction B, is limited by the equilibrium of the reaction, which results in low enantioselectivities at higher conversion and higher initial glycol ether substrate concentrations. *In-situ* removal of the byproduct ethanol from the reaction mixture should resolve these limitations. However, the technologies available to date are not capable of efficiently performing this separation. In this work, pervaporative separation of ethanol from the multicomponent mixture is described. Pervaporation is shown to be strongly influenced by interactions between the permeants and the membrane. Clearly, there is still much to learn about the interactions occurring during pervaporation of multicomponent mixtures. Studies in this field should bring forth new membranes and thus new opportunities for separation of reaction mixtures.

Modeling simulations presented in this thesis elucidate the importance of the position of reaction equilibrium for the conversion and enantioselectivity of a kinetic resolution. Hence, the equilibrium constant should be among one of the first parameters to be studied, when screening substrates for this class of reactions.

The key to successful and fast industrialization of enzyme driven processes is to gain comprehensive understanding of reaction, catalyst and process alternatives. Simultaneous engineering, i.e. the optimization of these alternatives in parallel, helps to achieve this goal. Such studies provide valuable information for sustainability studies, i.e. the economical, ecological and social picture, which should ultimately elucidate which reaction and process candidate is most beneficial for a class of substrates.

9

Materials and Methods

9.1 Materials

9.1.1 Chemicals

(R/S)-1-Methoxy-2-propanol, (R/S)-1-methoxy-2-propyl-acetat, purified R-1-methoxy-2-propyl-acetat (99% e.e.), vinyl acetate and ethyl acetate of 99% purity were kindly provided by The Dow Chemical Company, Stade, Germany. Ethanol, acetonitrile and pentanone of 99% purity originated from Sigma-Aldrich, Hannover, Germany.

9.1.2 Enzyme

Candida antarctica lipase B immobilized on a porous acrylic resin, Chirazyme L-2, c.-f., C2, with a wet particle density, ρ_p, of 200 $g \cdot L^{-1}$ and a particle diameter: 0.3-0.9 mm (Eigtved, 1992) originated from Roche Diagnostics GmbH, Mannheim, Germany.

9.1.3 Membrane

Dense Pervap 2256® membranes were kindly donated by Sulzer Chemtech, Linden, Germany. It is a membrane consisting of a chemically stable non-woven fabric as a sub-structure (~ 100 μm), a porous support of polyacrilonitrile (70 – 100 μm) and a selective poly-(vinyl alcohol) (PVA) membrane (6.25 μm) (Ortiz, et al., 2002; Sharma, et al., 2004).

9.2 Experimental Methods for Determination of Kinetics

The experimental methods used for determination of kinetic parameters differ for each reaction alternative and are described below.

9.2.1 Time Course Measurements of MPA Hydrolysis

The time course measurements described in Chapter 2 were performed at various initial MPA-concentrations in a 50 mL stirred tank reactor using 2 $g \cdot L^{-1}$ immobilized CAL-B at constant temperature and pH. For pH-control, a potentiometric titrator was used (Metrohm 719S, Filderstadt, Germany) in combination with a suitable buffer (e.g. 50 mM K_2PO_4 buffer for pH 7). Triplicate 100 µL samples were taken and extracted with 1 mL octanol containing 20 mM pentanone as internal standard (results not shown). The octanol phase was then used for GC-analysis.

9.2.2 Initial Rate Measurements of MP-EA Transesterification

The initial rate measurements presented in Chapter 3 are performed in a pure mix of substrates and products (MP, MPA, EA and EtOH) in a 10 mL stirred tank reactor using up to 20 $g \cdot L^{-1}$ immobilized CAL-B at 30°C. Triplicate 100 µL samples are taken and added to 1 mL octanol, containing 20 mM pentanone as internal standard. These samples are then analyzed by gas chromatography.

9.2.3 Time Course Measurements of MP-VA Transesterification

The time course measurements mentioned in Chapter 5 were performed at various initial substrate concentrations at constant temperatures (T=5-56°C). The reaction was started by adding typically 1 %v/v (i.e. 1-ε_L) of immobilized CAL-B to a temperature controlled 10 mL stirred tank reactor, which contained a defined mixture of MP and VA. Triple samples were taken at various intervals, diluted 1:50 with acetonitrile containing 10 mM Pentanone as internal standard and analyzed by GC.

9.3 Miniplant Experiments

9.3.1 Design, Construction, Start-up and Operation

In Figure 9.1, a detailed process information diagram (PID) of the fixed bed reactor are displayed. The miniplant was built within a Bosch-Rexroth frame (UTZ Ratio Technik, Korb). Process control equipment and software were supplied by National Instruments (Labview®, Austin, TX, USA).

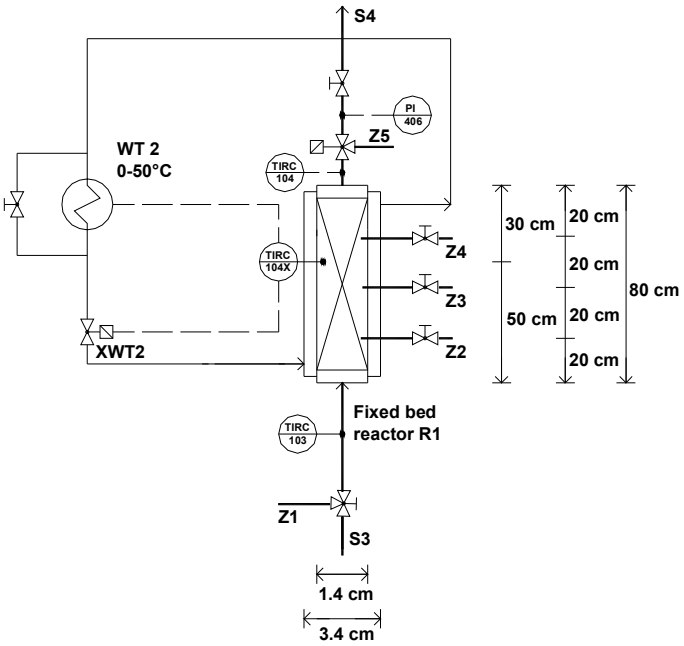

Figure 9.1 Detailed process information diagram of the miniplant reactor used for verification of the reactor model (PI: pressure sensor, S: stream, TIRC: temperature sensor, WT: cryostat, XWT: automatic valve, Z: sampling valve).

9.3.2 Typical Miniplant Operation and Measurements

Substrates were added separately to 25L stainless steel vessels (V1, V2) after which they were automatically pumped (gamma/L ProMinent Dosiertechnik GmbH, Heidelberg) in the correct ratio and amount to 20L glass vessels (V3, V4, HWS Labortechnik, Mainz) and mixed by air-driven stirrers (Gebr. Buddeberg GmbH, Mannheim). The temperature

of this mix was adjusted prior to being pumped by an Ismatec MCP-CPF process pump with QP-Q1 pump head (Wertheim, Germany) into the bottom of the jacketed fixed bed reactor (Glasgerätebau Ochs GmbH, Bovenden Lenglern). The temperature of the reactor was controlled using a PT100 sensor (RS Components GmbH, Mörfelden-Walldorf) at x=0.63 as set point for a cryostat (F33, Julabo, Seelbach), which employed a 50-50 mixture of water and ethanol as cooling medium. Flow rates were calibrated and measured accurately using Sartorius Combics 3 balances (HBH Ebinger, Fichtenberg).

Samples were taken at 25%, 50%, 75% and 100% relative reactor height at various conditions. These samples were further processed, by pipetting in triplicate 50μL of each sample into 950μL acetonitrile, containing 10 mM Pentanone as internal standard. These samples were further analyzed by gas chromatography to determine the local concentrations of R-MPA and S-MPA in the reactor.

In addition to these concentration measurements, the temperature of the reaction medium was measured continuously at 19%, 63% and 95% relative reactor height and the mass flow was determined by analyzing the loss of weight over time of the tanks containing the substrate mixture (V3, V4). The temperature in the reactor was controlled using the sensor at 63% relative reactor height.

9.4 Pervaporation Experiments

9.4.1 Setup

Scheme 9.2 shows schematically the experimental setup used for the pervaporation experiments of Chapter 4. To ensure quasi-stationary conditions of the feed, the volume of the membrane cell was expanded by circulating the feed mixture between the membrane cell and vessel V1 (5L) at 2 L/h (P1, P2: Beta dosing pumps, ProMinent Dosiertechnik GmbH, Heidelberg, Germany). The membrane cell was equipped with an electric motor (45W, maximum speed 3000 min^{-1}) to minimize concentration and temperature polarization on the surface of the membrane. For more details about this cell, see the paper of Indlekofer, et al. (1995). Membranes of 90 mm diameter were fixed on a PTFE-coated support plate (Millipore, Eschborn). The membrane upstream side was kept at atmospheric pressure and the downside pressure was controlled by a vacuum pump (P3, PIC 201: MD4, Vacuubrand, Wertheim). Due to atmospheric pressure in

vessel V2 as well as two condensers in stream S5 (HE3: Haake N6, at -30°C), the permeated vapor was condensed in V2. Each hour, the permeate was returned to V1 by another Beta dosing pump (P4) to maintain a constant feed composition. Temperature control of V1 and MR was maintained by MGW-Lauda thermostats, Lauda-Königshofen.

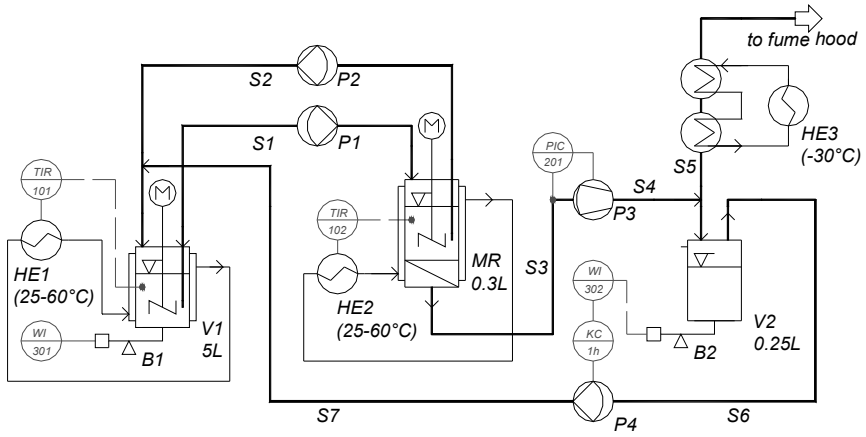

Scheme 9.2 Schematic diagram of the experimental system (B: balance; HE: heat exchanger; KC: time control; M: stirrer motor; MR: membrane cell; P: pump; S: stream; TIR: temperature identification & regulation; PIC: pressure identification & control; V: vessel; WI: weight identification).

9.4.2 Procedure

Prior to a typical pervaporation measurement, the dry Pervap 2256® membrane was first installed in the membrane cell. Next, the desired vacuum pressure was adjusted and as a final step the pumps P1 and P2 were turned on. This was done to prevent unwanted membrane swelling following the manufacture's advice.

During an operation time of >25h, 10 μL samples were taken out of vessel V2 and membrane cell MR, which were analyzed by gas chromatography. The total pervaporation flux was measured using balances. Once in two weeks a pervaporation experiment was performed with identical conditions to check reproducibility as well as long-term membrane quality. Over a period of several months, no changes have been observed. This was also true for the feed composition; indicating that the cooling

temperature of both condensers was sufficient as well as no leakage was present in the loop.

9.5 Analytical Methods: Gas Chromatography

A CP3800 gas chromatograph of Varian, Darmstadt, Germany, was used, equipped with two chiral columns: an α-dex 120 chiral capillary column (30 m x 0.25 mm x ID 0.25 µm, Supelco) and a β-dex column (25m x 0.25 mm x ID 0.25µm, CP7502, Varian). A single temperature program was used: 1 min at 40°C, 5°C·min^{-1} to 45°C, 10°C·min^{-1} to 100°C, 80°C·min^{-1} to 200°C, 2 min hold at 200°C. Helium was used as carrier gas (1.3 mL·min^{-1}) and the compounds were detected using a flame ionization detector (FID) at 250°C. The injector was set to 200°C and the split ratio was 1:20. Retention times for EtOH, EA, R-MP, S-MP, R/S-MPA on the α-dex column were 3.1, 4.0, 6.6, 6.8 and 10.2 min, respectively. Retention times for R/S-MP, S-MPA, R-MPA on the β-dex column were 6.3, 9.6 and 10.2 min, respectively.

9.6 Calculation Methods

9.6.1 Determination of Kinetic Parameters

The kinetic parameters of the model presented in Chapters 2 and 3 were determined using non-linear parameter estimation. For this purpose, the integrated software system at the institute of biochemical engineering was used, which consists of the commercial software packages OptdesX, Version 2.04, Design Synthesis Inc., Provo, UT, USA (optimization), ACSL, Huntsville, AL, USA (integration) and Maple, Waterloo, Ontario, Canada (symbolic model generation). During estimation, the relative error between measurement and model data was minimized.

For determination of kinetic parameters of the transesterification of 1-methoxy-2-propanol with vinyl acetate (Chapter 5), the coupled mathematical equations (5.12)-(5.17) are solved using implicit numerical methods with iterations, as described by Patankar (1982)[3].

[3] Numerical calculations were performed by Alexei Lapin at the IBVT, University of Stuttgart

9.6.2 Performing Reactor Simulations

The reactor simulations described in Chapter 3 are performed with the program Aspen Custom Modeler 11.1 (Aspen Technology, Cambridge, MA, USA) The modeling results of this program are transferred using Visual Basic scripting to Microsoft Excel (Microsoft Corporation, Redmond, USA) for comparison with experimental results and graphical representation.

9.6.3 Calculation of Effective Diffusion Coefficient

The rate of diffusion inside the porous matrix is determined by the effective diffusion coefficient, $D_{eff,i}$ (Equation (5.3)). It can be calculated using the following relationship, assuming the radius of the substrates, $r_{subs,i}$, are much smaller than the radius of the particle pores, r_{pore}:

$$D_{ep,i} = D_{0,i}\frac{\varepsilon_p}{\lambda}\left(1-\frac{r_{subs,i}}{r_{pore}}\right)^4 \approx D_{0,i}\frac{\varepsilon_p}{\lambda} \text{ for } r_{subs,i} << r_{pore} \qquad (5.21)$$

The porosity, ε_p, and tortuosity, λ, of the particle were assumed to be independent of concentration and temperature and equal to 0.5 and 6, respectively (Duan et al., 1997). The diffusivity at infinite concentration in organic solvents may be calculated by an empirical correlation (Scheibel, 1954):

$$D_{0,i} = \frac{8.2\cdot 10^{-8}\cdot T}{\mu_B \cdot \hat{V}_A}\left[1+\left(\frac{3\cdot\hat{V}_B}{\hat{V}_A}\right)^{2/3}\right] \qquad (cm^2\cdot s^{-1}) \qquad (5.22)$$

$\hat{V}_j$	saturated liquid volume	($cm^3\cdot mol^{-1}$)
λ	particle tortuosity	(-)
μ_j	viscosity	(cP)

j = A,B, where A and B denote the solute and solvent, respectively.

The viscosity of the solvent, μ_B, was assumed to be independent of concentration of the components and calculated by averaging the values obtained from the mixing rule for hydrocarbon mixtures at typical mol fractions, x_i (Perry, 1999):

$$\mu_B = \left[\sum_i^n \left(x_i \cdot \mu_i \right)^{0.33} \right]^3 \approx 1 Pa \cdot s \text{ with i = MP, VA, MPA, Ac} \quad (5.23)$$

The saturated liquid volume, $\hat{V}_i$, was calculated using the Rackett equation as modified by Spencer and Danner (1972):

$$\hat{V}_i^{-1} = \left(\frac{R \cdot T_{crit,i}}{P_{crit,i}} \right) Z_{RA,i}^{1+\left(1-\frac{T}{T_{crit}}\right)^{2/7}} \quad (\text{mol} \cdot \text{m}^3) \quad (5.24)$$

$T_{crit,i}$	critical temperature	(K)
$P_{crit,i}$	critical pressure	(Pa)
$Z_{RA,i}$	Rackett parameter	(-)

Thermophysical data for this equation was obtained from the NIST Chemistry WebBook (http://webbook.nist.gov/chemistry/) and the Korea Thermophysical Properties Data Bank (KDB; http://infosys.korea.ac.kr/kdb/): $T_{crit,\ MP}$ = 579.8 K; $T_{crit,\ VA}$ = 519.13 K; $P_{crit,\ MP}=41.85 \cdot 10^5$ Pa; $P_{crit,\ VA}=41.85 \cdot 10^5$ Pa; $Z_{RA,\ MP}$ = 0.2583; $Z_{RA,\ VA}$ = 0.2636.

List of Publications

I. Berendsen, W. R., Gendrot, G., Resnick, S. M., Reuss, M. (2006a). Kinetic modeling of lipase catalyzed hydrolysis of (R/S)-1-methoxy-2-propyl-acetate as a model reaction for production of chiral secondary alcohols. *Journal of Biotechnology*, **121**, 213-226, DOI: 10.1016/j.jbiotec.2005.07.006.

II. Berendsen, W. R., Gendrot, G., Freund, A., Reuss, M. (2006b). A kinetic study of lipase-catalyzed reversible kinetic resolution involving verification at miniplant-scale. *Biotechnology and Bioengineering*, **95**, 883-892, DOI: 10.1002/bit.21034.

III. Berendsen, W. R., Radmer, P., Reuss M. (2006c). Pervaporative Separation of Ethanol from an Alcohol – Ester Quaternary Mixture. *Journal of Membrane Science*, **280**, 684-692, DOI:10.1016/j.memsci.2006.02.029.

IV. Berendsen, W. R., Lapin, A., Reuss, M. (2006d). Investigations of reaction kinetics for immobilized enzymes – Identification of parameters in the presence of diffusion limitation. *Biotechnology Progress*, **22**, 1305-1312, DOI: 10.1021/bp060062e

V. Berendsen, W. R., Lapin, A., Reuss, M. (2007) Nonisothermal Lipase-Catalyzed Kinetic Resolution in a Packed Bed Reactor: Modeling, Simulation and Miniplant Studies, *Chemical Engineering Science*, **62**, 2375-2385, DOI: 10.1016/j.ces.2007.01.006

VI. Berendsen, W. R. and Samorski, M. (2006e) Einsatz und Potenzial der integrierten Miniplant-Technologie für die Enzymkatalyse, *Chemie Ingenieur Technik*, **78**, 1013-1021, DOI: 10.1002/cite.200600057

References

Al-Azemi, T. F. and Bisht, K. S. (2002) One-step synthesis of polycarbonates bearing pendant carboxyl groups by lipase-catalyzed ring-opening polymerization, *J. Polymer Sc. Part A: Polymer Chem.*, **40**, 1267-1274

Anderson, E.M., Larsson, K.M., and Kirk, O. (1998) One biocatalyst—many applications: The use of *Candida antarctica*, *Biocatal. Biotransform.*, **16**, 181–204

Appelhaus, P. (1998) Meßtechnik in miniplants: Erfolgbestimmender Faktor für das Gesamtprojekt, *Chem. Tech.*, **27**, 26-30

Atkinson, B., Lester, D. E. (1974) An enzyme rate equation for the overall rate of reaction of gel-immobilized glucose oxidase particles under buffered conditions. I. Pseudo-One Substrate Conditions, *Biotechnol. Bioeng.*, **16**, 1299-1320

Arroyo, M. and Sinisterra, J. V. (1994) High enantioselective esterification of 2-arzlpropionic acids catalysed by immobilized lipase from Candida antarctica: A mechanistic approach, *J. Org. Chem.*, **59**, 4410-4417.

Arroyo, M. and Sinisterra, J. V. (1995) Influence of chiral carvones on selectivity of pure lipase B from Candida antarctica, *Biotechnol. Lett.*, **17**, 525-530

Ayhan, F., Ayhan, H., Piskin, E., Tanyolaç, A. (2002) Optimization of urease immobilization on non-porous HEMA incorporated poly(EGDMA) microbeads and estimation of kinetic parameters, *Bioresource Technol.*, **81**, 131-140

Bailey, J. E. and Ollis, D. F., (1986) Biochemical Engineering Fundamentals, 2nd ed. McGraw-Hill, New York

Bare, J. C., Norris, G. A., Pennington, D. W., McKane, T. (2003) *J. Ind. Ecol.*, **6**, 3

Bartling, K., Thompson, J. U. S., Pfromm, P. H., Czermak, P., Rezac, M. E. (2001) Lipase catalyzed synthesis of geranyl-acetate in n-Hexane with membrane-mediated water removal, *Biotechnol. Bioeng.*, **75**, 676-681

Baumann, M., Hauer, B. H., Bornscheuer, U. T. (2000) Rapid screening of hydrolases for the enantioselective conversion of „difficult to resolve substrates“, *Tetrahedron: Asymmetry*, **11**, 4781-4790

Behr, A., Brehme, V. A., Ewers, C. L. J., Groen, H., Kimmel, T., Kueppers, S., Symietz, I. (2004) New developments in chemical engineering for the production of drug substances, *Eng. Life Sci.*, **4**, 15-24

Behr, A., Ebbers, W., Wiese, N. (2000) Miniplants - Ein Beitrag zur inhärenten Sicherheit? *Chem.-Ing.-Tech.*, **72**, 1157-1166

Bocola, M. (2002) Strukturelle und kinetische Untersuchungen zum Mechanismus und Vorhersage der stereoselektiven Substraterkennung von Lipasen, Thesis, Lübeck

Bornscheuer, U. T. and Kazlauskas, , R. J. (1999) Hydrolases in organic synthesis, Wiley-VCH, Weinheim

Bousquet, M. P., Willemot, R. M., Monsan, P., Boures, E. (2000) Enzymatic synthesis of alpha-butylglucoside linoleate in a packed bed reactor for future pilot scale-up, *Biotechnol. Prog.*, **16**, 589-594

Bousquet-Dubouch, M. P., Graber, M., Sousa, N., Lamare, S., Legoy, M. D. (2001) Alcoholysis catalyzed by *Candida antarctica* lipase B in a gas/solid system obeys a ping pong bi bi mechanism with competitive inhibition by the alcohol substrate and water, *Biochim. Biophys. Acta*, **1550**, 90-99

Brun, J. P., Larchet, C., Melet, R., Bulvestre, G. (1985) Modeling of the pervaporation of binary mixtures through moderately swelling, non-reacting membranes, *J. Membr. Sci.*, **23**, 257-283

Buschulte, T. K. and Heimann, F. (1995) Verfahrensentwicklung durch Kombination von Prozeßsimulation und Miniplant-Technik, *Chem.-Ing.-Tech.*, **67**, 718-723

Carrara, C. R., Mamarella, E. J., Rubiolo, A. C. (2003) Prediction of the fixed-bed reactor behaviour using dispersion and plug-flow models with different kinetics for immobilized enzyme, *Chem. Eng. J.*, **92**, 123-129

Chang, C. S., Tsai, S. W., Kuo J. (1999) Lipase-catalyzed dynamic resolution of naproxen-2,2,2-trifluoroethyl thioester by hydrolysis in isooctane, *Biotechnol. Bioeng.*, **64**, 120-126

Chang, R. (1981) Physical chemistry with applications to biological systems, 2nd ed., Macmillan Publishing Co. Inc., New York

Chen, C.-S., Wu, S.-H., Girdaukas, G., Sih, G.J. (1987) Quantitative analysis of biochemical kinetic resolution of enantiomers. 2. Enzyme-catalyzed esterifications in water-organic biphasic systems, *J. Am. Chem. Soc.*, **109**, 2812-2817

Chen, K. C., Wu, J. Y., Yang, W. B., Hwang, S. C. J. (2003) Evaluation of effective diffusion coefficient and intrinsic kinetic parameters on azo dye biodegradation using PVA-immobilized cell beads, *Biotechnol. Bioeng.*, **83**, 821-832

Ching, C. B., Chu, K. H. (1988) Modelling of a fixed bed and a fluidized bed immobilized enzyme reactor, *Appl. Microbiol. Biotechnol.*, **29**, 316-322

Chulalaksananukul, W., Condoret, J. S., Combes, D. (1992) Kinetics of geranyl acetate synthesis by lipase-catalyzed transesterification in n-hexane, *Enzyme Microb. Technol.*, **14**, 293-298

Degueil-Castaing, M., De Jeso, B., Drouillard, S., Maillard, B. (1987) Enzymatic reactions in organic synthesis: 2-ester interchange of vinyl esters, *Tetrahedron Lett.*, **28**, 953-954

Drauz, K. and Waldmann, H. eds. (1995) *Enzyme catalysis in organic synthesis*, Wiley-VCH, Weinheim

Duan, G., Ching, C. B., Lim, E., Ang, C. H. (1997) Kinetic study of enantioselective esterification of ketoprofen with n-propanol catalysed by a lipase in an organic medium, *Biotechnol. Lett.*, **19**, 1051-1055

Eigtved, P. (1992) Immobilization of lipase by adsorption on a macroporous resin, Patent, US 5,156,963

Faber, K., (1997) Biotransformations in organic chemistry, 3rd ed., Springer, Berlin

Faqir, N. M. and Attarakih, M. M. (2002) Optimal temperature policy for immobilized enzyme packed bed reactor performing reversible Michaelis-Menten kinetics using the disjoint policy, *Biotechnol. Bioeng.*, **77**, 163-173

Faqir, N. M. (2004) Optimization of operating temperature for an continuous immobilized glucose isomerase reactor with pseudo linear kinetics, *Eng. Life Sci.*, **4**, 450-459

Favre, E., Nguyen, Q. T., Clement, R., Neel J. (1996) The engaged species induced clustering (ENSIC) model : A unified mechanistic approach of sorption phenomena in polymers, *J. Membr. Sci.*, **117**, 227-236

Feng, X. and Huang, R. Y. M. (1996) Estimation of activation energy for permeation in pervaporation, *J. Membr. Sci.*, **118**, 127-131

Ferscht, A. R. (1985) Enzyme structure and mechanism. 2nd edn. WH Freeman and Company, San Francisco

Fishman, A., Eroshov, M., Dee-Noor, S. S., van Mil, J., Cogan, U., Effenberger, R. (2001) A two-step enzymatic resolution process for large-scale production of (S)- and (R)-ethyl-3-hydroxybutyrate, *Biotechnol. Bioeng.*, **74**, 256-263

Flores, M. V. and Halling, P. J., (2002) Full model for reversible kinetics of lipase-catalyzed sugar-ester synthesis in 2-methyl-2-butanol, *Biotechnol. Bioeng.*, **78**, 794-800

Goedkoop, M. and Spriensma, R. (2000) The Eco-indicator 99. A damage oriented method for life cycle impact assessment, methodology report, Zürich, http://www.pre.nl

Ghanem, A., Aboul-Enein, H. Y. (2004a) Application of lipases in kinetic resolution of racemates, *Chirality*, **17**, 1-15.

Ghanem, A., Aboul-Enein, H. Y. (2004b) Lipase-mediated chiral resolution of racemates in organic solvents, *Tetrahedron: Asymmetry*, **15**, 3331-3351

Ghoreyshi, S. A. A., Farhadpour, F. A., Soltanieh, M. (2002) Multicomponent transport across nonporous polymeric membranes, *Desalination*, **144**, 93-101

Giordano, R. L. C., Giordano, R. C., Cooney, C. L. (2000) A study on intra-particle diffusion effects in enzymatic reactions: glucose-fructose isomerization, *Bioproc. Eng.*, **23**, 159-166

Gonçalves, L. R. B., Suzuki, G. S., Giordano, R. C., Giordano, R. L. C. (2001) Kinetic and mass transfer parameters of maltotriose hydrolysis catalyzed by glycoamylase immobilized on macroporous silica and wrapped in pectin gel, *Appl. Biochem. Biotechnol.*, **91-93**, 691-702

González, G., Caminal, G., de Mas, C., Lopez-Santin, J. (1989) An approach in mathematical modeling of an upflow packed-bed reactor for enzymatic hydrolysis of wheat straw, *Biotechnol. Bioeng.*, **34**, 242-251

González, B. G. and Uribe, I. O. (2001) Mathematical modeling of the pervaporative separation of methanol – methyl *tert*-butyl ether mixtures, *Ind. Eng. Chem. Res.*, **40**, 1720-1731

Greenlaw, F. W., Shelden, R. A., Thompson, E. V. (1977) Dependence of diffusive permeation rates on upstream and downstream pressures II. Two component permeant, *J. Membr. Sci.*, **2**, 333-348

Greß, D., Hartmann, H., Kaibel, G., Seid, B. (1979) Einsatz von mathematischen Simulationen und Miniplant-Technik in der Verfahrenstechnik, *Chem.-Ing.-Tech.*, **51**, 601-611

Guisán, J. M., Melo, F. V., Ballesteros, A. (1981) Determination of intrinsic properties of immobilized enzymes. 2. Kinetic studies on sepharose-saphylococcal nuclease in the presence of diffusional limitations, *Appl. Biochem. Biotechnol.*, **6**, 37-51

Hasanoğlu, A., Salt, Y., Keleşer, S. Özkan, S. Dinçer, S. (2005) Pervaporation separation of ethyl acetate – ethanol binary mixtures using polymethylsiloxane membranes, *Chem. Eng. Process.*, **44**, 375-381

Hassan, M. M., Atiqullah, M., Beg, S. A., Chowdhury, M. H. M. (1995) Analysis of non-isothermal tubular reactor packed with immobilized enzyme systems, *Chem. Eng. J.*, **58**, 275-283

Hassan, M. M., Atiqullah, M., Beg, S. A., Chowdhury, M. H. M. (1996) Effects of enzyme microcapsule shape on the performance of a nonisothermal packed-bed tubular packed bed reactor, *J. Chem. Technol. Biotechnol.*, **66**, 41-55

Heimann, F. (2003) Process intensification through the combined use of process simulation and miniplant technology, *Comput. Aided Chem. Eng.*, **14**, 155-160

Hein, S. and Vortmeyer, D. (1995) Wandgekühlte chemische Festbettreaktoren und deren Modellierung mit Ein- und Zweiphasenmodellen, *Z. Naturforsch.*, **50a**, 568-576

Heinsman, N. W. J. T., Valente, A. M., Smienk, H. G. F., Padt, van der A., Franssen, M. C. R., Groot, de A., Riet, van 't, K. (2001) The effect of ethanol on the kinetics of

lipase-mediated enantioselective esterification of 4-methylocatnoic acid and the hydrolysis of its ethyl ester, *Biotechnol. Bioeng.*, **76**, 193-199

Henke, E., Schuster, S., Yang, H., Bornscheuer, U. T. (2000) Lipase-catalyzed resolution of ibuprofen, *Monatshefte für Chemie*, **131**, 663-638

Hofen, W., Körfer, M., Zetzmann, K. (1990) Scale-up-Probleme bei der experimentellen Verfahrensentwicklung, *Chem.-Ing.-Tech.*, **62**, 805-812

Hoff, B.H., Waagen, V., Anthonsen, T. (1996) Resolution of 1-phenoxy-, 1-phenylmethoxy- and 1-(2-phenyletoxy)-2-propanol and their butanoates by hydrolysis with lipase B from *Candida antarctica*, *Tetrahedron: Asymmetry*, **7**, 3181-3186

Holmes, J. L. and Lossing F. P. (1982) Heats of formation of the ionic and neutral enols of acetaldehyde and acetone, *J. Am. Chem. Soc.*, **104**, 2648-2652

Houlton, S. (2002) Chirals gain in importance, *Chemical Week*

Hu, C. H., Brinck, T., Hult, K. (1998) Ab initio and density functional theory studies of the catalytic mechanism for ester hydrolysis in serine hydrolases, *Int. J. Quantum Chem.*, **69**, 89-103

Indlekofer, M., Brotz, F., Bauer, A., Reuss, M. (1996) Stereoselective bioconversions in continuously operated fixed bed reactors: modeling and optimization, *Biotechnol. Bioeng.*, **52**, 459-471

Indlekofer, M., Funke, M., Claassen, W., Reuss, M. (1995) Continuous enantioselective transesterification in organic solvents. Use of suspended lipase preparations in a microfiltration membrane reactor, *Biotechnol. Prog.*, **11**, 436-442

Indlekofer, M., Reuss, M., Barth, S., Effenberger, F. (1993) Kinetic analysis and simulation studies for lipase-catalyzed resolution of racemic 2-methyl-1-pentanol, *Biocatalysis*, **7**, 249-266

Jacobsen, E. W. Skogestad, S. (1994) Instability of Distillation Columns, *AIChE J.*, **9**, 1466-1478

Ji, W., Sikdar, W. K., Hwang, S.-T. (1994) Modeling of multicomponent pervaporation for removal of volatile organic compounds from water, *J. Membrane Sci.*, **93**, 1-19

Jiraratananon, R., Chanachai, A., Huang, R. Y. M. (2002) Pervaporation dehydration of ethanol-water mixtures with chitosan/hydroxyethylcellulose (CS/HEC) composite membranes. II Analysis of mass transport, *J. Membr. Sci.*, **199**, 211-222

Jonquières, A., Clément, R., Roizard, D., Lochon, P. (1996) Pervaporative transport modelling in a ternary system : ethyltertiarybutylether / ethanol / polyurethaneimide, *J. Membrane Sci.*, **109**, 65-76

Jung, H. J. and Bauer, W. (1992) Determination of process parameters and modelling of lipase-catalyzed transesterification in a fixed bed reactor, *Chem. Eng. Sci.*, **15**, 341-348

Kazlauskas, R. J. and Bornscheuer, U. T. (1998) Biotransformations with lipases. Biotechnology-Series. Eds.: Rehm, H. J., Reed, G., Pühler, A., Stadler, P. J. W. and Kelly, D. R., Weinheim, VCH-Wiley, 8a, 37-191

Kielbasinski, P., Omelanczuk, J., Mikolajczyk, M. (1998) Lipase-promoted kinetic resolution of racemic, P-chiral hydroxymethylphosphonates and phosphinates, *Tetrahedron: Asymmetry*, **9**, 3283-3287

Kirchner, G., Scollar, M. P., Kilbanov, A. M. (1985) *J. Am. Chem. Soc.*, **107**, 7072-7076

Kraut, J. (1977) Serine protease: structure and mechanism of catalysis. *Annu. Rev. Biochem.*, **46**, 331-358

Krishna, S.H., Karanth, N.G. (2002) Lipases and lipase-catalyzed esterification reactions in nonaqueous media. *Cat. Rev. - Sci. Eng.*, **44**, 499-591

La Ferla, B. (2002) Lipases as useful tools for the stereo- and regioselective protection and deprotection of carbohydrates, *Monatsh. Chem.*, **133**, 351-368

Lapin, A., Müller, D., Reuss, M. (2004) Dynamic behavior of microbial populations in stirred bioreactors simulated with Euler-Lagrange methods – traveling along the lifelines of single cells, *Ind. Eng. Chem. Res.*, **43**, 4647-4656

Lapin, A., Schmid, J., Reuss, M. (2006) Modeling the dynamics of *E. coli* populations in the three-dimensional turbulent field of a stirred-tank bioreactor — A structured–segregated approach, *Chem. Eng. Sci.*, **61**, 4783-4797

Lee, W. H., Kim, K.-J., Kim, M. G., Lee, S. B. (1995) Enzymatic resolution of racemic ibuprofen esters: effects of organic cosolvents and temperature, *J. Ferm. Bioeng.*, **80**, 613-615

Liang, Y., Wu, Y., Dinghuo, L., Wang, C., Liu, Y., Songsheng, Q., Zou, G. (1997) Thermokinetic models of enzyme-catalyzed reactions in batch and plug-flow reactors, *Thermochim. Acta*, **307**, 149-153

Lida, T. and Mase, T. (2002) Scalable enantioselective processes for chiral pharmaceutical intermediates, *Curr. Opin. Drug Discov. Devel.*, **5**, 834-851

Lin, S. H. (1972) Nonisothermal immobilized enzyme reaction in a packed bed reactor, *Biophysik*, **8**, 302-309

Lin, S. H. (1991) Optimal feed temperature for an immobilized enzyme packed-bed reactor, *J. Chem. Technol. Biotechnol.*, **50**, 17-26

Lortie, R. (1994) Evaluation of the performance of immobilized enzyme reactors with Michaelis-Menten kinetics, *J. Chem. Technol. Biotechnol.*, **60**, 189-193

Lortie, R. and Thomas, D. (1986) Heterogeneous one-dimensional model for fixed bed enzyme reactors, *Biotechnol. Bioeng.*, **28**, 1256-1260

Lozano, P., Daz, M., de Diego, T., Iborra, J.L. (2003a) Ester synthesis from trimethylammonium alcohols in dry organic media catalyzed by immobilized *Candida antarctica* lipase B, *Biotechnol. Bioeng.*, **82**, 352-358

Lozano, P., Diego, de T., Carrie, D., Vaultier, M., Iborra, J. L. (2003b) Lipase catalysis in ionic liquids and supercritical carbon dioxide at 150 degrees C, *Biotechnol. Prog.*, **19**, 380-382

Magnusson, A. O., Rotticci-Mulder, J. C., Santagostino, A., Hult K. (2005) Creating space for large secondary alcohols by rational redesign of Candida antarctica lipase B, *ChemBioChem*, **6**, 1051-1056

Maier, S. and Kaibel, G. (1990) Verkleinerung verfahrenstechnischer Versuchsanlagen - Was ist erreichbar? *Chem. Ing. Tech.*, **62**, 169-174

Marrazzo, W. N., Merson, R. L., McCoy, B. J. (1975) Enzyme immobilized in a packed-bed reactor: kinetic parameters and mass transfer effects, *Biotechnol. Bioeng.*, **17**, 1515-1528

Marsh, D. R. and Tsao, G. T. (1976a) A heat transfer study on packed bed reactors of immobilized glucoamylase, *Biotechnol. Bioeng.*, **18**, 349-362

Marsh, D. R. and Tsao, G. T. (1976b) A theoretical and computational study of the heat effects on packed-bed reactors of immobilized enzymes, *J. Solid-Phase Biochem.*, **1**, 67-79.

Martinelle, M. and Hult, K. (1995) Kinetics of acyl transfer reactions in organic media catalyzed by *Candida antarctica* lipase B, *Biochim. Biophys. Acta*, **1251**, 191-197

Marx, S., Gryp, P. v. d., Neomagus, H., Everson, R., Keizer, K. (2002) Pervaporation separation of methanol from methanol/*tert*-amyl methyl ether mixtures with a commercial membrane, *J. Membr. Sci.*, **209**, 353-362

Masoud, F., Nasrin, M., Saeed, M., Reza, M., Manouchechr, V., Reza, B. M. (2002) Kinetic behaviour of α-galactosidase produced by Absidia griseola: a comparison between free and immobilized forms of the enzyme, *World J. Microb. Biotechnol.*, **18**, 649-653

Mei, Y., Miller, L., Gao, W., Gross, R.A. (2003) Imaging the distribution and secondary structure of immobilized enzymes using infrared microspectroscopy, *Biomacromolecules*, **4**, 70-74

Meuleman E. B. (1999) Modeling of liquid/liquid separation by pervaporation: toluene from water, *AIChE J.*, **45**, 2153-2160

Moynihan, H.J., Lee, C.K., Clark, W., Wang, N.H.L. (1989) Urea hydrolysis by immobilized urease in a fixed bed reactor: analysis and kinetic parameter estimation, *Biotechnol. Bioeng.*, **34**, 951-963

Murty, V. R., Bhat, J., Muniswaran, P. K. A. (2002) Hydrolysis of oils by using immobilized enzyme: a review, *Biotechnol. Bioeng.*, **7**, 57-66

Nagy, E. (2004) Nonlinear, coupled mass transfer through a dense membrane, *Desalination*, **163**, 345-354

Neel, J. (1991) "Introduction to pervaporation", in pervaporation membrane separation processes, Ed.: R. Y. M. Huang, Elsevier Science Publishers, Amsterdam

Nishiyama, T. (1998) Uphill diffusion and a new nonlinear diffusion equation in ternary electrolyte system, *Phys. Earth Planet. Int.*, **107**, 33-51

Nol, M., Lozano, P., Vaultier, M., Iborra, J. L. (2004) Kinetic resolution of *rac*-2-pentanol catalyzed by Candida antarctica lipase B in the ionic liquid, 1-butyl-3-methylimidazolium bis[(trifluoromethyl)sulfonyl]amide, *Biotechnol. Lett.*, **26**, 301-306

Orrenius, C., Hæffner, F., Rotticci, D., Öhrner, N., Norin, T., Hult K. (1998) Chiral recognition of alcohol enantiomers in acyl transfer reactions catalysed by *Candida antarctica* lipase B, *Biocatal. Biotransform.*, **16**, 1-15

Orsat, B., Wirz, B., Bischof, S. (1999) A continuous lipase-catalyzed acylation process for the large-scale production of vitamin A precursors, *Chimia*, **53**, 579-584

Ortiz, I., Alonso P., Urtiaga, A. (2002) Pervaporation of azeotropic mixtures ethanol/ethyl tert-butyl ether: influence of membrane conditioning and operation on pervaporation flux, *J. Membr. Sci.*, **149**, 67-72

Otto, R.T., Scheib, H., Bornscheuer, U.T., Pleiss, J., Syldatk, C., Schmid, R.D. (2000) Substrate specificity of lipase B from *Candida antarctica* in the synthesis of arylaliphatic glycolipids, *J. Mol. Catal. B: Enzyme*, **8**, 201-211

Ottosson, J., Fransson, L. Hult, K. (2002) Substrate entropy in enzyme enantioselectivity: An experimental and molecular modeling study of a lipase, *Protein Sc.*, **11**, 1462-1471

Ottosson, J. and Hult K. (2001) Influence of the acyl chain length on the enantioselectivity of Candida antarctica lipase B and its thermodynamic components in kinetic resolution of sec-alcohols, *J. Mol. Catal. B: Enzym.*, **11**, 1025-1028

Ottosson, J., Rotticci-Mulder, J. C., Rotticci, D., Hult, K. (2001) Rational design of enantioselective enzymes requires considerations of entropy, Protein Sc., 10, 1769-1774

Overmeyer, A., Lippelt, S. S., Kasche, V., Brunner, G. (1999) Lipase catalysed kinetic resolution of racemates at temperatures from 40°C to 160°C in supercritical CO_2, *Biotechnol. Lett.*, **21**, 65-69

Ozdemir, S. S., Dincer, S., Savasci, D. T. (1999) Separation of alcohol-ester binary mixtures by pervaporation, *Eurasian Chemtech J.*, **1**, 33-37

Pamies, O. and Bäckvall, J. E. (2004) Chemoenzymatic dynamic kinetic resolution, *Trends in Biotechnol.*, **22**, 130-135

Park, B.-G. (2004) Pervaporation Characteristics of Polyetherimide/γ-Alumina Composite Membrane for a Quaternary Equilibrium Mixture of Acetic Acid-Ethanol-Ethyl Acetate-Water, *Korean J. Chem. Eng.*, **21**, 882-889

Patankar, S. V. (1982) Numerical methods in heat transfer. In: Proc Seventh Intern Heat Transfer Conference, München, **1**, 83–90

Patel, M.T., Nagarajan, R., Kilara, A. (1996) Lipase-catalyzed biochemical reactions in novel media. A review., *Chem. Eng. Commun.*, **152-153**, 365-404

Patel, R.N. (2002) Enzymatic preparation of chiral pharmaceutical intermediates by lipases. In: Lipid Biotechnology, (Kuo, T.M., Gardner, H.W., eds.), 527-561

Patwardhan, V.S. and Karanth, N.G. (1982) Film diffusional influences on the kinetic parameters in packed-bed immobilized enzyme reactors, *Biotechnol. Bioeng.*, **24**, 763-780

Pereira, E. B., Castro, H. F., Moraes, F. F., Zanin, G. M. (2001) Kinetic studies of lipase from Candida rugosa. A comparative study between free and immobilized enzyme on porous enzyme beads, *Appl. Biochem. Biotechnol.*, **91-93**, 739-752

Perry, R. H. (1999) Perry's Chemical Engineerings' Handbook. Eds. Green, D.W., Maloney, J.O., McGraw-Hill, New York

Rakels, J. L. L., Romein, B., Straathof, A. J. J., Heijnen, J. J. (1993) Kinetic analysis of enzymatic chiral resolution by progress curve evaluation, *Biotechnol. Bioeng.*, **43**, 411-422.

Rautenbach, R. and Hömmerich, U. (1998) Experimental study of dynamic mass transfer effects in pervaporation, *AIChE J.*, **44**, 1210-1215

Raza, S., Fransson, L., Hult, K. (2001) Enantioselectivity in *Candida antarctica* lipase B: A molecular dynamics study, *Protein Sci.*, **10**, 329-338

Resnick, S. M., Donate, F. A., Frank, T. C., Thyne T. C., Foley, P. (2003) Enzymatic Resolution of Propylene Glycol Alkyl (or Aryl) Ethers and Ether Acetates, Patent, WO 03,083,126

Rizzi, M., Stylos, P., Riek, A., Reuss, M. (1992) A kinetic study of immobilized lipase catalysing the synthesis of isoamyl acetate by transesterification in n-hexane, *Enz. Microb. Technol.*, **14**, 709-714

Robbins, L. A. (1979) The miniplant concept, *Chem. Eng. Prog.*, **75**, 45-48

Rogalska, E., Ransac, S., Carriere, F., Verger, R., (2000) Stereoselective hydrolysis of glycerides by lipases. In: Fat Digestion and Absorption (Christophe, A.B., De Vriese, S., eds.), 47-59

Romero, M. D., Calvo, L., Alba, C., Daneshfar, A., Ghaziaskar, H. S. (2005) Enzymatic synthesis of isoamyl acetate with immobilized *Candida antarctica* lipase in *n*-hexane, *Enz. Microb. Technol.*, **37**, 42-48

Rotticci, D., Mulder, J. C., Denman, S., Norin, T., Hult, K. (2001a) Improved enantioselectivity of a lipase by rational protein engineering, *Protein Sc.*, **2**, 766-770

Rotticci D., Ottosson J., Norin T., and Hult, K. (2001b) Candida antarctica Lipase B: A Tool for the Preparation of Optically Active Alcohols. *Methods in Biotechnol. Vol 15: Enzymes in Nonaqueous Solvents: Methods and Protocols*. Vulfson EN, Halling PJ, Holland HL (eds). Humana Press, Totowa, NJ

Roy, I., Gupta, M. N. (2004) Hydrolysis of starch by a mixture of glycoamylase and pullulanase entrapped individually in calcium alginate beads, *Enzyme Microb. Technol.*, **34**, 26-32

Rubin, B. and Dennis, E. A. eds. (1997a) *Methods in Enzymology: Lipases, Part A: Biotechnology*, **284**, Academic Press, New York

Rubin, B. and Dennis, E. A. eds. (1997b) *Methods in Enzymology: Lipases, Part B: Enzyme characterization and utilization*, **286**, Academic Press, New York

Rusnak, M. (2004) Untersuchungen zur enzymatischen Enantiomerentrennung von Glykolethern und Etablierung neuer Methoden des synthetischen Shufflings, Thesis, Institute of Technical Biochemistry, University of Stuttgart, Stuttgart

Santano, E., Pinto, M. C., Macías, P. (2002) Chlorpromazine oxidation by hydroperoxidase activity of covalent immobilized lipoxygenase, Biotechnol. *Appl. Biochem.*, **36**, 95-100

Scheibel, E. G. (1954) *Liquid Diffusivities, Ind. Eng. Chem.*, **46**, 2007-2013

Schnell, B., Faber, F., Kroutil, W. (2003) Enzymatic racemisation and its application to synthetic biotransformations, *Adv. Synth. Catal.*, **345**, 653-666

Secundo, F., Carrea, G., Soregaroli, C., Varinelli, D., Morrone, R. (2001) Activity of different Candida antarctica lipase B formulations in organic solvents, *Biotechnol. Bioeng.*, **73**, 157-163

Segel, I. H., (1993) Enzyme kinetics – Behavior and analysis of rapid equilibrium and steady state enzyme systems. John Wiley & Sons, Inc. New York., 957p

Sharma, A., Thampi, S. P., Suggala S. V., Bhattacharya, P. K. (2004) Pervaporation from a Dense Membrane: Roles of Permeant-Membrane Interactions, Kelvin Effect, and Membrane Swelling, *J. Membr. Sci.*, **20**, 4708-4714

Sheldon, R. A., Lau, R. M., Sorgedrager, M. J., Rantwijk, van F., Seddon, K. R. (2002) Biocatalysis in ionic liquids, *Green Chem.*, **4**, 147-151

Shibatani, T., Nakamichi, K., Matsumae, H. (1990) Patent, EP 362 556

Shin, J. S. and Kim, B. G. (1998) Kinetic modeling of ϖ-transamination for enzymatic kinetic resolution of α-methylbenzylamine, *Biotechnol. Bioeng.*, **60**, 34-540.

Smitha, B., Suhanya, D., Sridhar S., Ramakrishna, M. (2004) Separation of organic-organic mixtures by pervaporation – a review, *J. Membrane Sci.*, **241**, 1-21

Spencer, C. F. and Danner, R. P (1972) Improved equation for prediction of saturated liquid density, *J. Chem. Eng. Data*, **17**, 236-241

Sridhar, S., Smitha, B., Shaik, A. (2005) Pervaporation based separation of Methanol/MTBE-mixtures – a review, *Sep. Purif. Rev.*, **34**, 1-33

Stadler, H.-G. (2005) Entwicklung eines kontinuierlichen Verfahrens zur enzymkatalysierten Synthese eines strukturierten Triglycerides, Ph.D.-Thesis, University of Stuttgart

Steen, B. (2000) A systematic approach to environmental priority strategies in product development (EPS), Version 2000 – Models and Data of the Default Method, Göteburg

Steude, H. E., Deibele, L., Schröter, J. (1997) Miniplant-Technik - ausgewählte Aspekte der apparativen Gestaltung, Chem.-Ing.-Tech., 69, 623-631

Stinson, S. C. (2000) Chiral Drugs: New intermediates, catalysts, and reactions fuel continued industry growth, *Chem. Eng. News*, **78**, 55-78

Theil, F. (2001) Enantioselective lipase-catalyzed transesterifications in organic solvents. In: Methods in Biotechnology, 277-289

Toullec, J. (1990) Keto-enol equilibrium constants. in: Z. Rappaport (Ed.), The chemistry of enols, Wiley, New York, pp.323-398

Tran Minh, C., Bougnol-Bilvou, V., Lancelot, F. (1976) Enzymatic reactor using high activity immobilized enzyme during exothermic reaction, Proceedings of the 4th International Symposium in Chemical Reaction Engineering, DECHEMA, Frankfurt/Main, 125-134

Tsotsas, E. (2002) Wärmeleitung und Dispersion in durchströmten Schüttungen, in: VDI-Wärmeatlas, 9. Ed., Mh1-14, Springer Verlag, Berlin

Turner, N. J. (2004) Enzyme catalysed deracemisation and dynamic kinetic resolution reactions, *Curr. Opin. Chem. Biol.*, **8**, 114-119

Turner, N.A., Vulfson, E.N. (2000) At what temperature can enzymes maintain their catalytic activity? *Enzyme Microb. Technol.*, **27**, 108-113

Uppenberg, J., Hansen, M. T., Patkar, S., Jones, T. A. (1994) The sequence, crystal structure determination and refinement of two crystal forms of lipase B from Candida antarctica, *Structure*, **2**, 293-308

Uppenberg, J., Öjrner, N., Norin, M., Hult, K., Klezwegt, G. J., Patkar, S., Waagen, V., Anthonsen, T. and Jones, T. A. (1995) Crystallographic and molecular modeling

studies of lipase B from Candida antarctica reveal a stereospecific pocket for secondary alcohols, *Biochemistry*, **34**, 16838-16851

Urtiaga, A., Gorri D., Ortiz, I. (2002) Mass-transfer modeling in the pervaporation of VOCs from diluted solutions, *AIChE J.*, **48**, 572-581

Watanabe, K., Koshiba, T. Yasufuku, Y., Miyazawa, T., Ueji, S. (2001) Effects of substituent and temperature on enantioselectivity for lipase-catalyzed esterification of 2-(4-substituted phenoxy) propionic acids in organic solvents, *Bioorg. Chem.*, **29**, 65-76

Wörz, O. (1995) Process development via a miniplant, *Chem. Eng. Proc.*, **34**, 261-268

Xiu, G.-H., Jiang, L., Li, P. (2001) Mass transfer limitations for immobilized enzyme catalyzed kinetic resolution of racemate in a fixed-bed reactor, *Biotechnol. Bioeng.*, **74**, 29-39

Yu, X., Li, Y., Wang, C., Wu, D. (2004) Immobilization of Aspergillus niger tannase by microencapsulation and its kinetic characteristics, *Biotechnol. Appl. Biochem.*, **40**, 151-155

Zhang, H. Y., Wang, X., Ching, C. B., Wu, J. C. (2005) Experimental optimization of enzymatic kinetic resolution of racemic flurbiprofen, *Biotechnol. Appl. Biochem.*, **42**, 67-71